University of Southampton

Faculty of Engineering, Science and Mathematics

School of Engineering Sciences

Sensors for Thermal Conductivity at High Temperatures

by

Jaromir Bilek

Thesis submitted for the degree of

Doctor of Philosophy

June 2006

UNIVERSITY OF SOUTHAMPTON

ABSTRACT

FACULTY OF ENGINEERING, SCIENCE AND MATHEMATICS

SCHOOL OF ENGINEERING SCIENCES

Doctor of Philosophy

SENSORS FOR THERMAL CONDUCTIVITY AT HIGH TEMPERATURES

by Jaromir Bilek

This thesis describes research undertaken to improve a technique for the measurement of the thermal conductivity of molten materials. The research follows on from the work of previous researchers who designed and tested an instrument for the measurements of the thermal conductivity of molten metals up to 750 K. The previously used transient hot-wire technique, which consisted of the experimental measurement of the voltage response of a sensor and a subsequent inverse finite element analysis, has been significantly upgraded.

The experimental part of the technique has been improved by the introduction of a new design of the sensor for the measurement of the thermal conductivity. Both the new and the original designs have been used to investigate the same material samples in order to demonstrate the robustness and repeatability of the experimental technique. Additionally, the finite element analysis employed has also undergone various major improvements and resulted in a new finite element model which not only represents the true geometry of the experimental device but also employs a more accurate solution of the transient, conductive heat transfer.

The significant upgrade of the technique and the availability of two different sensor designs have helped to uncover systematic errors which could not have been previously identified and may have resulted in deviations of the measured thermal conductivity. Five original sensors and five sensors with the new design have been used to investigate the thermal conductivity of molten indium, tin and lead at various temperatures up to 750 K. The results have been compared to previously published data and the discrepancies have been discussed and explained. Each metal has been measured using at least two sensors and the consistency of the measured data has also been verified by using two different samples of pure tin. Besides the pure metals, the thermal conductivity of several metal alloys currently used in industry has been investigated within the same temperature range. The overall uncertainty of the measurements of the thermal conductivity is estimated to be ±3 %.

Contents

List of Tables

List of Figures

Declaration of Authorship

I, Jaromir Bilek, declare that the thesis entitled *Sensors for Thermal Conductivity at High Temperatures* and the work presented in it are my own. I confirm that:

- this work was done wholly or mainly while in candidature for a research degree at this University;
- where any part of this thesis has previously been submitted for a degree or any other qualification at this University or any other institution, this has been clearly stated;
- where I have consulted the published work of others, this is always clearly attributed;
- where I have quoted from the work of others, the source is always given. With the exception of such quotations, this thesis is entirely my own work;
- I have acknowledged all main sources of help;
- where the thesis is based on work done by myself jointly with others, I have made clear exactly what was done by others and what I have contributed myself;
- parts of this work have been published as papers at scientific conferences. The published papers are presented in *Appendix C Publications*.

Signed: .....[redacted].....

Date: .....15.6.2006.....

Acknowledgements

I would like to express my deepest thanks to my supervisors Dr John Atkinson and Prof Bill Wakeham for their valuable professional advice and kind encouragement throughout the course of my postgraduate research.

My warmest thanks go out to my friends and colleagues within the Electro-Mechanical Group at the School of Engineering Sciences, in particular to Dr Liza Lam, Dr Gary Zhang and Mrs Karen Ragan, as their help and guidance have been vital for me during my stay at the University of Southampton.

In addition, I would like to mention Dr Ed Young and Mike Webb from the Cryogenic Laboratory and Erik Roszkowiak from the Transportation Systems Research Laboratory who provided the essential technical support for the experimental part of my PhD project. I also cannot miss out my friend Moss (Lt Nuttaphon Sathon), who helped me with the experiment with the infrared camera, and Dr Peter Quested from National Physical Laboratory, who provided me with the data about the demand for the thermophysical properties.

I would also like to take this opportunity to thank my parents and my fiancée Miss Yiping Shen for their help, patience and constant encouragement. I deeply appreciate all the support that they have given me to help make my stay in Southampton a wonderful and fruitful experience.

Definitions of Symbols and Abbreviations

Greek symbols

α	linear thermal coefficient of electrical resistance [K^{-1}]
β	quadratic thermal coefficient of electrical resistance [K^{-2}]
γ	Euler's constant ($\gamma = 0.5772157\ldots$)
λ	thermal conductivity [$W \cdot m^{-1} \cdot K^{-1}$]
ρ	mass density [$kg \cdot m^{-3}$]
σ	electrical conductivity [$S \cdot m^{-1}$]

Other symbols

A	area [m^2]
a	thermal diffusivity [$m^2 \cdot s^{-1}$]
C_P	specific heat capacity [$J \cdot kg^{-1} \cdot K^{-1}$]
d	thickness of a gap or interface [m]
f	interface coefficient between two materials (λ/d) [$W \cdot m^{-2} \cdot K^{-1}$]
l	length [m]
l_w	length of the finite part of an infinite hot wire [m]
Q	heat flux [$W \cdot m^{-2}$]
$\overline{Q}$	heat flow rate [W]
q_{gen}	heat generation [$W \cdot m^{-3}$]
q	heat generated per unit length [$W \cdot m^{-1}$]
r	radius [m]
T	thermodynamic (absolute) temperature [K]
$T(t)$	temperature at time t [K]
$\Delta T(t)$	change of the temperature at time t, i.e. $T(t) - T(0)$
T_C	Celsius temperature [°C]
T_m	thermodynamic (absolute) temperature of melting point [K]
t	time [s]
v	velocity [$m \cdot s^{-1}$]

Electronic bridge analysis

$R(t)$	electrical resistance at time t [Ω]
$\Delta R(t)$	change of the resistance at time t, i.e. $R(t) - R(0)$
R_1	resistance for the tuning of the Wheatstone bridge
R_2	additional (padding) resistance
R_{bare}	resistance of the bare wire (not encapsulated)
R_{leadin}, $R_{leadout}$	lead resistances of the sensor
R_{short}	short wire resistance (part of the hot wire)
R_{long}	long wire resistance (part of the hot wire)
R_w	resistance of the hot wire as a part of an infinitely long wire
R_0	resistance R_w at temperature 273.15 K (0°C)
R_{LL}	resistance of one half of the electrical current path
S_L	ratio between short and long wire, i.e. R_{short}/R_{long}
V_S	supply voltage (voltage applied on the bridge)
$V_B(t)$	voltage measured at terminal B at time t
$\Delta V(t)$	Wheatstone bridge output at time t

General abbreviations

FE	Finite Element
FEM	Finite-Element Method
THW	Transient Hot Wire
TCR	Temperature Coefficient of Resistance
TCE	Temperature Coefficient of Expansion

The definitions above show the most frequent symbols and abbreviations in the thesis. Other symbols are described and explained in the text where they are used.

1. Introduction

The chapter explains the importance of measurements of the thermophysical properties of materials which are used in industry. The first section briefly describes both an obsolete and a modern approach to the product design-to-manufacture process and presents data from a survey conducted within the project "*THERMOLAB*". The following section describes the previous stages of the current research and the last section reveals the structure of the thesis, which may help readers to orientate themselves in the text.

1.1. Demand for Properties of Materials

The demand for accurate data of material properties has been sharply increasing recently. The increase has been mainly supported by the introduction of computational modelling of artefacts and manufacturing process, which has become a key process in the design of almost every industrially fabricated device. Product design is no longer based just on manufactured prototypes and their subsequent testing. Nowadays, most production processes are accompanied by some degree of computation and mathematical models, which are used to predict behaviour of the components and materials during the fabrication stages. It has become apparent that the computational modelling is one of the main design tools and therefore the accuracy of its output is highly desirable.

In order to create a realistic model of any production process, material properties must be very precisely defined at specific conditions and for every temperature, at which the material is used or a component mounted. Well-defined material properties then allow a highly precise computational modelling and subsequently help to improve performance of the final product and optimise its cost. Inevitably, materials data and their temperature and ageing characteristics are crucial input parameters to any modelling and if a thermal or thermo-mechanical analysis is required, thermophysical properties have to be known.

At present, almost every industrial fabrication process is dealing with some kind of molten material. For example the electronics industry is working with molten solders, the casting industry with molten metals and alloys, or a moulding processes are used wherever plastic materials are fabricated. In the past, the knowledge of the exact thermophysical properties of molten materials was not so significant because the design-to-production process relied heavily on testing of prototypes. An example of such process in the casting industry is illustrated in Figure 1.1 and shows the production steps of an obsolete technique where the prototype was observed and tested after the fabrication process. The faults that emerged during the fabrication were recognised (slow mould filling, quick solidification or visible cracks), but it was not possible to distinguish clearly, which of the processing parameters had to be adjusted. Therefore the optimisation of the fabrication was rather slow and required large number of fabricated

prototypes. Such a means of production was not time and cost effective and that is why there is a demand to model fabrication processes or calculate the final product properties based on available material properties.

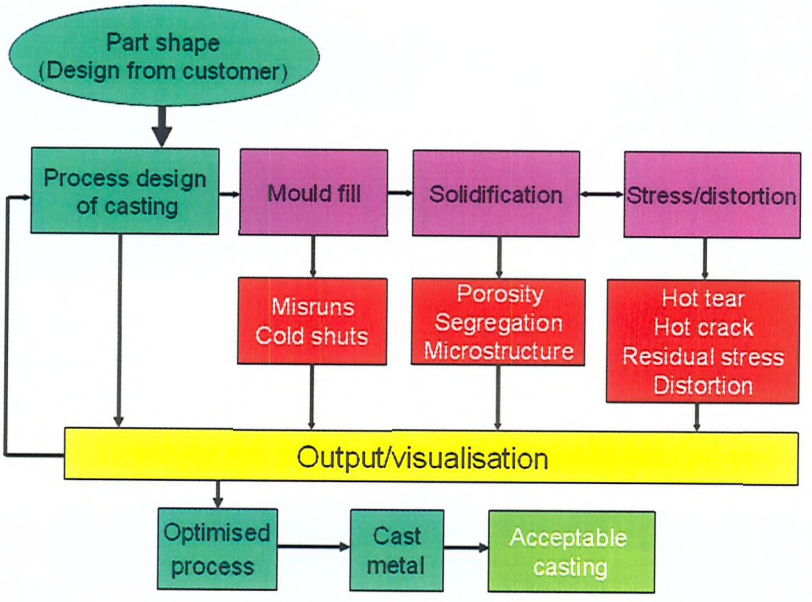

Figure 1.1 Obsolete design-to-production process in the casting industry [1]

An example of a modern design-to-process production preparation in the casting industry is described in Figure 1.2. It shows groups of thermophysical properties which are used as input values for the computational modelling of the fabrication processes. The results from the model help to determine optimal parameters of the production process and achieve smooth, reliable and high quality production of a device.

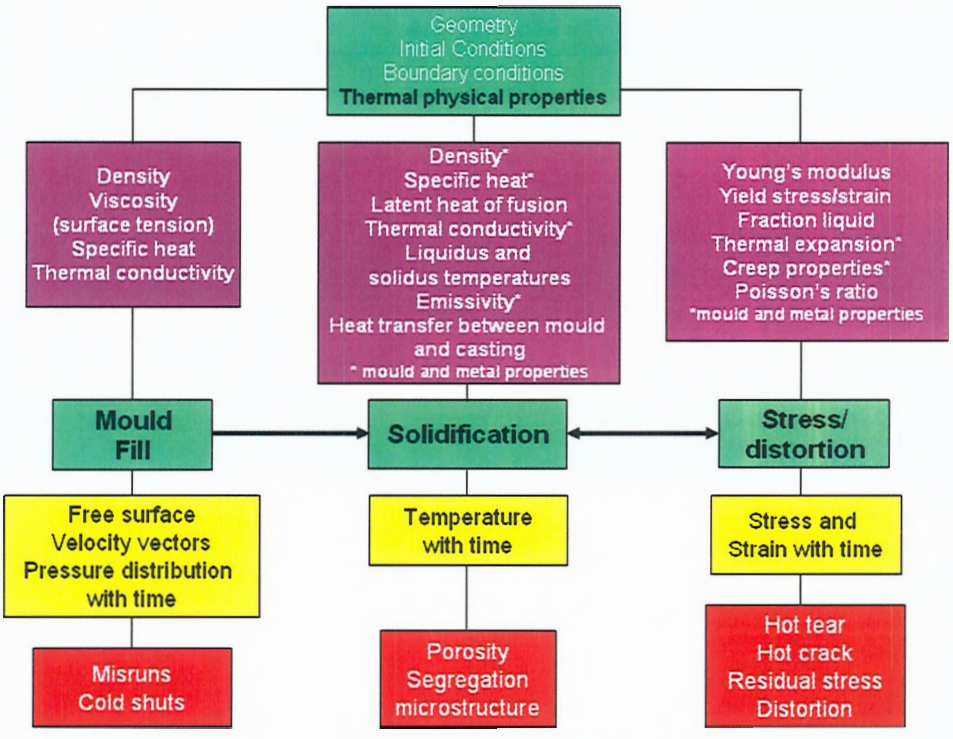

Figure 1.2 Parameters of the modern design-to-production process in the casting industry [2]

Recently, National Physical Laboratory in London has participated in the project which aimed to obtain a reasonable picture of the demand for the thermophysical properties. A survey "*Industrial Need for Thermophysical Property Data*" was conducted as a part of an ESA Project "*THERMOLAB*". About one thousand questionnaires were sent around Europe to industrialists and trade associations and about three hundred of them replied. Some significant results from the survey can be seen in the figures below.

Figure 1.3 shows a distribution of the required thermophysical properties in different industrial areas. It can be seen that the thermal conductivity is the 'most wanted' material property because more than one third of all returned questionnaires identified as such. Figure 1.4 then illustrates an expected use of material properties data, again distinguished by application area and it shows that the thermophysical data of materials are mainly required for

- Computer modelling
- Gaining scientific understanding
- Process control

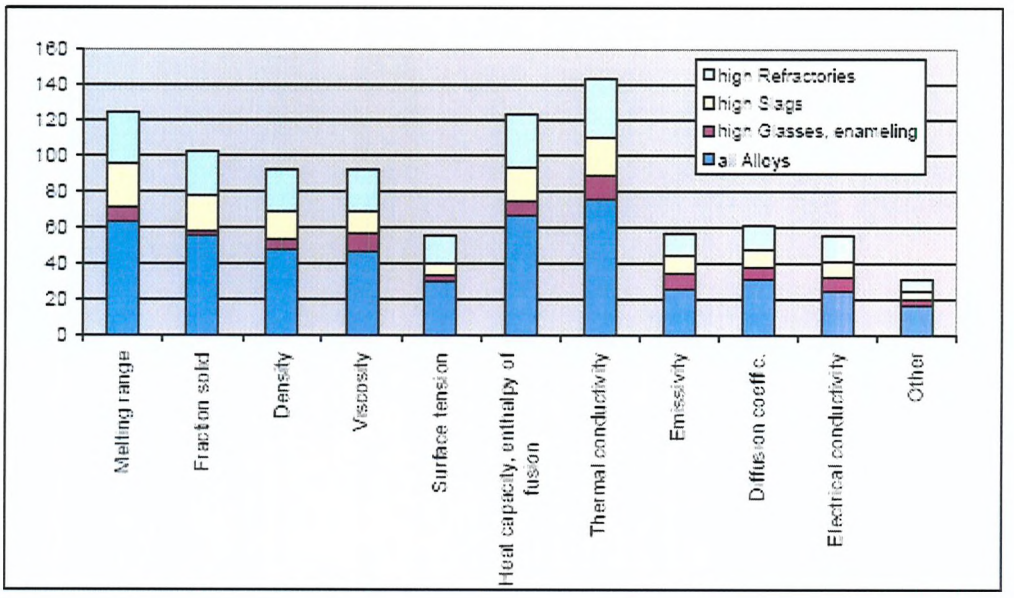

Figure 1.3 Histogram showing the distribution of thermophysical properties ranked "high" importance according to material type [2]

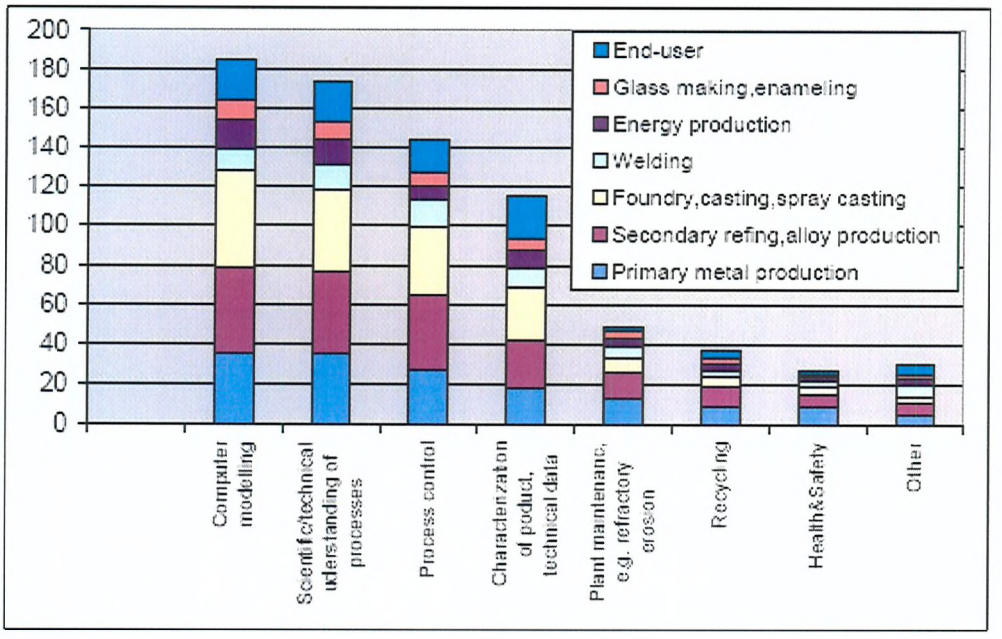

Figure 1.4 Histogram showing intended use of material properties (Europe) [2]

The survey showed that the thermal conductivity of materials is the most required thermophysical property and is mostly used as an input data for the modelling of the manufacturing and solidification processes. Knowledge of the thermal conductivity also

helps to understand physical relationships in other applications and optimise thermal management of utilised equipments, such as thermal baths, furnaces, etc.

Over the years, the scientists have developed various techniques for measurements of the thermal conductivity of materials. Every technique allows measurements of certain materials at specified conditions (phase, pressure, temperature) and very reliable data can be obtained for solids in wide range of temperatures. However, the measurements of the thermal conductivity of molten materials are less straightforward and offer many challenges. This work has focused on the development of the technique for the measurements of the thermal conductivity of molten materials with an aim to provide highly accurate data within wide range of temperatures.

1.2. Previous Research

Since the introduction of the thermal conductivity measurements, various methods have been used to analyse solids, liquids and gases, and a brief overview can be found in chapter *2.Methods for the Measurements of the Thermal Conductivity*. Accurate techniques were developed for the measurements of the thermal conductivity of fluids and a number of instruments were designed and tested in the second half of the last century [3-5]. However such experimental techniques could not be directly applied to the measurement of the thermal conductivity of electrically conductive fluids at elevated temperatures.

A new approach to this task was considered during the European project which started in 1992 and was called "*An Instrument for the Measurement of Thermal Conductivity of High Temperature Melts*". The European project focused on an introduction of a modified transient hot-wire technique which is one of the methods for precise thermal conductivity measurements and is described in detail in chapter *3.Transient Hot-Wire Technique*. The project explored the application of the transient hot-wire technique for aggressive conditions of molten metals and for this purpose a bare metallic wire characteristic for early works [6, 7] was replaced by a wire encapsulated in an alumina substrate. An implementation of thick film technology into the manufacturing process of the sensor was also one of the significant changes in the sensor fabrication technology [8].

The research in Imperial College London, where a significant part of the European project was carried out, continued and focused on the measurements of the thermal conductivity of several molten metals [9-13]. The research was terminated in 2001 and a year later the measuring equipment was moved from Imperial College London to University of Southampton. The current postgraduate research project started in January 2003 with a fundamental goal to confirm that the technique used in Imperial College London is capable to provide repeatable data. Subsequently, the technique was improved, the design of the sensor upgraded and several new metals and alloys analysed. This work describes the improvements and presents results from the measurements of the thermal conductivity.

1.3. Scope

This introduction is followed by chapter *2.Methods for the Measurements of the Thermal Conductivity*, which describes the methods that are currently available for the measurements of the thermal conductivity. The chapter briefly explains both steady-state and transient methods and discusses their suitability for the measurement of the thermal conductivity of fluids at high temperatures. The method that is used for the measurement in this work is introduced in chapter *3.Transient Hot-Wire Technique*. The fundamental theory is thoroughly described and compared to the modified technique that is used in this work for the measurements of the thermal conductivity of electrically conductive fluids at high temperatures. The modified technique is also comprehensively explained and a detail analysis of uncertainty is carried out.

The following chapter *4.Experimental Arrangements* describes the sensor, instrumentation and experimental procedures. A new sensor design is introduced and the importance of calibration of the sensors is discussed. The technique of measurements and subsequent evaluation of the signal from the sensor is fully explained. In conclusion the accuracy of the measurements is discussed.

Chapter *5.Results* then lists all the data of the thermal conductivity, which have been measured during the current project. The thermal conductivity as the function of temperature is presented for pure indium, tin and lead and also for alloys which are currently used in electronics industry and are commonly known as solders. The thermal conductivity data are compared to values measured by other researchers and discussed.

The last chapter *6. Future Work* gives suggestions for the following projects and lists several tasks, which could not be carried out in the current project due to the limited time given for the postgraduate research. *Appendix A* then summarises the thermophysical properties of the investigated molten materials, *Appendix B* lists the source code for the analysis in ANSYS® and *Appendix C* presents the papers which have been published since the beginning of this postgraduate research.

2. Methods for the Measurements of the Thermal Conductivity

A brief overview of various methods for the measurements of the thermal conductivity is presented in this chapter. The primary goal is to introduce the main-stream methods, explain their fundamental principles and provide a reader with links to other sources. The chapter is divided into two main sections, which summarise steady-state and transient techniques. The chapter also analyzes the suitability of the techniques for the measurements of the thermal conductivity of liquids at elevated temperatures and discusses the accuracy and possible sources of uncertainty for the values of the measured thermal conductivity or thermal diffusivity.

2.1. Steady-State Methods

Steady-state methods generally rely on measurements of the heat flux necessary to maintain a temperature difference constant in time, between two surfaces in the fluid as a means of determining the thermal conductivity of the fluid. Alternatively one can measure the temperature difference generated by the application of the known constant heat flux within the measured fluid. The two surfaces are usually formed by concentric cylinders or by two parallel plates. All steady-state instruments are characterised by much higher simplicity and simpler working equations than transient methods.

The difficulties in their use derive from a need for extremely accurate alignment of the two surfaces, because defects in alignment make a first-order contribution to the inaccuracy of the measured thermal conductivity. Another significant source of inaccuracy arises from the fact that the temperature gradient must always be applied in a gravitational field. A buoyancy force is then inevitable which acts as a driving force for convective fluid motion. And finally, all steady-state methods encounter a certain error because of the radiation of the heated surface. The radiation generated in the heated surface penetrates through the measured sample to the second surface where it is absorbed. If the measured sample is transparent, the influence of the radiative part of the heat transfer can be described by equations and evaluated. However once the measured sample absorbs a part of the radiation from the heated surface, the radiative heat transfer cannot be evaluated accurately and this imposes a certain error on the measured thermal conductivity.

2.1.1. Coaxial-Cylinder Method

The coaxial-cylinder method was first used more than one hundred and thirty years ago and many concentric-cylinder cells for the measurements of gases and liquids have been designed since [3]. In principle, the method assumes a thin layer of homogeneous fluid with a uniform thermal conductivity λ, enclosed between two coaxial cylinders of infinite length. The classical arrangement of the method is shown in Figure 2.1. The external radius of the inner cylinder is r_1 and the internal radius of the external cylinder r_2. In the steady-state conditions, the temperatures of the external surface of the inner cylinder and of the internal surface of the outer cylinder will be respectively T_1 and T_2.

The amount of the heat transferred by conduction per unit time per unit length through the fluid layer is given by Fourier's law [4]. Using L as the length of the inner cylinder, a heat input rate $\overline{Q}$ instead of the heat flux, and reordering Fourier's law, the thermal conductivity can be calculated from the equation

$$\lambda = \frac{\overline{Q} \cdot \log(r_2 / r_1)}{2\pi \cdot L \cdot \Delta T} \tag{2-1}$$

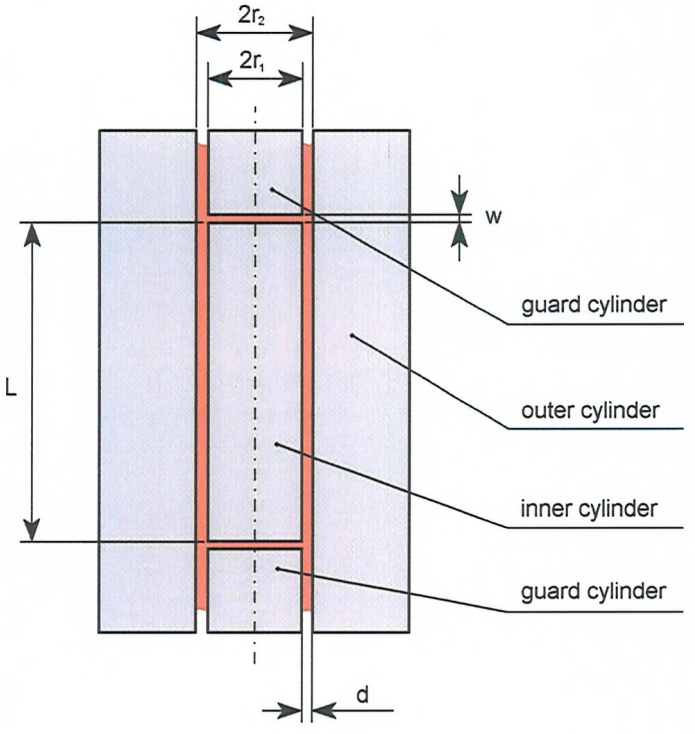

Figure 2.1 Schematic diagram of the concentric cylinders

Guard cylinders shown in Figure 2.1 are separated from the heat source by a width w, approximately equal to d. When the guard cylinders are kept at the same temperature as the heat source, all of the heat is transferred radially and equation (2-1) can be applied to obtain the thermal conductivity of the fluid. The method has been used to determine the thermal conductivity of a wide range of fluids, mostly with an accuracy claimed to be within a range of ±5 %. An overview of measured fluids and a large list of other references can be found in [3, 5]. A few concentric-cylinder cells were also designed for the measurements of fluids at elevated temperatures, for example works published by Sklyarchuk [14] and Abdulagatov [15]. These researchers reported an uncertainty of up to ±7 % of the measured thermal conductivity.

2.1.2. Parallel-Plate Method

In the parallel plate method the fluid to be investigated is confined between two horizontal plates. The system is heated from above and the thermal conductivity is again calculated using the phenomenological relationship known as Fourier's law. In practice the specimen is kept between two circular plates of a metal with a high thermal conductivity, usually copper. The upper plate is supplied with thermal energy with the heat flow rate $\overline{Q}$ uniformly distributed over the plate area. The basic equation is then written as

$$\lambda = \frac{\overline{Q} \cdot d}{A \cdot \Delta T} \tag{2-2}$$

where A is the area of the plates, d is distance between the plates, and ΔT is a temperature difference between the plates. The diagram of the parallel plate method is illustrated in Figure 2.2.

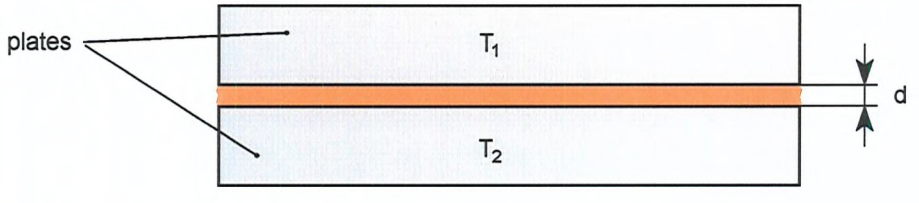

Figure 2.2 Schematic diagram of the parallel plate method

The history of this method dates back to 1881 and thereafter the method has been used and modified by many investigators [3]. The method is mainly used for solids, however an accuracy suitable for many practical applications can also be reached for liquids at temperatures up to 770 K (500 °C). The parallel plate method minimises convection, allows proper consideration of radiation and other corrections due to the simple cell geometry and possibility of measuring with different plate distances [3].

The method has been used by Osipenko [16] to measure the thermal conductivity of molten antimony, indium, tin and lead with an uncertainty of about ±5 %.

2.1.3. Heat Flow Methods

These techniques can be divided into two categories according to the geometry of the instrument, i.e. axial and radial heat flow methods. The principle is that a known heat input is applied to one end of the sample and removed at the other end of the sample by a heat sink. This inevitably results in a temperature drop along the sample from which the thermal conductivity can be calculated. These methods are in principle very similar to parallel-plate and coaxial-cylinder methods and that is why very similar equations are employed to derive the thermal conductivity. The only difference is that the temperature drop along the sample is measured by thermocouples, which are not placed on the heated plate and the heat sink but immersed in the measured sample.

The axial heat flow technique was used by Hemminger [17-19] to determine the thermal conductivity of molten tin and lead with a total estimated uncertainty of ±5 %. A different axial heat flow apparatus was used by Duggin [20], who also claimed an uncertainty of ±5 % for the measurements of the thermal conductivity of molten indium and lead. A comparison between results of both researchers shows that the thermal conductivity of lead at the melting point measured by Hemminger [19] differs by about 3 % from the value measured by Duggin but the differences are much greater at higher temperatures (up to 20 % at 750 K).

Goldratt and Greenfield [21, 22] used a slightly different approach but still their method can be classified as the axial heat flow technique. They derived the thermal conductivity of molten indium from the measurements of the temperature profile along the sample, which was enclosed in the thin-walled stainless steel cylinder. They placed the cylinder in the vacuum, heated its top end with a known heat flow input and then observed the temperature profile along the cylinder using an infrared camera. They derived the thermal conductivity from the heat losses caused only by radiation and claimed the accuracy of such measurements to be about ±1 %.

2.2. Transient Methods

The main difficulty in performing accurate measurements of the thermal conductivity of fluids lies in the isolation of the conduction process from other mechanisms of heat transfer. This isolation cannot be fully achieved in steady-state techniques and that is why the transient methods have been developed. The success of the transient techniques is based on the fact that the characteristic time for the acceleration of the fluid by buoyancy forces can be made to be much longer than the propagation time of a temperature wave originated by a strong and localised temperature gradient.

Transient methods can be divided into several groups following different criteria. One criterion can be the method for the heat generation in time, i.e. pulse or step function. The methods can be also judged by the geometry of the employed instruments and source of the heat (cylinder, plate, disc, wire, etc). Another parameter of the method distinguishes whether the sensing probe is inserted into the measured medium or whether the method is non-contact. A detailed overview of the transient contact methods can be found in [23] and a brief description of the non-contact transient methods with references to other sources is also given in [3].

In the following subsections, the principles of several transient techniques are reviewed. The experimental method, which has been used in our research, is described in detail in chapter *3.Transient Hot-Wire Technique* and that is why it is not included in the following overview.

2.2.1. Temperature Waves

The principle of the periodically generated temperature waves is that the sample is heated periodically at one end and the temperature along the sample varies with the same period but diminishing amplitude. In addition, as the temperature waves travel along the sample with a finite velocity, there is a varying phase relationship and the time lag along the sample is determined. Under the ideal conditions envisaged (no heat losses), the thermal diffusivity can be derived from the measurement of the amplitude decrement and either the phase difference or velocity of the temperature wave. Either radial or plane temperature waves can be used for the measurement of the thermal conductivity. Radial temperature waves have been widely used by Fillipov and his

various co-workers [24, 25] for the measurements of a wide range of materials, including thermal diffusivities of liquid tin and lead at temperatures above 800 °C with reported errors of ±6 % [26]. The periodic plane temperature waves are analogous to the radial temperature waves but, because it is not always possible to provide a sample in the form of a long rod, the methods apply to thin plate specimens. Plane temperature waves have been widely used by Zinovyev and co-workers [27] to measure the thermal diffusivity of high-melting metals. The uncertainty of these methods is mainly influenced by the phenomenon of the convection within the measured fluid. The periodic pulses heat up the measured liquid and the convectional heat transfer inevitably occurs within a certain time.

2.2.2. Laser Flash Technique

The basic configuration of this non-contact method is shown in Figure 2.3. In principle, the front surface of the measured sample is irradiated by a pulse of energy from a high power laser source. The back surface is monitored by an infrared detector and the temperature as a function of time is obtained. The resulting time dependency exhibits a maximum ΔT_{max} and it is customary to determine the time t_1 required to obtain $0.5 \cdot \Delta T_{max}$. The thermal diffusivity of the measured sample of thickness d can be then calculated from the measured data as

$$a = 0.1388 \frac{d^2}{t_1} \tag{2-3}$$

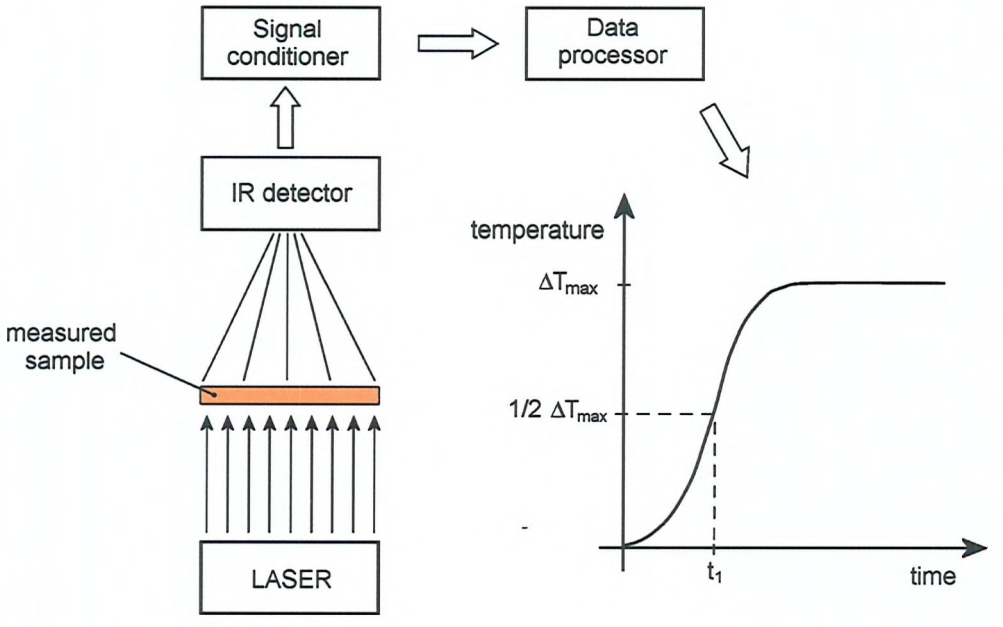

Figure 2.3 Schematic diagram of the laser flash technique

This non-contact method and the conventional way to calculate the thermal diffusivity of the measured sample was firstly proposed by Parker et al in 1961 [28]. The method is well-proved and widely used for the measurement of solids [29, 30]. The latest extensive review of the laser flash method was published by Vozar and Hohenauer [31] who also subsequently analysed the uncertainty of the method [32].

The laser flash technique also expanded into the measurements of the thermal diffusivity of liquids at elevated temperatures [33-35], however here its accuracy still remains uncertain. The IR detector is sensing a surface of the container with the measured fluid and this can result in misleading values due to the multilayer system and/or convective flow within the sample. For example, Maeda [36] reported that the measurements of the thermal diffusivity of melts at high temperatures showed deviations of about ±6 % and concluded that a number of uncertainties are present.

2.2.3. Interferometry

During the last thirty years there have been rapid developments of optical techniques to the measurements of the thermal properties of fluids. These techniques are applicable to a wide range of optically transparent fluids and they were found to be valuable especially within the critical region of the fluids, i.e. the region of temperatures and

pressures at which the liquid state of the matter ceases to exist. In this region, the most of other methods fails to work properly due to the large temperature gradients applied and geometry limitations.

The interferometry technique has been developed by Becker and Griggull [37]. During the measurements, an infinitesimally thin, uniform source of heat is located at the junction of two semi-infinite materials, usually solid and fluid. Initiation of the heat source causes a temperature rise of the fluid. The temperature distribution in the fluid at any instant can be determined by means of the effect of the refractive index of the fluid using optical interferometry. In the simplest approach an interference pattern is produced in the fluid at a uniform temperature in a plane perpendicular to the heater surface by the superposition of two laser beams. Any subsequent non-uniformity of temperature induced by the transient heating perturbs the fringe pattern. This perturbation can be described by equations [3] and therefore, in principle, measurements of perturbation could be used to determine the thermal diffusivity of the fluid and subsequently thermal conductivity of the fluid.

2.2.4. Forced Rayleigh Scattering Method

The most recent optical technique, which was originally designed to determine the thermal diffusivity of fluids under extreme condition, is called forced Rayleigh scattering.

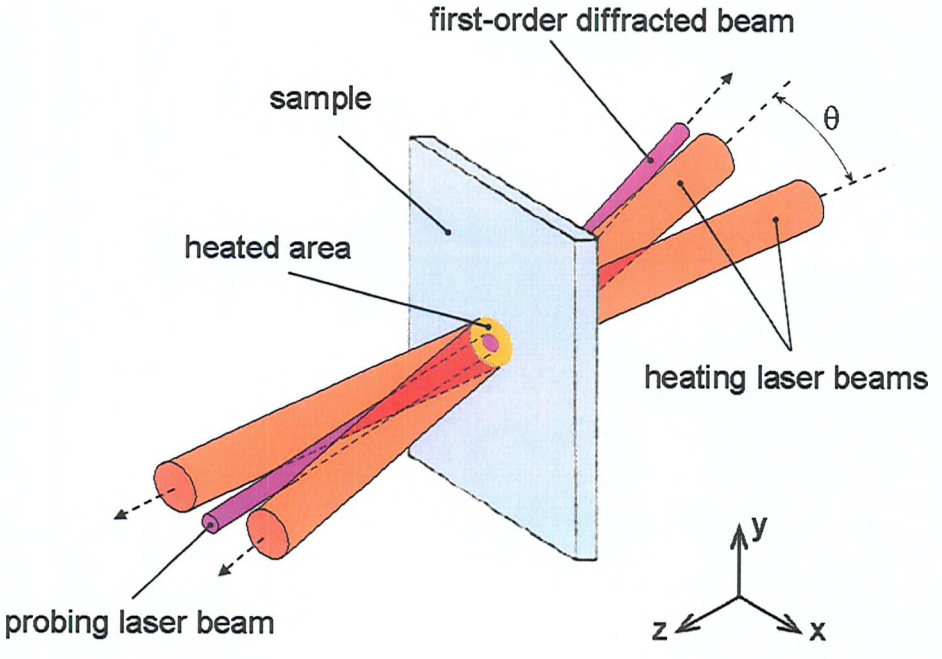

Figure 2.4 Principle of the forced Rayleigh scattering method [38]

The principle of the method is shown in Figure 2.4. A heating laser beam is divided into two beams by a splitter. If the beams are focused on the sample surface, an interference fringe pattern is formed. When the beams of light are absorbed in the material a sinusoidal temperature distribution is generated in the sample. It induces a distribution of the refractive index which acts as an optical grating for another probing laser beam with a different wavelength. If the probing laser beam is aimed at the heated area of the specimen, a diffracted beam whose intensity is proportional to the square of refractive index amplitude can be observed. If heating is terminated in a short time, an exponential decay of the excited temperature distribution takes place due to heat conduction in the specimen. Since the distribution of the refractive index also decays, the intensity of the diffracted beam relaxes with time. That means that the thermal diffusivity of the material can be deduced by measuring the decay rate of the intensity of the diffracted beam.

Details, error analysis and examples of the application of this technique can be found in [3, 38, 39]. In comparison with other methods for the measurement of the thermal diffusivity, the main features of the forced Rayleigh scattering can be summarised as a contact-free method, short time measurements (< 1ms), small temperature rise (< 0.1 K), small sample volume (< 10 mm^3) and applicability to anisotropic materials. Due to these very good characteristics the method has great potential to become reliable at high temperatures.

In 1988, Nagasaka [40] measured the thermal conductivity of molten KCl up to 1000 °C (1273 K) and claimed an accuracy of ±7 %. However, more recent measurements of the thermal conductivity of water carried out by Motosuke [41] at low temperatures by the same technique suffered very large deviations from the reference data (up to 30%) and application of suitable corrections or significant improvements of the apparatus seem to be necessary.

2.2.5. Thermoelectric Measurements

This method is based on the measurement of an increase in the resistance of a small area of an investigated sample, owing to heating by a static electric field. The principle of the technique was originally described by Borelius [42] and further investigated by Cutler [43] who suggested that 'the decay curve of the resistance of the small-area contact depends on the thermal diffusivity of the material in the vicinity of the metal contact'. He described the phenomenon by a set of equations and introduced specific conditions when the thermal diffusivity can be measured without knowing the geometry of the contact. Yurchak later designed the instrument for the measurements of the thermal conductivity of molten metals, measured the thermal conductivity of molten gallium [44] and indium [45] with a scatter of approximately ±2 % and estimated the experimental error to approximately ±4 %.

The main advantage of this technique is the small dimensions of the sample and the instrument and relative simplicity of the working equations because the geometry of the small-area contact does not have to be known. On the other hand, the precise measurements of very small resistances (10^{-7} Ω) within time are required and the 'decay curve' of the resistance can be influenced by electric capacitances which inevitably occur in every electrical circuit.

2.3. Summary

A number of available steady-state and transient methods for the measurements of the thermal conductivity of liquids have been introduced. However all the presented techniques were found inadequate for application to molten metals if the uncertainty of the thermal conductivity is required to be better than ±5 %. The steady-state techniques and the transient temperature waves cannot be used because of the presence of the conventional heat transfer within the measured sample. The laser flash technique and the transient optical techniques have also been left out because their application for molten metals is difficult mainly due to the high reflectance of the surface of the melt.

Therefore it has been decided to choose a transient technique which has been widely tested during the measurements of the thermal conductivity of fluids for last forty years and offers accuracy superior to other techniques. This contact transient technique is called Transient Hot-Wire (THW) method and is described in detail in the following chapter.

3. Transient Hot-Wire Technique

The chapter describes the most accurate technique for the measurement of the thermal conductivity of fluids currently available. The fundamentals of the method are explained and discussed in detail, the overview of derived techniques is given and, subsequently, the FE-based method used for the extraction of the thermal conductivity from a transient thermal response of the hot wire encapsulated in a substrate is introduced. The FE model and solution technique are described in detail and a step-by-step process of an inverse FE analysis is presented. The last section then discusses possible deviations of the FE solution from true values and demonstrates that the measured thermal conductivity is unique within a range of uncertainty and cannot be altered by changing other parameters in the FE model.

3.1. Background Theory

The transient hot-wire method is an absolute technique for the measurements of thermal conductivity and the instruments based on its principle are considered capable of providing the highest accuracy possible at present. The transient hot-wire technique was firstly used by Stalhane and Pyk in 1931 [46] when they empirically investigated the relationship between the time and temperature rise of the wire subjected to a heat step input to the wire. They also published the first results for the thermal conductivity of water, glycerine and castor oil. However it took an additional eighteen years until van der Held and van Drunen [47] used the method to provide the first reasonable results.

Over the years, the method was significantly upgraded and a range of measurement devices have been designed depending on the type of application e.g. hot-wire apparatus employed by Haran and Wakeham for gases [48] or Assael for electrically conductive liquids [49] and solids [50]. At the same time the fundamental theory of the transient technique was extended. At present, a number of modifications of the basic THW technique exists, such as the Hot Strip Methods [51-55], the Short Hot Wire Technique [56] or the Modified Transient Hot-Wire Technique [29].

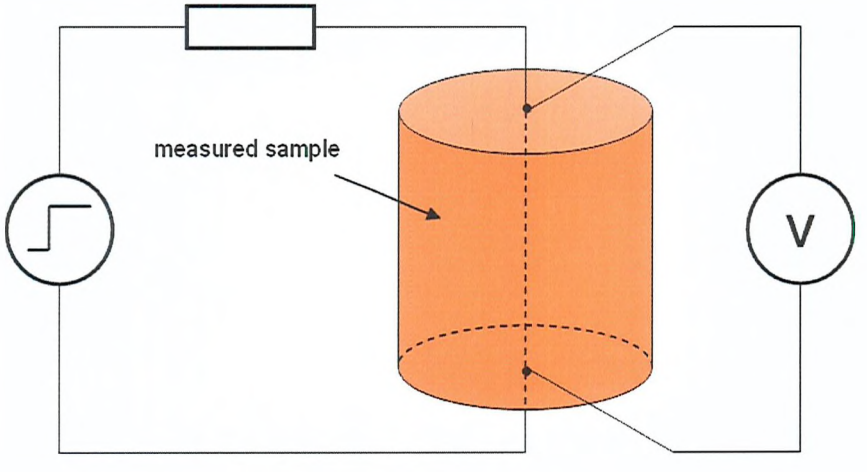

Figure 3.1 Concept of the transient hot-wire technique

The fundamental principle of the method is simple and its concept is illustrated in Figure 3.1. A step voltage is applied to the vertical 'hot wire' and the voltage along the wire is monitored in time. As the wire is heated up its resistance increases with the

temperature hence the monitored voltage also increases. From this voltage transient characteristic, the temperature change of the wire and the applied heat flux are calculated. The heat flux values are then used as an input for the mathematical model which relates the thermal conductivity of the sample to the measured temperature response.

The transient hot-wire method was chosen as the most suitable technique at the very first stages of the previous research work [8, 13]. The main reason for its employment is the fact that it offers the highest accuracy from all currently known methods. This high accuracy feature is underpinned by avoidance of the effects of convectional part of the heat transfer which inevitably occurs during measurements in the earth's gravity. A response to a heat step function is observed during just the first second from the start of the experiment and this time is small enough to ensure that the fluid movements driven by the inevitable change of density of a measured fluid are too small to influence the outcome.

All transient techniques operate under specific conditions which allow a simplification of the energy conservation equation for viscous, isotropic and incompressible fluid [3]. After those simplifications, the fundamental equation can be written as

$$\rho \cdot C_P \cdot \frac{DT}{Dt} = -\nabla \cdot \vec{Q} + \phi \tag{3-1}$$

where ρ and C_P are fluid thermal properties, $\vec{Q}$ is the heat flux vector and ϕ is the internal energy increase owing to viscous dissipations. The notation *D/Dt* represents a substantive derivative, also called conductive derivative, Lagrangian derivative or Stokes derivative, which is a derivative taken with respect to a moving coordinate system [57].

A general solution of equation (3-1) is not possible and that is why it is necessary to apply some restrictions. Firstly, it must be ensured that temperature gradients are small, so that a near-equilibrium state is maintained. Secondly, any fluid movement must be avoided and therefore $\phi = 0$ so that the substantive derivative can be changed into a partial derivative. Such simplifications make higher demands on the measurement process, because a fluid movement must be suppressed to its minimum possible value prior to the measurements of the temperature response. The previous research work [58]

also concluded that a wire must be kept in vertical position and a response should be measured within the first second after applying heat input.

The heat flux vector $\vec{Q}$ can be written in general as

$$\vec{Q} = -\lambda \cdot \nabla T + \vec{Q}_r \tag{3-2}$$

where $\vec{Q}_r$ is the heat flux arising from radiation. Although there is always some contribution from radiative transport there are specific circumstances under which it is negligible, such as low emissivity of the heater material and small temperature gradients. The influence of the radiation in the transient hot-wire technique was investigated and evaluated in detail in the previous work [13]. Thus, for an isotropic fluid with a temperature-independent thermal conductivity and with an internal heat generation, the density and heat capacity equation (3-1) can be rewritten as

$$\rho \cdot C_P \cdot \frac{\partial T}{\partial t} = \lambda \cdot \nabla^2 T + q_{gen} \tag{3-3}$$

Equation (3-3) is the basis of all transient experimental methods for the measurement of the thermal conductivity [3]. In order to derive the thermal conductivity from this equation, the second order differential equation has to be solved. In an ideal case, where the hot wire is directly immersed into the fluid and other important conditions are met, a remarkably accurate analytical solution exists.

In the ideal model, an infinitely-long, vertical, line source of heat possessing zero heat capacity and infinite thermal conductivity is immersed in an infinite isotropic fluid, with physical properties independent of temperature and in thermodynamic equilibrium with the line source at time $t = 0$. The transfer of energy from the line source, when a stepwise heat flux per unit length q is applied, is assumed to be entirely conductive (note that $q_{gen} = q/A$, where A is a cross-sectional area of the line source). The temperature rise in the fluid at a distance r from the wire, at time t is written as

$$\Delta T(r,t) = T(r,t) - T_0 \tag{3-4}$$

where T_0 is the equilibrium temperature of the fluid. With the additional condition that the thermal diffusivity a is constant, the exact solution of the fundamental transient equation (3-3) can be written as [59]

$$\Delta T(r,t) = \frac{q}{4\pi\lambda} E_1\left(\frac{r^2}{4at}\right) \tag{3-5}$$

where λ and a are the thermal properties of the measured fluid and $E_1(x)$ is the exponential integral with the expansion [60]

$$E_1(x) = \int_x^\infty \frac{e^{-y}}{y}\, dy = -\gamma - \ln x - \sum_{n=1}^{\infty} \frac{(-x)^n}{n \cdot n!} \tag{3-6}$$

Therefore the exact solution shown in equation (3-5) can be written at $r = r_0$ as

$$\Delta T(r_0,t) = \frac{q}{4\pi\lambda}\left[\ln\left(\frac{4at}{r_0^2 e^{\gamma}}\right) + \frac{r_0^2}{4at} - \frac{1}{4}\left(\frac{r_0^2}{4at}\right)^2 + \frac{1}{18}\left(\frac{r_0^2}{4at}\right)^3 + \ldots\right] \tag{3-7}$$

where r_0 is the wire radius. If the wire radius and the time are chosen such that the second and following terms on the right hand side of equation (3-7) are less than 0.01% of ΔT, the temperature rise can be written as [3]

$$\Delta T(r_0,t) = \frac{q}{4\pi\lambda} \ln\left(\frac{4at}{r_0^2 e^{\gamma}}\right) = \frac{q}{4\pi\lambda}(\ln t + C) \tag{3-8}$$

where C is a constant. Equation (3-8) is the fundamental working equation of the transient hot-wire technique. It suggests the possibility of obtaining the thermal conductivity from the slope of the line ΔT vs ln t, while thermal diffusivity may be obtained from its intercept or, more correctly, from the absolute value of ΔT at a fixed time.

Since the introduction of the THW technique, the ideal analytical solution has been used and experiments have been carried out at various conditions and configurations. A number of departures from the ideal in the transient hot-wire technique have been observed, mathematically evaluated and essential corrections introduced. The corrections are applied to the experimentally measured temperature rise using the equation

$$\Delta T(r_0,t) = \Delta T_w(t) + \sum_i \delta T_i \tag{3-9}$$

where $\Delta T_w(t)$ is the temperature rise measured experimentally and the second term on the right hand side is a sum of the applied corrections. A list of currently available corrections can be found in various sources [3, 61].

The most important correction for our type of experiment is the inclusion of hot-wire material properties into calculations. The ideal model assumes a line source of the heat flux and evaluates the temperature at a distance which equals the wire radius. The correction is defined as [61]

$$\delta T_1 = \frac{q}{4\pi\lambda}\left[\frac{r_0^2\left[(\rho C_P)_w - \rho C_P\right]}{2\lambda t}\ln\frac{4at}{r_0^2 e^{\gamma}} - \frac{r_0^2}{2at} + \frac{r_0^2}{4a_w t}\right] \tag{3-10}$$

where the subscript *w* indicates material properties of the wire material. The correction is valid if [58, 59]

$$\frac{4at}{r_0^2 e^{\gamma}} >> 1 \tag{3-11}$$

Other corrections apply to specific experimental configurations and do not contribute to the temperature rise of the wire in our experiment.

3.2. Modified Techniques

Despite the availability of various types of corrections to the ideal model, the measurement of the thermal conductivity of electrically conductive fluids at elevated temperatures still belongs among the most challenging tasks. The sample liquid has to be isolated from the hot wire and this inevitable means that the properties of the isolating layer influence the overall temperature rise of the hot wire as a function of time. At low temperatures, it is sufficient to use platinum wire coated with a thin, uniform polyester layer and to deal with the modification of the ideal model analytically [62]. Unfortunately for application at high temperatures, finding a material that can withstand temperatures greater than 375 K (100 °C) and can be coated on the wire is exceedingly difficult.

Nakamura et al [63, 64] developed an instrument, which consisted of a hot wire printed on a relatively thick alumina substrate and coated with an additional 60-μm-thick alumina layer. They employed the transient hot-wire method of comparison introduced by Takegoshi [65] and measured the thermal conductivity of several molten metals and semiconductors [66, 67]. They also investigated the influence of the convection inside the measured sample by conducting the experiments in microgravity environment [68]. However the usage of the rather simplified equations for the description of the temperature response of the complex instrument means that the accuracy of this technique cannot be reliably evaluated and large deviations from the true values are very likely.

Yamasue et al [69] have been able to obtain a layer of silica on the wire by dipping the probe into a silica slurry, and carried out measurements of molten tin and lead up to 1473 K (1200 °C). However, the imprecisely defined thickness of the silica layer and non-uniformity of the silica coating may explain the very significant departures of the measured thermal conductivity values from data published by other researchers such as Hemminger [18, 19] (steady-state method), Peralta [11] (transient technique) or Touloukian [70], Ho [71] and Mills [72] (recommended values).

Another possible solution for the high temperature isolation was suggested by Zhang et al [73]. They managed to sputter platinum wire only 8.7 mm long and 51 μm diameter with a layer of aluminium oxide (Al_2O_3) and carried out measurements of several

polymers and molten salts up to 973 K (700 °C) using the short-hot-wire technique [56]. However the accuracy of such a technique is mostly affected by heat transfer to the ends of the short hot wire.

Research teams from Imperial College London (UK), Aristotle University in Thessaloniki (Greece) and University of Lisboa (Portugal) used another approach. They encapsulated the hot wire into a high temperature co-fired ceramic, which had been mainly used for advanced applications in space and electronics research, and derived the thermal conductivity of several molten metals using a finite element analysis [8, 13]. Their work became the basis for the current research. An overview of the employed FE model and the manner of extraction of the thermal conductivity from FE model is discussed in details in the following sections.

3.3. Finite Element Analysis

All transient hot-wire methods for measuring electrical conductive fluids employ an additional layer outside of a metallic wire and such a layer usually greatly influences the thermal response of the hot wire. Therefore the ideal model together with a small analytical correction is no longer sufficient to provide an accurate description of the measurement and another means of extraction of the thermal conductivity from the measured temperature response needs to be found.

With the introduction of computational mathematical modelling during the last decade of the twentieth century, a complicated but very accurate numerical solution of the equation (3-3) became possible. The solution is based on an inverse mathematical problem where the thermal conductivity is derived from the calculated characteristic response of the sensor. Computational modelling, in particular the Finite Element Method (FEM), also allows the need for cylindrical symmetry of the instrument to be released. It is this which opens a wider range of possibilities for the construction of a suitable sensor.

3.3.1. Introduction to FEM

The FEM is not simply a modern technique as it may seem from its recent wide and popular use in almost every technical area. The FEM has been developing since the beginning of the twentieth century from Matrix Structure Analysis (MSA) [74, 75]. The very first book published about FEM dates back to 1967 [76] and since then more than five hundred books have been published about the theory and applications of FE analysis in various fields of science. A very useful online source for FE books, conference proceedings and journals can be found in [77], which may help readers to understand the background of FEM in detail.

In the previous projects, in which the THW sensor and fabrication technology were introduced [8, 13], the FE analysis was carried out using a special purpose computer program. Right at the beginning of the current research, it was decided to use one of the available commercial FE packages and therefore enhance the solution in many ways. Originally the FE programme was written in FORTRAN language. The code was able to accommodate only square finite elements and did not allow any further

improvements without re-writing the entire programme. The cross-section of the wire also could not be defined properly and a rectangular shape had to be applied instead of the real circular cross-section of the wire [8, 12, 13]. This was a major simplification and a possible source of inaccuracy in the solution, especially at very short times during the transient run. Besides this, the old model was inflexible in terms of a suitable size of the finite elements, time-stepping options, definition of material properties and post-processing of results. The switch to the FEM commercial ANSYS® software was therefore a natural step towards much higher flexibility of the employed FE analysis.

The ANSYS® software works with general physical equations which describe physical laws in many fields of science such as mechanics, thermal management, electromagnetism etc. In our case the governing equation for the thermal analysis is given as

$$\rho \cdot C_P\left(\frac{\partial T}{\partial t}+v_x\frac{\partial T}{\partial x}+v_y\frac{\partial T}{\partial y}+v_z\frac{\partial T}{\partial z}\right)=\frac{\partial}{\partial x}\left(\lambda_x\frac{\partial T}{\partial x}\right)+\frac{\partial}{\partial y}\left(\lambda_y\frac{\partial T}{\partial y}\right)+\frac{\partial}{\partial z}\left(\lambda_z\frac{\partial T}{\partial z}\right)+q_{gen} \qquad (3\text{-}12)$$

where v_x, v_y, v_z are velocities for mass transport of heat and λ_x, λ_y, λ_z are thermal conductivities in element x, y and z directions. It can be seen that the governing equations (3-3) and (3-12) are the same, assuming that the measured fluid is not in motion and the thermal conductivity is isotropic.

At the beginning of the analysis in ANSYS®, appropriate finite elements are chosen according to the model geometry (one up to three dimensional) and character of the analysis (stress, thermal, magnetic, etc.). Once the geometry and material properties are defined, the model is meshed, time options can be set and subsequently a solution is run. The details of such a general analysis process and a detailed description of ANSYS® software is given in [78]. The parameters, which have been chosen for the FE analysis in this work, are described in the sections below.

3.3.2. Comparison between an Ideal Model and FE Solution

Since the FE solution was first implemented in the accurate measurements of the thermophysical properties, there has been a discussion whether such measurements can provide reliable values. It has been also shown in the section above that the FE analysis has undergone significant changes since it was used for the first time with THW measurements and it was essential to verify the new FE solution in every possible way. Therefore significant attention has been given to justification of the modelling technique and applied parameters.

A simple FE model had been constructed to allow comparison with the analytical solution of the transient hot-wire equation (3-3). The test model has a circular cross-section of the hot wire and the material properties of pure platinum and alumina are used. There are a few key parameters that can be set for the FE analysis. The two most important are the density of the mesh of the model and the time stepping of the transient run.

The mesh density has a great influence on the solution at very short times of the transient run. Significant departures from the true transient response can be seen up to several hundreds microseconds from the start depending on the coarseness of the mesh. A meshed model, which was used for the comparison to the analytical solution, is shown in Figure 3.2 together with a description of available thermal finite elements in ANSYS® analysis.

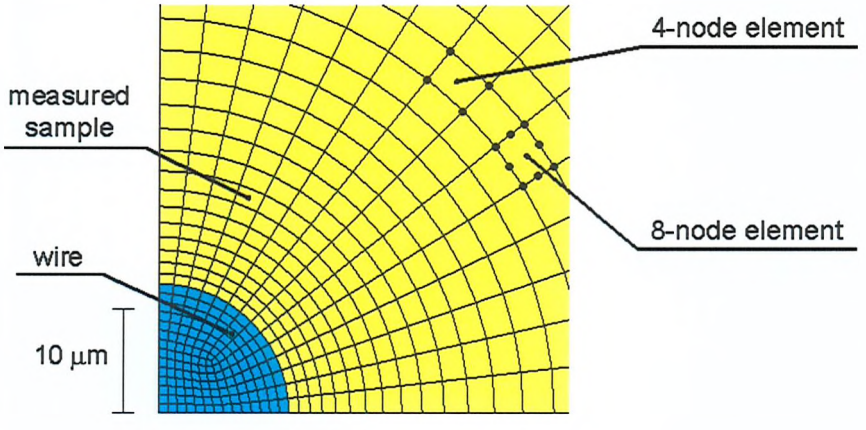

Figure 3.2 Mesh of the model used for comparison to analytical solution

The model of the wire surrounded by a measured sample is cylindrically symmetric and the symmetry allows using finer mesh and less computational resources. In Figure 3.2, the blue colour of elements illustrates the platinum hot wire with 25 μm diameter while the yellow colour is used for the test material. The dimensions of the test material are virtually unlimited as the temperature increase at the edges at the end of the first second is equal to zero. It means that the borders of the test material will not affect the increase in temperature of the hot wire in any way even if they are finite.

The second parameter, the time stepping, has a significant influence over the entire time of the transient run. In principle, only one time step could be applied from the start of the solution to the end. However, if the time increment is set to 1 μs and is not changed during the analysis, the number of calculated time points will be 10^6, and the computational time and resources needed for storing the results would be unfeasibly high.

Therefore, a number of tests were carried out to find an optimal time stepping for the solution of the transient analysis. Several values of the time steps were tested and a summary of them is given in Table 3.I. The term 'step' refers to one decade of the time spectrum, i.e. if the first step is 1 μs then the following step is 10 μs (one decade) and this step is divided into a number of sub-steps according to the time increment.

Table 3.I Summary of tested time-stepping for the transient run

	Previous Works	*Timestep10*	*Timestep100*	*Timestep200*	*Timestep500*
Start of the transient run	1μs	0.1μs	0.1μs	0.5μs	0.2μs
First step	100μs	1μs	10μs	100μs	100μs
Increment within each step	step/100	step/10	step/100	step/200	step/500
Number of steps	5	7	6	5	5
Total number of substeps	460	64	550	920	2300

In the figures below, the comparison among different time steps is presented. The FE solution is subtracted from the temperature rise, ΔT, calculated from the analytic solution for one typical set of conditions. The values are plotted as a function of time and should be found to be close to zero. The comparison with the results obtained from previous work [13] is not included, because the geometry of this model was different (rectangular cross-section of the wire) and the algorithm of that model is no longer used.

The analytical solution is calculated using the first three terms of the expansion in equation (3-7) and in addition, the correction from equation (3-10) is applied. It was mentioned above in section *3.1.Background Theory*, that the correction is not valid throughout the whole time region, see equation (3-11). That is why the accuracy of the analytical solution is not acceptable for validation purposes at very short times, i.e. below 10ms in our case, and the graphs below show only time regions from 1ms to 1s. However, this does not affect the accuracy of the FE model at shorter times and it is expected that an absolute deviation of the FE model from the reality is within the same ranges as for the validated time regions.

In both ideal and FE solution, the same step heat flux input is applied. The analytical solution is calculating the temperature rise at distance $r = r_0$ from the middle of the wire and for an optimal comparison, the values from the FE solution are also taken at this position.

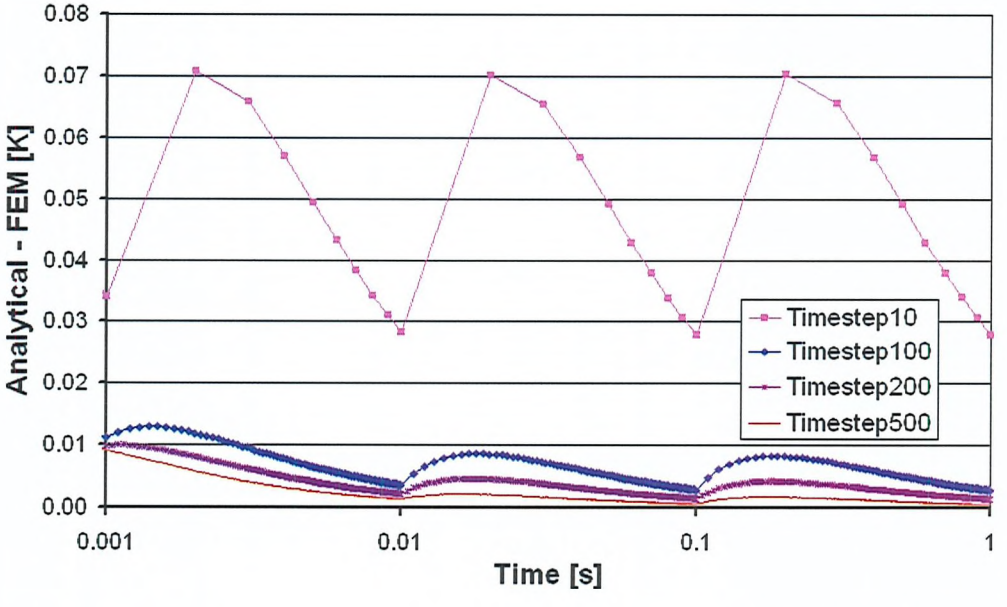

Figure 3.3 Comparison of various time steps applied to the model

The overall temperature rise of the wire within the first second is approximately 6.5 K. It can be seen immediately from Figure 3.3, that the values generated by the FEM using Timestep10 lead to significant (~1%) departures of the temperature rises given by the FE model and the analytical solution. When the finer time steps are applied, the departures decrease. A better comparison between finer time steps can be seen in Figure 3.4.

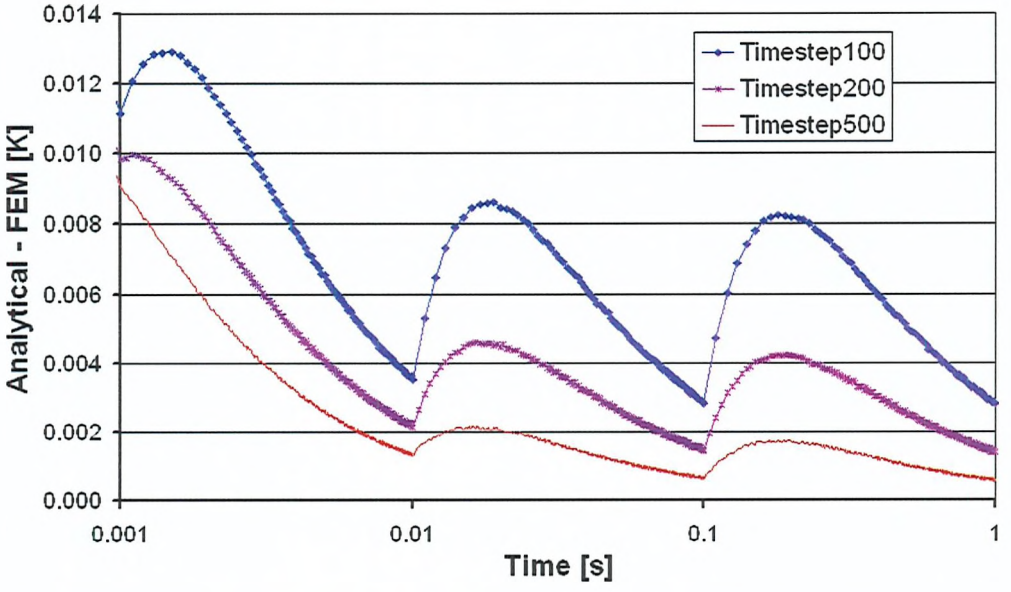

Figure 3.4 A detailed comparison of applicable time steps

It can be anticipated from the figures that when the number of time steps increases, the solution becomes more accurate and converges to the analytical solution more quickly. This fact itself is one of the validations of the model. Next, the absolute difference between FE solution and analytical results is of order of 10^{-3} K in the time region where the analytical solution is remarkably accurate. The maximum absolute deviation from an ideal model is not greater than 9 mK for Timestep100 throughout the transient run and it can be stated that the Timestep100 configuration is sufficient enough to be used for a comparison with an experimental measured response from the sensor, because the accuracy of experimental measurement of the response is not higher.

3.3.3. FE Model of the Encapsulated Hot Wire

It has been verified that the FEM can be used for measurements of the thermal properties of the material that is surrounding the hot wire. In order to measure the thermal properties of electrically conductive liquids, a new layer of the measured liquid is introduced into the FE model, which results in a layered wire-isolation-fluid structure as shown in Figure 3.5.

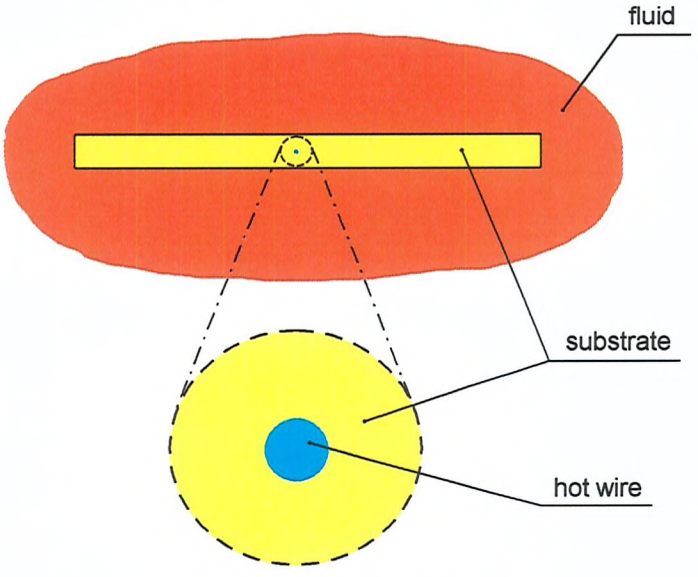

Figure 3.5 Cross-section of the structure where the hot wire is isolated from the fluid by a rigid substrate

When a heat flux is applied on the hot wire, the heat wave travels from the wire to an isolating material (substrate) and subsequently reaches the measured sample. This results in a certain temperature rise of the hot wire which can be divided into several time regions. Every time region then reflects the nature of the heat transfer in the material and can be used to evaluate its thermal properties. In other words, as the heat wave transfers through the structure of material which surrounds the hot wire, the material, which is in direct contact with the hot wire, affects the temperature rise at very short times and its thermal properties governs the temperature rise as long as the heat wave does not reach another material. The heat wave then propagates further and other materials start to influence the temperature rise as well. A typical example of such behaviour is illustrated in Figure 3.6.

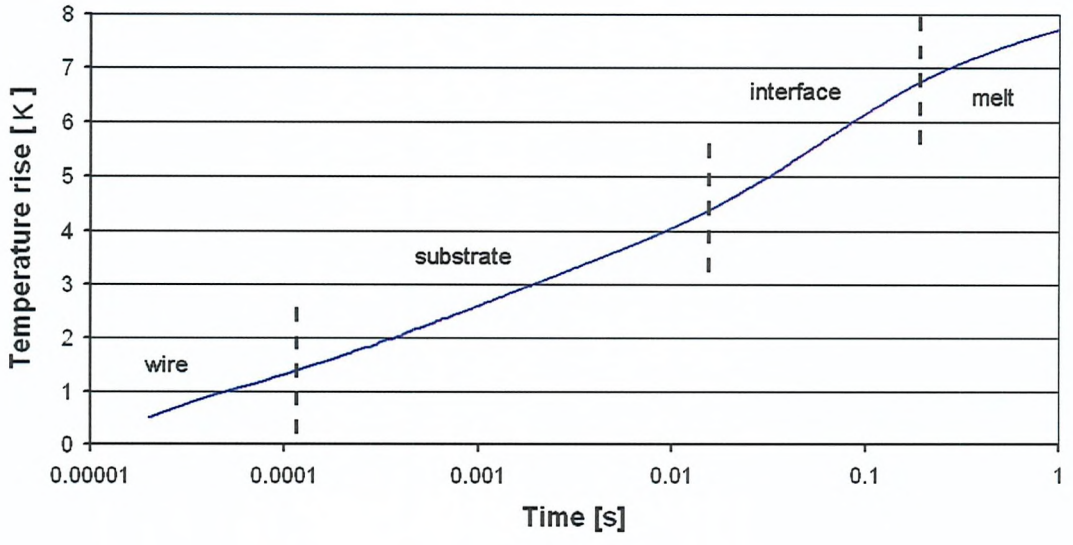

Figure 3.6 Example of the temperature rise of the hot wire

The parts of the transient response are affected by the following properties:

- Wire – hot-wire diameter, thermal properties of the hot wire (λ_w, $\rho_w \cdot C_{Pw}$) and wire-substrate interface coefficient (f_{ws})
- Substrate – wire + thermal properties of the substrate (λ_s, $\rho_s \cdot C_{Ps}$)
- Interface – wire + substrate + substrate thickness + substrate-melt interface coefficient (f_{sm})
- Melt – wire + substrate + interface + thermal properties of the melt (λ_m, $\rho_m \cdot C_{Pm}$)

The geometrical and thermal properties of the hot-wire instrument are usually well known unlike all other parameters, which need to be extracted from the measured temperature rise. Within each region shown in Figure 3.6, in very trivial terms, the thermal conductivity of a material determines the rate of the temperature increase while the product $\rho \cdot C_P$ governs the total magnitude of the response. Therefore the analysis of the transient temperature response of the hot wire allows measurements of the thermal properties of both the substrate and the fluid.

It was found that interface layers between wire, substrate and melt materials need to be introduced in order to describe the behaviour of the hot-wire temperature rise [79]. The interface layers characterize a temperature discontinuity which inevitably occurs at every junction between two solid materials when a temperature gradient is applied. This

discontinuity occurs at a molecular level. The FE model uses very thin layers of a material with low thermal conductivity to describe such temperature discontinuities and their effect on the measured transient response of the wire. The schematic diagram of the FE model with both interfaces and the thermal parameters of all layers are shown in Figure 3.7.

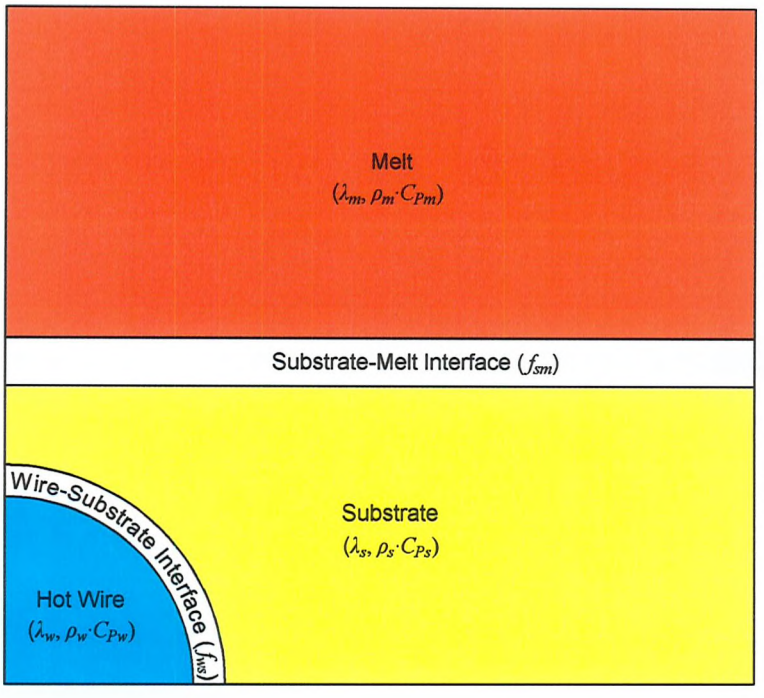

Figure 3.7 Schematics of the FE model geometry

The FE model of the layered structure is constructed as a 2-D model of the sensor cross-section with the assumption that the hot-wire diameter is the same along its whole length. The symmetrical cross-section allows further simplification of the modelled geometry, because the thermal wave travels from the centre of the circular hot wire to the rectangular substrate. That is why only one quarter of the cross-section of the hot-wire sensor can be used for the entire analysis without any impact on the overall accuracy.

It has been observed that the thickness of the interface layer between the hot wire and the substrate is temperature dependent because of the different coefficients of thermal expansions (CTE) of platinum and substrate material. On the other hand, the thicker substrate-melt interface does not show this kind of behaviour but produces a greater temperature rise. It was proved in the past that the interfaces can be modelled using a thin layer of air [79] although it is more likely that the interfaces are created by a layer

of various oxides (surface soil, metal oxides). That is why the interface coefficients, f_{ws} and f_{sm}, have been introduced above. They refer to ratios between interface thermal conductivity, λ_i, and interface thickness, d. The ratio λ_i/d defines the only essential thermal property because the interface thickness is so thin that its density and specific heat capacity do not contribute to its thermal behaviour.

During the FE analysis, the geometrical model is meshed in order to create a net of finite elements and compile a matrix which is subsequently solved. The net (mesh) structure needs to be very well controlled. The geometry of the sensor consists of a combination of very thin interfaces and relatively thick substrate and melt. A suitable balance has to be found in order to minimize errors in calculations which usually occur when elements have very disproportional length/height ratio. Ideally the length and the height of the element should be the same. Unfortunately this is not feasible especially for interface elements because their height (interface thickness) is too small in comparison with the dimension of the smallest element of the hot wire as it is shown in Figure 3.8.

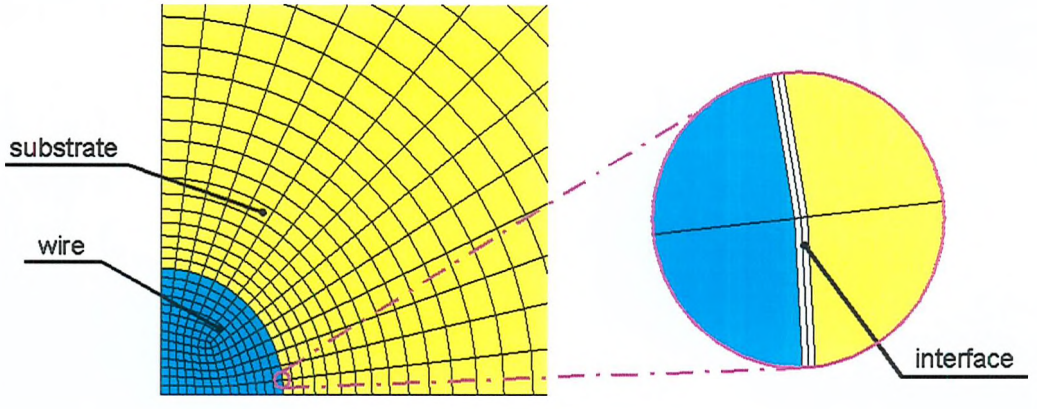

Figure 3.8 Meshed hot wire and detail view of the wire-substrate interface

The ANSYS® software recommends a maximum element length/height ratio of between 0.05 and 20, stating that further disproportion in the element dimensions may introduce errors in results. However the ratio can be up to 1:2000 for the wire-substrate interface and up to 1:500 for the substrate-melt interface. These values are much higher than the recommendations and that is why their use must be verified. The validation has been carried out by replacing the simple interface elements with more complicated ANSYS® thermal contact elements where a thickness of the gap does not have to be defined and

only the thermal conductivity of the contact is an input parameter. The final thermal conductivity of the measured fluid was identical for both analyses and therefore it has been decided to use the simpler and quicker analysis with the interface elements.

Besides the requirements for the length/height ratio, the mesh is also required to be denser at areas where a higher temperature gradient is expected, because it minimizes propagation of small calculation errors to other elements. In our case, the hot wire is the only source of the heat in the FE model and that is why the density of the elements is much higher in the hot-wire region than at the edge of the melt. A detailed view of the meshed wire with wire-substrate interface is shown in Figure 3.8, the substrate mesh with substrate-melt interface can be seen in Figure 3.9 and the overall FE meshed model is illustrated in Figure 3.10.

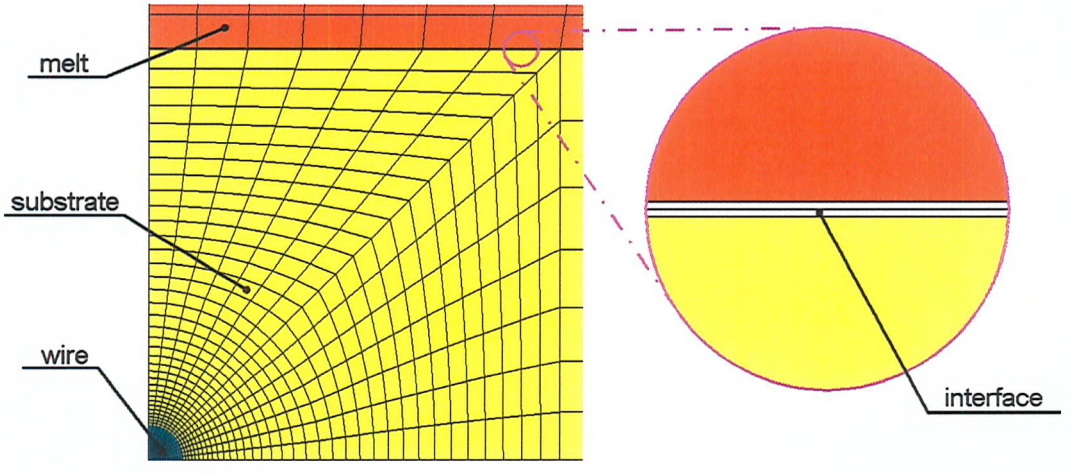

Figure 3.9 Meshed substrate in the area near the hot wire plus a detail view of the substrate-melt interface

Altogether the presented FE model consists of 2966 elements. The type of elements can be chosen from the available set of the thermal elements in the ANSYS® element library. The analysis does not require the use of 3-D elements and also elements for other types of analyses (thermo-mechanical, magnetic or electrical) can be ignored. Therefore the thermal elements PLANE55 (4-node) and PLANE77 (8-node) are found to be adequate for the FE model. The difference between 4-node and 8-node elements is illustrated in Figure 3.2.

More nodes in the model, i.e. when element PLANE77 is used, usually lead to a more accurate solution. On the other hand, the total number of nodes and respectively

elements cannot be set too high because it would significantly affect the overall computation time. The matrix, which contains all the nodes, has to be calculated at every time point during the transient run. The time analysis in the section *3.3.2. Comparison between an Ideal Model and FE Solution* showed that the number of time steps per decade must be at least 100. This means that a minimum of 550 calculations of the matrix need to be carried out for the analysis from 1μs to 1s. The solution of the model presented above with the finite elements PLANE55 (quicker solution) can be obtained approximately within 10 minutes, using a machine with Pentium IV, 3.2 GHz, 512 MB RAM and the size of the ANSYS result file is approximately 1GB. Therefore a suitable structure and density of the mesh had to be considered also according to available time and computational resources.

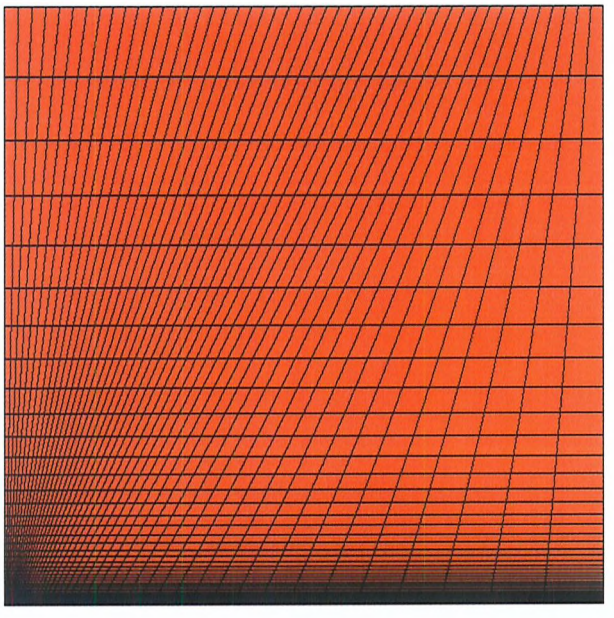

Figure 3.10 Full view of the 2D meshed model

3.3.4. Solution - Transient Analysis

Before the solution of the FE model can be carried out, the initial and boundary conditions (in ANSYS® commonly called 'loads') have to be defined. In our case, the only thermal load in the model is the heat generation within the platinum wire. The calculated heat flux is divided by the number of nodes and applied directly as a heat generation at every node within the hot wire. Several trial transient analyses proved that a higher density of nodes within the hot-wire cross-section leads to a significantly more accurate solution at very short times.

The solution of the FE model is carried out by an ANSYS® in-built Sparse Direct Solver [78]. This is a default solver which is recommended when robustness and solution speed are required and also for nonlinear analyses. The Sparse Direct Solver is also suitable for ill-conditioned matrices, such as poorly shaped elements. At first, the solver needs to be set according to the analysis requirements because the ANSYS® solver uses a number of parameters to adjust and tune the solution and format output files.

Probably the most important parameter of the solver for the transient analysis is the time stepping. The time stepping has been closely investigated and the results have already been partially presented in the section *3.3.2.Comparison between an Ideal Model and FE Solution*. However, it has been found that the modelled response suffers from 'periodical' downgrade of the results accuracy. Figure 3.3 and Figure 3.4 show that at the beginning of every time decade the deviation from the ideal model sharply increases and later returns to its previous values. This phenomenon repeats every decade and may have significant effect on the thermal conductivity measurements especially when a large heat flux is applied on the hot wire. Differences presented in Figure 3.4 were calculated for a total temperature rise of 6.5 K.

The problem was investigated and discussed at the international conference EuroSimE 2005 [80] leading to significant changes in the whole temperature rise analysis. The work published by Palacín et al [81] suggests use of logarithmic time stepping, so-called 'log-spaced time steps'. Every time decade is divided into specific time regions which are equally distributed on the logarithmic time axis. The equation for logarithmic time steps can be written as

$$\log t_{\log} = \frac{i}{N} + \log t_{\text{start}} \tag{3-13}$$

where t_{start} is the time at the beginning of the decade, i is a substep number, N is the total number of substeps within the decade and t_{log} is an adequate time for which the solution is calculated.

This log-spaced time stepping has been applied in our transient analysis in ANSYS® and a direct comparison of the ideal model, linear spaced (original) and the newly introduced log-spaced time steps for one hundred substeps per decade is given in Figure 3.11. It can be seen that the new log-spaced time steps result in monotonically varying accuracy throughout the whole response and the absolute deviation does not affect the slope of the temperature rise which is the most important feature for the THW thermal conductivity measurements.

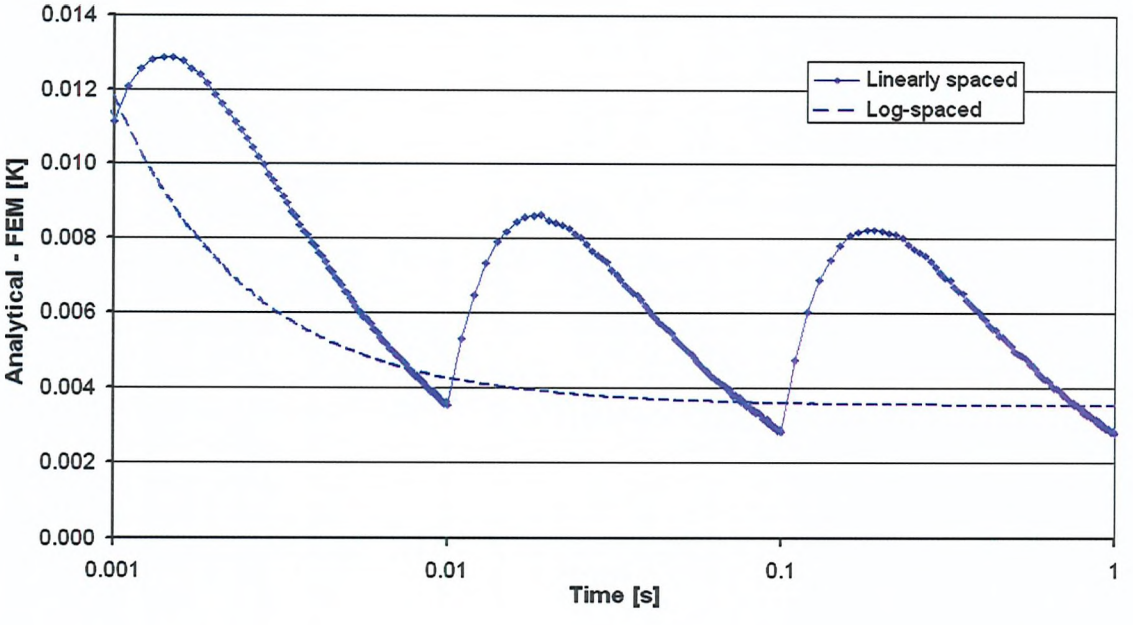

Figure 3.11 Absolute differences between ideal model and different time stepping

3.3.5. Post-Processing

During the solution of the large matrix equations in ANSYS®, raw output results are stored in large data files (typically more than 1GB for the FE model presented above). Required results then have to be read from the file and prepared for a comparison with experimental values, i.e. post-processed. From all the output data, only the hot-wire temperature at every analysed time point is of interest. It can be seen in Figure 3.12 that the temperature is not uniform across the whole wire cross-section because the wire has a finite thermal conductivity. The figure is acquired from ANSYS® and represents the thermal distribution within the platinum hot wire encapsulated in the substrate with the thermal conductivity of 10.2 $W \cdot m^{-1} \cdot K^{-1}$ after the heat flux of 55 $W \cdot m^{-1}$ was applied for 1 s.

Because of the non-uniform thermal distribution, the overall hot-wire temperature at a specified time point is taken as an arithmetic average of the temperatures at all nodes, which shape the hot wire. The array of time and average temperature is then stored into a text file together with the geometrical and thermal parameters of the FE model. Such a simple text file (size about 12 KB) is the final output of the analysis and it can be subsequently processed in any available spreadsheet program and archived without extreme requirements for the data storage.

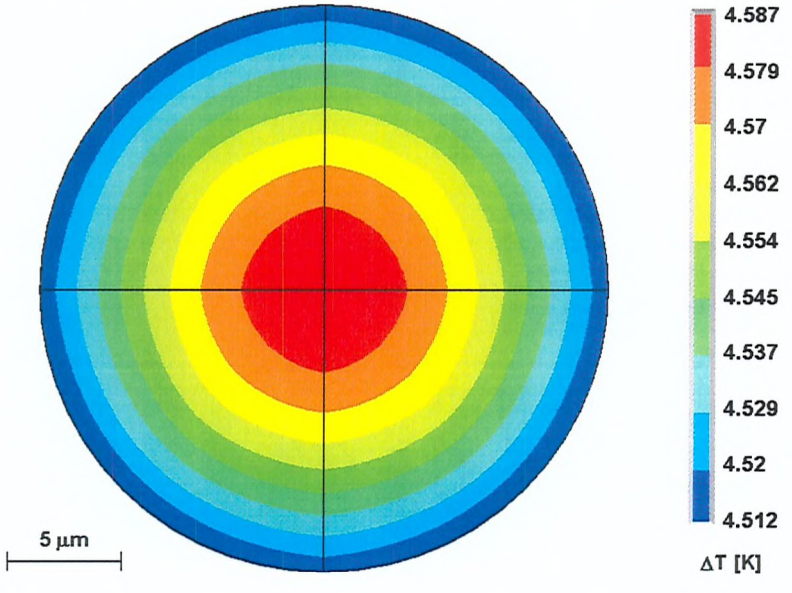

Figure 3.12 Typical modelled temperature distribution within the hot wire

3.3.6. Material Properties Measurements

In order to derive all the unknown properties of the materials of the wire/substrate/melt system, the calculated temperature rise has to be matched to the values observed experimentally by means of iterative adjustments. At the beginning of the inverse analysis, the thermal properties of materials, which influence the temperature rise at very short times, are adjusted and results observed. The thermal properties of the hot wire are well known and that is why only changes of wire-substrate interface (f_{ws}) and substrate thermal properties (λ_s, $\rho_s \cdot C_{Ps}$) influence the shape of the transient curve. Once a match between experiment and model is satisfactory, i.e. typically ±0.01 K as it is shown in Figure 3.13, the two following time regions (substrate-melt interface and melt) can be also analysed.

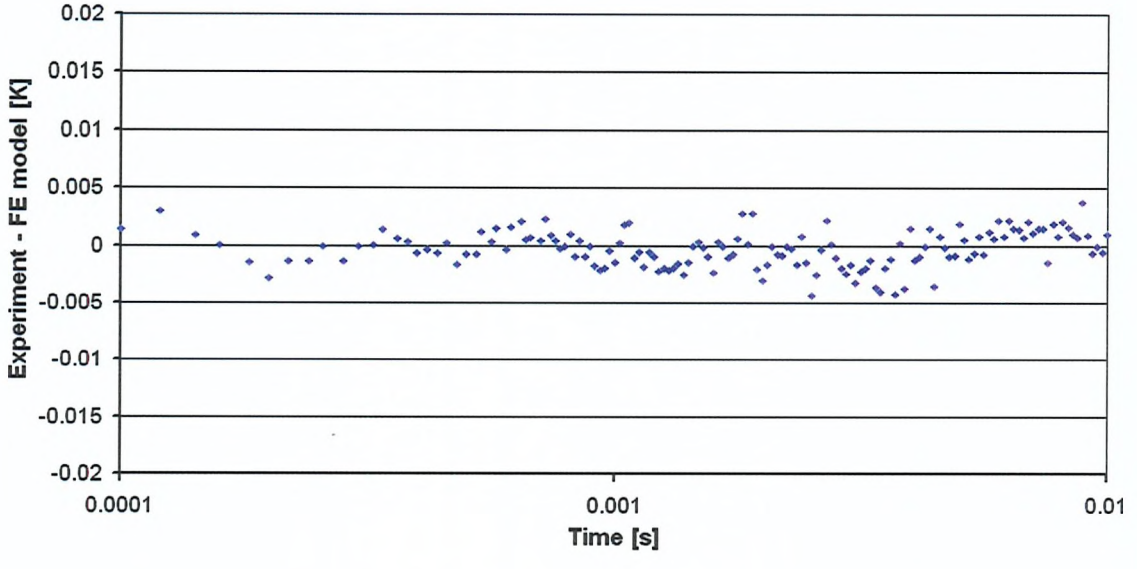

Figure 3.13 Typical comparison between FE model and experiment in the time regions where the substrate properties affect the nature of the hot-wire temperature rise

The substrate-melt interface properties have a significant effect on the transient response from the moment when the heat wave leaves the substrate material (about 0.01 s) up to about 0.1 s when the thermal properties of the melt become a major shaping factor. Again the properties of the interface and the melt are adjusted as long as the deviation from the experimentally measured temperature rise is more than ±0.01 K.

A typical overall comparison between experimental and modelled hot-wire behaviour is presented in Figure 3.14.

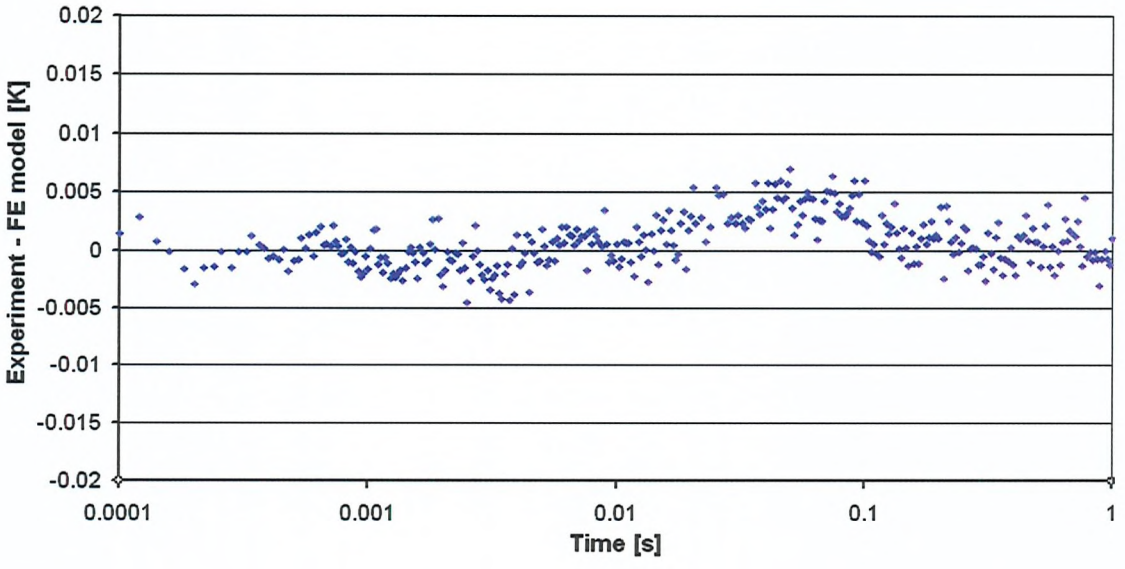

Figure 3.14 Comparison between experiment and FE model in all time regions of the measured hot-wire temperature rise

Once a satisfactory match is obtained for one measured response at a certain temperature, the identical model settings are applied to several other thermal responses measured at the same temperature. These thermal responses should be obtained at the same temperature but with different heat input into the hot wire. In other words, various temperature rises from 4 K up to 10 K should be analysed using the same settings of the FE model. If significant differences occur between responses, it suggests that either the model does not represent the actual experimental circumstance or the measured responses are not repeatable and the experiment procedures have to be checked for possible errors.

3.4. Discussion

It has been shown above that finite element description can provide a very close matching (±0.01 K) with the experimentally measured values of the temperature rise of the wire embedded in a substrate and immersed in a molten material. It has also been presented that certain material properties influence the transient hot-wire response at certain times. This section further discusses the behaviour of the modelled response and evaluates the overall accuracy of the measurement of the thermal conductivity.

In order to evaluate the accuracy of the model, the exact geometry of the hot wire instrument has to be defined. A typical model is constructed from a wire with a radius 12.5 μm, a substrate with overall thickness of 580 μm and width 30 mm, and a melt placed around the substrate extending up to 15 mm from the hot wire in the y-axis direction, i.e. a quarter of the modelled sensor cross-section has dimensions 15 mm × 15 mm. Table 3.II then lists the thermal properties of the materials specified by suppliers for platinum (Goodfellow) and alumina (Coorstek), the previously published data for molten tin [71] and interface coefficients [13].

Table 3.II Material properties of the model used for evaluation of the sensitivity

Model section	$\lambda\ [W{\cdot}m^{-1}{\cdot}K^{-1}]$	$\rho{\cdot}C_P\ [J{\cdot}m^{-3}{\cdot}K^{-1}]$	$f\ [W{\cdot}m^{-2}{\cdot}K^{-1}]$
Hot Wire (Pt)	70.35	2.855E+06	---
Wire-Substrate Interface	---	---	2.0E+07
Substrate (Al_2O_3 @ 250°C)	15	3.682E+06	---
Substrate-Melt Interface	---	---	7.0E+04
Melt (Sn @ 250°C)	30	1.684E+06	---

Equation (3-7), which is the analytical solution of the fundamental transient hot-wire equation (3-3), shows that the accuracy of the derived thermal conductivity of the material, which surrounds the hot wire, depends on the accuracy of the measured heat flux q, i.e. if the heat flux is measured with an uncertainty of ±1 %, the uncertainty of the derived thermal conductivity must be greater than ±1 %.

However not all the parameters of the FE solution can be assessed using analytical methods. That is why the solution of the typical model is evaluated and subsequently one of the geometrical or material properties is altered and the model solved again. The

two responses are then compared and the observed differences help to define the overall uncertainty of the measured thermal properties.

Equation (3-7) also suggests that small changes of the radius of the hot wire have very little influence on the derived thermal conductivity of the material around the wire. Figure 3.15 illustrates the magnitude of these changes and proves that only the offset of the temperature response changed, and the slope of the curve remained the same in the last three time decades of the temperature response. Similar behaviour has been observed for the coefficient of the wire-substrate interface and it is also shown in Figure 3.15.

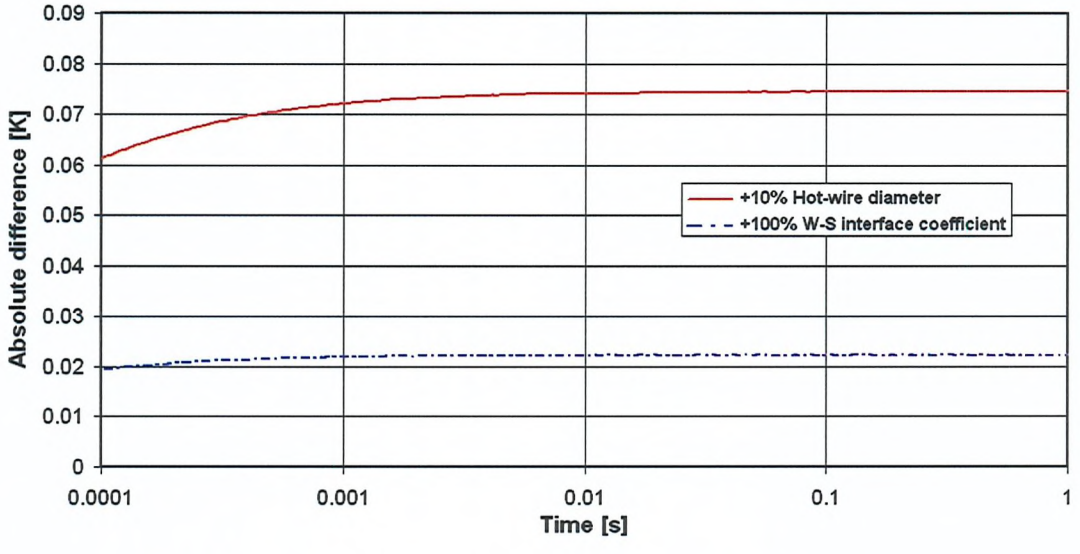

Figure 3.15 Absolute comparison between the typical model and model with altered hot-wire diameter and wire-substrate interface coefficient

Unlike the wire properties, an alteration of the substrate thermal parameters imposes significantly greater differences on all time regions of the temperature rise of the hot wire as can be seen in Figure 3.16. However the nature of such differences is very specific so that they can be identified. The most important feature of an inadequately set product of density and specific heat capacity is a peak which occurs in the time decade from 0.01 s to 0.1 s. This peak is unique and cannot be suppressed by any change of parameters other than density or specific heat. The only parameter which also imposes a peak in the same time decade is inappropriately measured thickness of the substrate. However the thickness of the substrate can be measured with a maximum uncertainty of ±10 μm, i.e. ±1.7 %, and therefore the product of density and heat capacity of the substrate can be also derived with a corresponding accuracy.

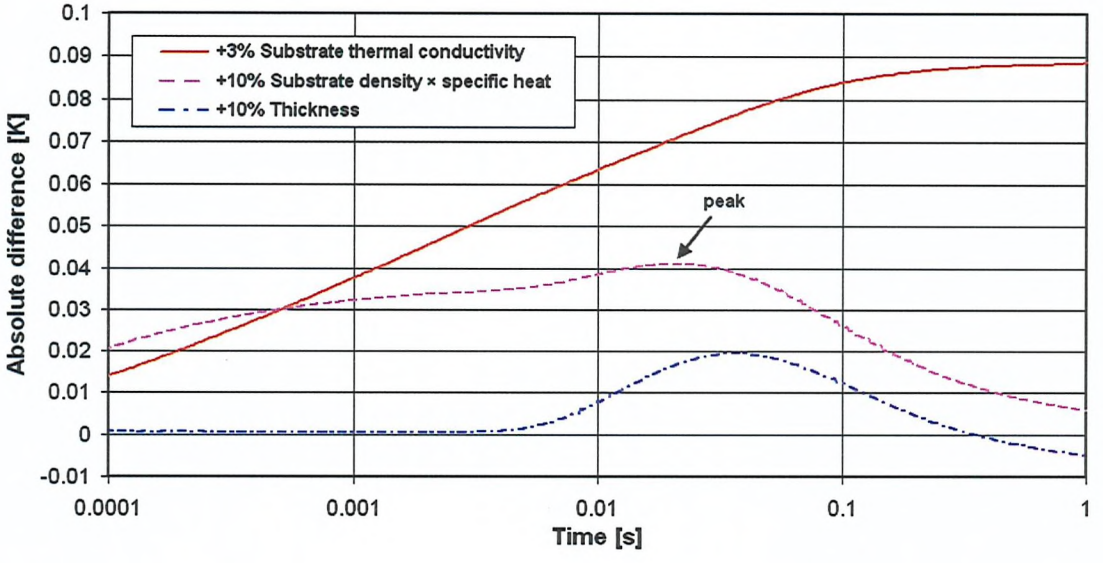

Figure 3.16 Absolute comparison between the typical model and model with altered parameters of the substrate

It can be seen in Figure 3.17 that the substrate-melt interface coefficient is a major parameter for fitting the slope of the temperature rise in the decade from 0.01 s to 0.1 s. The thermal conductivity of the melt then plays the most significant role in the last time decade from 0.1 s to 1 s, where the influence of the thickness of the interface layer is very small.

Nevertheless the product of density and specific heat capacity of the melt also partly influences the temperature rise and it imposes the main error on the slope of the curve within the last time decade. It can be deduced from Figure 3.17 that an uncertainty of ±10 % in the product $\rho \cdot C_P$ of the measured fluid results in about ±1.6 % change in the slope of the temperature rise. The heat capacity data for molten metals varies rather significantly or is given with wide uncertainty regions as it is presented in chapter *5.Results*. However even heat capacity values with large deviation of 10 % can be used in our technique to extract the thermal conductivity with an accuracy better than 2 %.

It has been stated above that a change of the heat flux applied on the hot wire results in the same relative change of the derived thermal conductivity of the material surrounding the wire. The influence of the change of the applied heat flux has also been investigated for our 'sandwich' structure and the results are illustrated in Figure 3.18

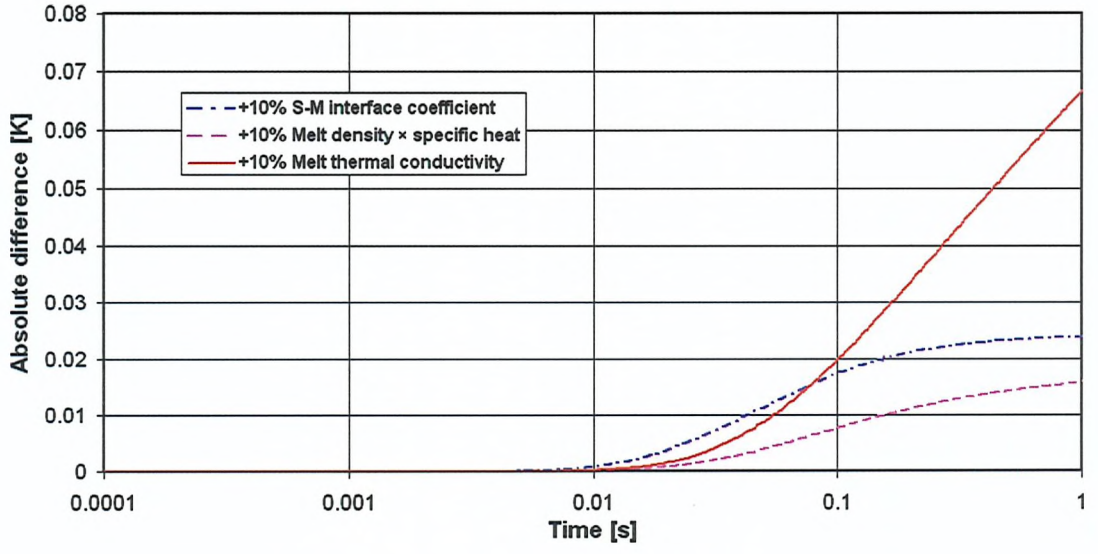

Figure 3.17 Absolute comparison between the typical model and model with altered parameters of the melt and the substrate-melt interface

It can be observed in Figure 3.18 that the FE model follows the ideal model and a -2 % change of the applied heat flux has the same effect on the temperature rise from 0.1 ms to 10 ms as a -2 % change of the thermal conductivity of the substrate. However due to the geometry of the instrument, the influence on the measured thermal conductivity of the melt is not as high and is about -1.3 %.

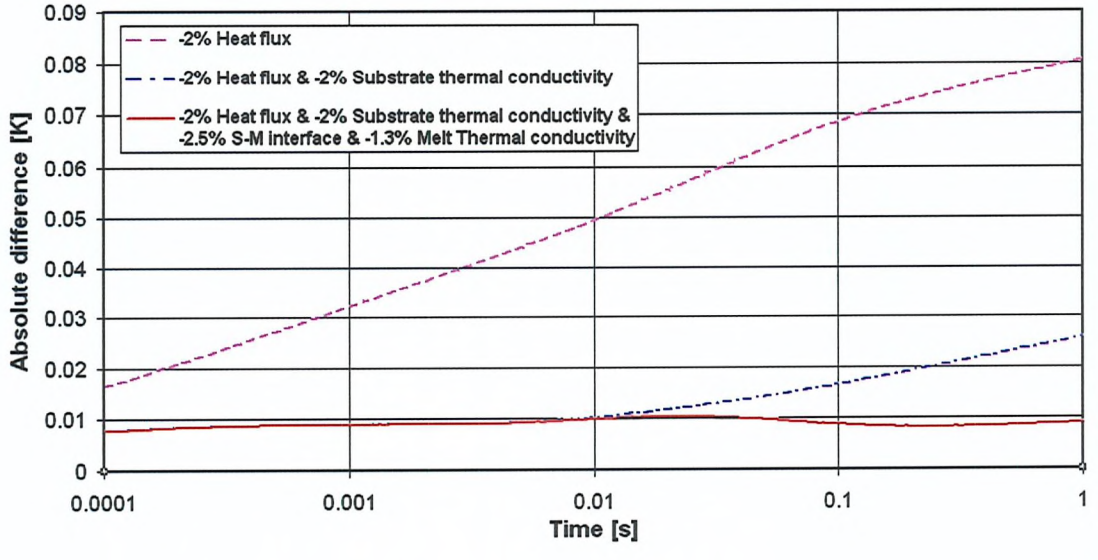

Figure 3.18 The analysis of applied heat flux and subsequent influence on the measured thermal conductivity

4. Experimental Arrangements

The chapter describes the design, fabrication and calibration of the transient hot-wire sensor. Subsequently the experimental set-up is introduced, explained in detail and the accuracy of the various measuring devices is examined. The procedures for the measurements of temperature, resistance and voltage are presented. It is then shown how the experimentally acquired voltage response from the sensor is processed in order to derive the temperature rise of the hot wire and the applied heat flux. The overall analysis of the experiment is given and the uncertainty in the results estimated.

4.1. Sensor Design

The design of the THW sensor is influenced by three major factors. Firstly, the theory behind the transient hot-wire technique requires a vertical, infinite line source of the heat flux (refer to section *3.1.Background Theory*). The line source can be substituted by a wire of a small diameter if an appropriate correction is applied. However the wire is not infinite and cannot even serve as a part of an infinitely long wire because the ends of the wire always encounter certain heat losses to the leads of the hot wire. This phenomenon has been experimentally cancelled by measurements of the temperature rise of the two wires with identical cross-sectional area but different length. The fundamental idea is that if the same heat flux is applied on the two wires, the subtraction of their resistances gives a resistance of a finite part of an infinite hot wire. The principle is graphically explained in Figure 4.1. The two-wire configuration is essential for accurate thermal conductivity measurements and has to be therefore included in the design of the THW sensor.

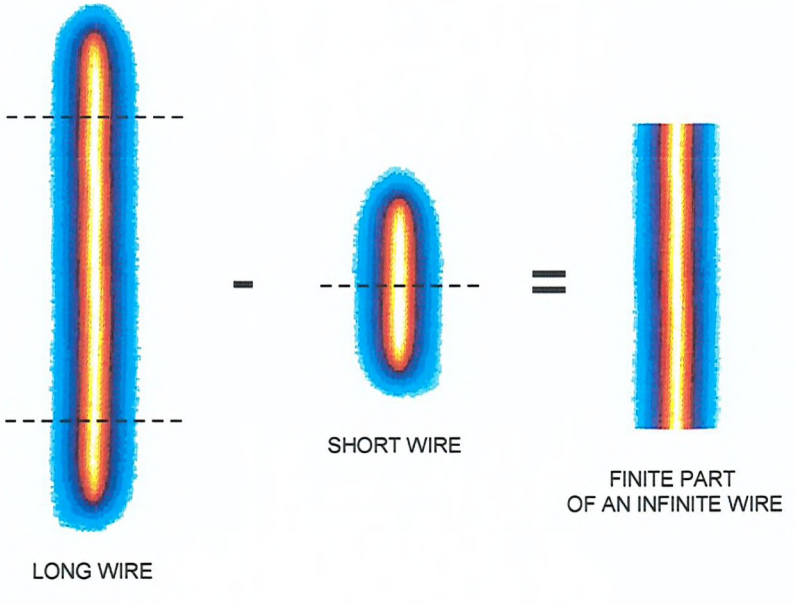

Figure 4.1 Principle of cancellation of the heat losses at the ends of the finite hot wire

Secondly the design depends on availability of appropriate fabrication technologies. The fundamental idea is that the hot wire and all connection leads are electrically insulated from the measured fluid by a substrate, which is required to be uniform, homogeneous and symmetrically placed around the wire. The substrate should also provide a decent mechanical support for the fragile hot wire and is required to sustain highly chemically aggressive environment and elevated temperatures at the same time. Figure 3.5 suggests an acceptable configuration where the hot wire is placed in the middle of a rigid substrate, for which a theoretical model was developed in chapter *3.Transient Hot-Wire Technique*.

These requirements had been challenged during the very first stages of previous research [8, 13] and the ceramic technology called High Temperature Co-fired Ceramics (HTCC) was evaluated as the most suitable fabrication technique. HTCC is a specific type of ceramic which allows electrically conductive paths to be buried inside a rigid alumina substrate so that they are electrically, chemically and optically isolated from the ambient environment. The HTCC material is usually available in the form of flexible sheet which is commonly called 'alumina tape'. The printed conductive pattern is then clamped in-between two alumina tapes and the whole HTCC module is sintered at high temperatures. The HTCC is a planar technology and has been mainly used for high-performance electronics for the space and military applications.

And finally, the geometrical design of the THW sensor is also limited by dimensional constraints of available equipment such as inner dimensions of a furnace chamber used for the thermal conductivity measurements or dimensions of the crucible with the measured fluid. In our case, the crucible is cylindrical with inner diameter of 60 mm and height of 100 mm.

4.1.1. Original Sensor Design

The original sensor design was created during a European project in 1990's [8] and it is shown in Figure 4.2. The sensor has altogether five measuring terminals. Terminals A and C are used to supply the heating electric current to the hot wire while the terminals B, D and E are used for voltage or 4-wire resistance measurements. The measuring terminals are created by printed conductive paths and foils. A detail description of the step-by-step fabrication process and used materials is given in section *4.2.Fabrication Process*.

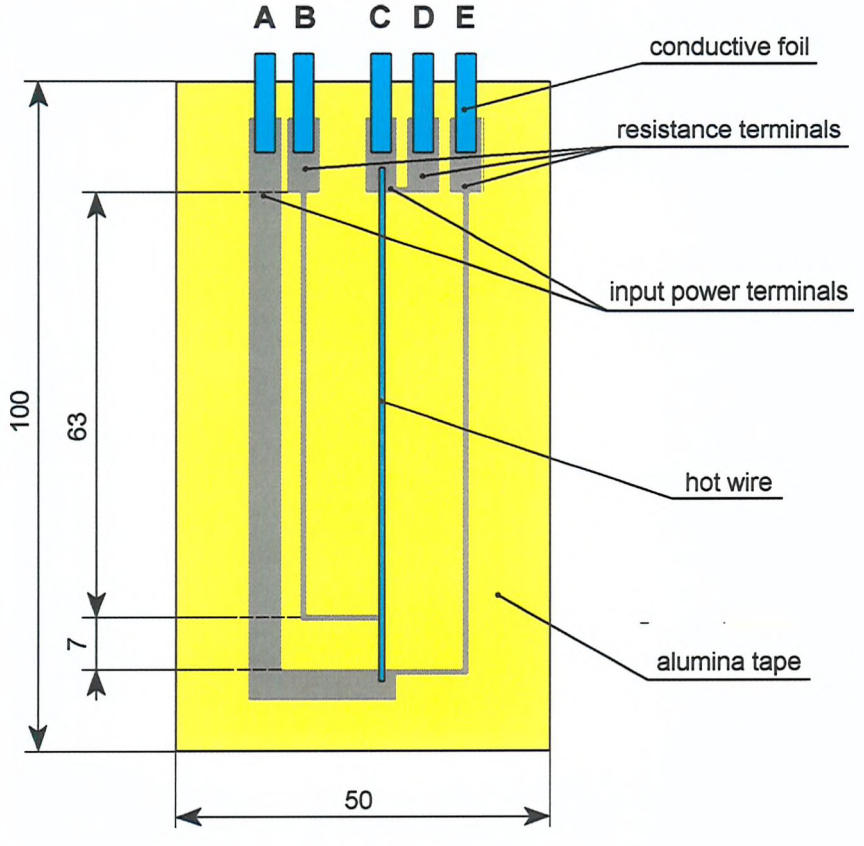

Figure 4.2 Original design of the THW sensor (dimensions in mm)

The hot wire is placed in the middle of the sensor and virtually divided into two parts with the ratio of 1:9. Figure 4.3 explains the principle of the end-effect cancellation for this kind of design and shows an infrared image of the sensor acquired at room temperature. The voltage, measured at the terminal B while the electric current I is heating up the hot wire, can be then evaluated as

$$\Delta V = I \cdot (\Delta R_L - \Delta R_S) = I \cdot \Delta R_w \qquad (4\text{-}1)$$

The measured voltage ΔV therefore characterises the temperature increase of the finite part of an infinitely long wire. The length of the finite part in the original design is 56 mm and its resistance R_w is typically about 11 Ω at the room temperature..

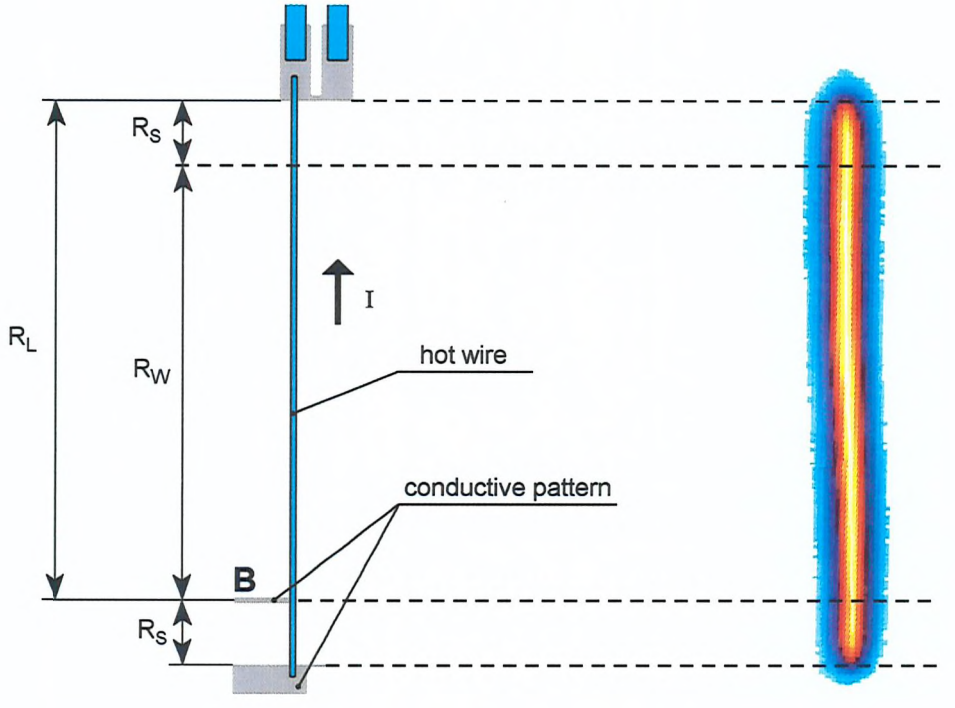

Figure 4.3 End-effect cancellation in original design

The infrared image, which helps to understand the cancellation of the end-effects, was acquired by infrared camera DeltaTherm™ and the data evaluated using DeltaVision software from Stress Photonics Inc. For the experiment with the infrared camera, the sensors had to be coated with a black paint in order to achieve high and uniform emissivity of the sensor surface. The acquired thermal images confirmed the assumption that the heat is generated only within the hot wire and the conductive pattern and foils do not contribute to the thermal distribution on the sensor. The full infrared image of the coated sensor taken after one second from the moment, when the electric current I of about 340 mA was applied, are shown in Figure 4.4 together with the temperature scale in degrees Celsius.

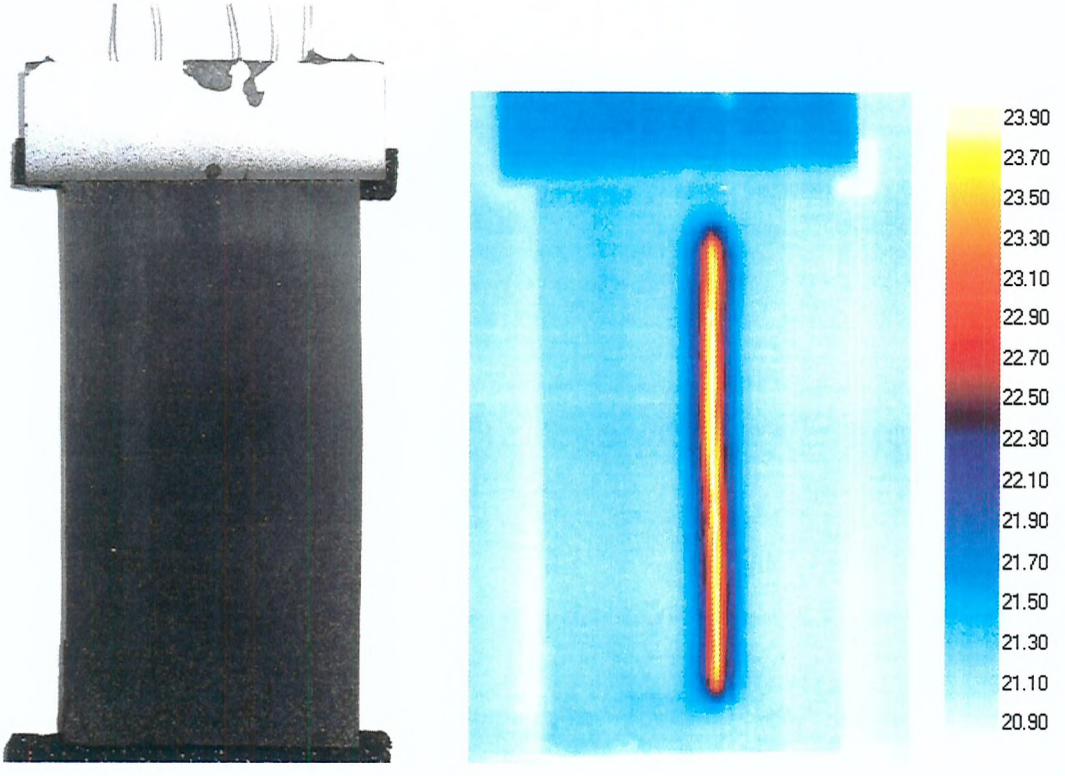

Figure 4.4 Sensor with black paint coating and its image acquired using IR camera

4.1.2. New Sensor Design

During the experiments with the original THW sensors it has been found that unless a large heat flux is applied on the hot wire, the change of the resistance of the 56 mm long hot wire is relatively very small. The temperature rise could not be measured with high sensitivity because of natural low-level noise imposed on every measurement of very small voltages. In order to increase the overall sensitivity of the measurements hence the accuracy of the whole method, a new design of the THW sensor has been introduced and is shown in Figure 4.5.

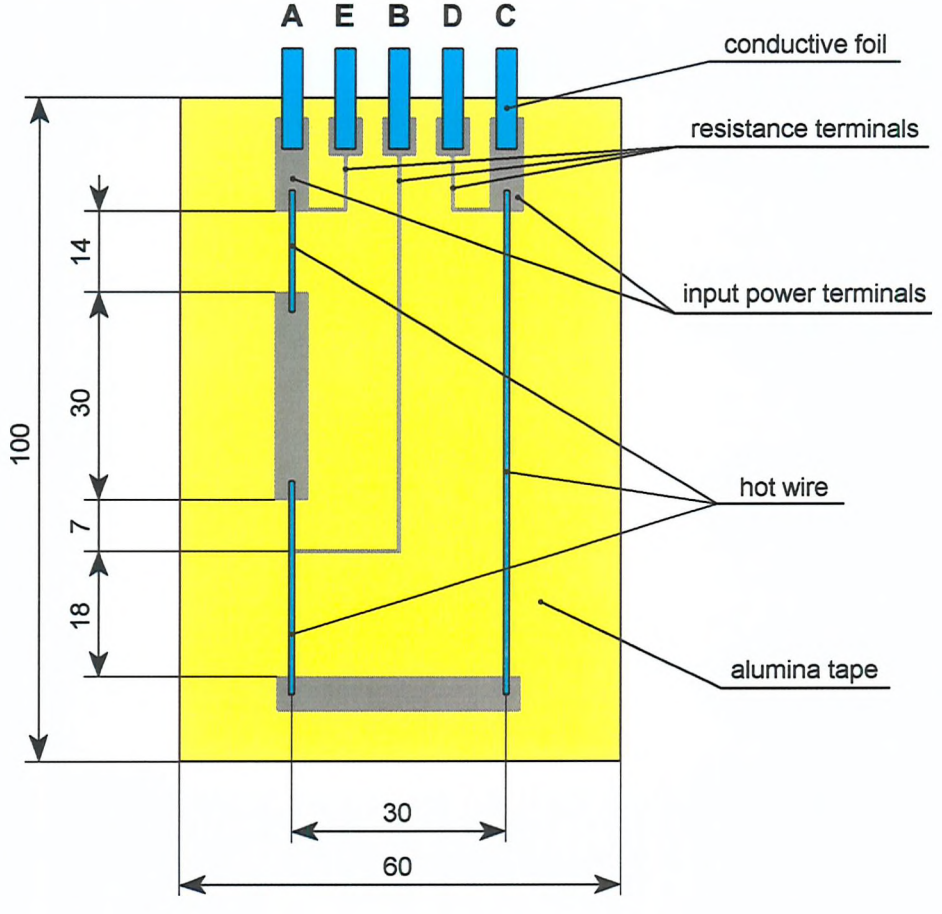

Figure 4.5 New design of the THW sensor (dimensions in mm)

The new design is based on the hot wire which is divided into three thermally independent parts. The key feature of the new design is that the length of the hot wire is extended to 108 mm and the ratio between short and long part of the wire is about 1:4. Extension of both parts of the wire ensures that the measurements of the voltage

changes at the terminal B do not show noisy behaviour and result in more sensitive and accurate extraction of the thermal conductivity. On the other hand, the use of the thermally independent sections means that the cancellation of the heat losses at the ends of the wires is more complicated as it can be seen in Figure 4.6. The change of the voltage at the terminal B can be evaluated as

$$\begin{aligned}\Delta V &= I\cdot\left(\Delta R_{\text{long}} - \Delta R_{\text{short}}\right) = I\cdot\left(3\cdot\Delta R_{\text{S}} + \Delta R_{\text{W1}} + \Delta R_{\text{W2}} + \Delta R_{\text{P}} - 3\cdot\Delta R_{\text{S}} - \Delta R_{\text{P}}\right) = \\ &= I\cdot\left(\Delta R_{\text{W1}} + \Delta R_{\text{W2}}\right) = I\cdot\Delta R_{\text{w}}\end{aligned} \tag{4-2}$$

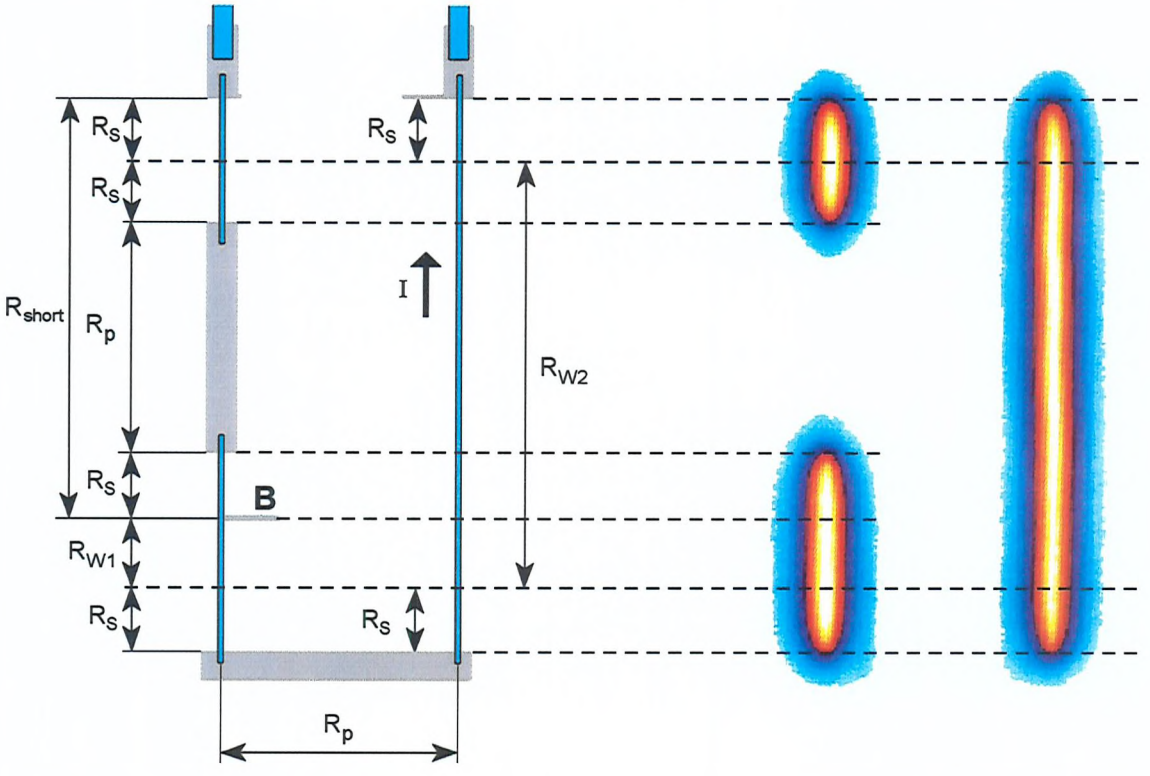

Figure 4.6 Cancellation of the end-effects in the new design

The new designed length of the finite part of an infinitely long hot wire is 66 mm, i.e. extension by 18 % if compared to the original design. At the same time the new sensor does not require any upgrades of the original measuring devices and changes in configuration of the equipment.

Figure 4.7 shows an infrared image of the whole new sensor, captured at room temperature. The thermal distribution proves that the wide conductive lines which connect the three parts of the hot wire do not contribute to the heat generation on the

sensor. However even if there is any minor temperature rise in these two wide conductive lines, the changes in resistance again cancel each other and the voltage measured at the terminal B stays intact. The infrared image also proves that all three sections of the hot wire are thermally independent, i.e. do not influence each other. Moreover the 'thermal distance' between the three sections is quite large and the length of the buried conductive lines with resistance R_p can be reduced by up to 50 %, which would further significantly improve the performance of the THW sensor. This and further suitable design improvements will be explained and discussed in chapter *6. Future Work.*

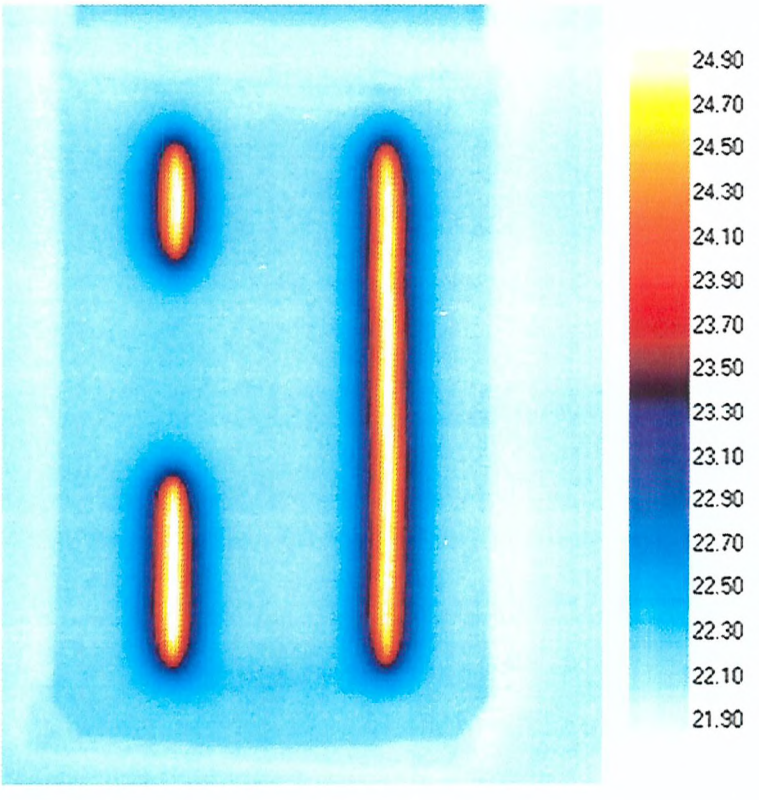

Figure 4.7 Infrared image of the sensor with the new design

4.2. Fabrication Process

The fabrication of a single sensor takes from four to five days and the process is divided into several steps. The sensor is not required to be fabricated in a very clean environment, however the alumina tape should not come into contact with any chemicals, water or skin prior its sintering in order to produce clean and homogenous alumina substrate at the end. The fabrication stages are described in detail in the following sections.

Table 4.I lists all materials currently used in the fabrication process. The original alumina tape was supplied by a company which no longer exists in the market. A single stock of the tape has been used during last ten years and that is why all measurements have been carried out using the alumina tape from one supplier. Unfortunately, it was not possible to obtain material datasheets from the manufacturer and also the thermal properties of the alumina tape which were measured in previous experiments were not published. Currently a new HTCC tape from ESL is being tested in order to continue with the research after the stock of the original alumina tape is exhausted.

Table 4.I Overview of the materials required for fabrication of the THW sensor

Material	*Supplier*	*Maximum Application Temperature [K]*
Platinum wire	Goodfellow	2000
Platinum foil	Goodfellow	2000
Platinum thick film paste	Ferro, ESL	unknown
Nickel wire	Goodfellow	1728
Alumina tape (HTCC)	*unknown*	cca 1500
Kapton® film	Katco Ltd	600
Zirconium powder	Zircar Products Inc	cca 2100
High temperature glue	Fortafix Ltd	cca 1700

4.2.1. Thick Film Technology

A conductive pattern is created on the alumina tape using thick film technology. The technology is based on the screen printing process which is probably the oldest method of graphic art reproduction [82].The modern screen printing process is illustrated in Figure 4.8 where the printing medium (ink, paste) is forced through open areas of a mesh-reinforced screen onto a surface of the solid substrate and creates a desired pattern.

The modern thick film technology uses finely meshed stainless steel screens and well defined thick film pastes. The pastes can be virtually made of any material and can form any required pattern with minimum width of the printed line about 300 μm. If a higher resolution is required, specially designed screens and pastes should be used and it is essential to employ etching processes for the resolution finer than 80 μm. The printed pattern is usually from 10 μm to 20 μm thick depending on a type of the screen and settings during the printing process

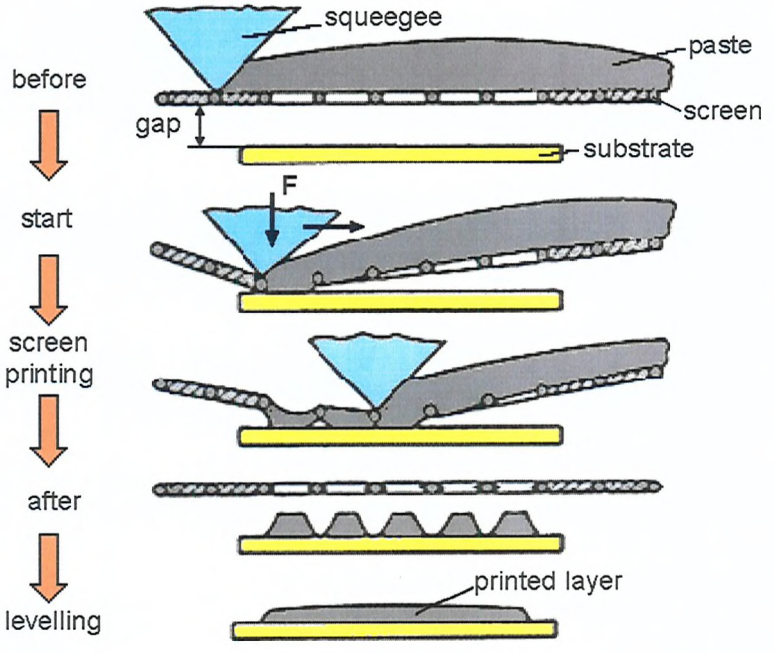

Figure 4.8 Screen printing process

Recently the thick film technology has been widely used also in HTCC and mainly LTCC (Low Temperature Co-fired Ceramics) electronic modules [83]. In both technologies, the thick film pattern is printed onto a flexible alumina based tape. The tapes are then aligned, vertically pressed together and sintered so that the conductive pattern is buried in the solid ceramic module [84]. As mentioned above, such technology was found ideal for the fabrication of the THW instrument.

Due to the high temperature requirements of our application, the buried conductive pattern must be made of a metal with a high melting point. Therefore the platinum based thick film pastes are used, supplied by Ferro (paste number 7336-1HV) and ESL (paste number 5545). Both pastes provide satisfactory printing and performance results,

although they are not originally designed to be cured between alumina tapes and the recommended firing temperature is also different.

The screen with the original design was fabricated by DEK Ltd with 325 mesh count per inch, the mesh filaments in angle 45° to the screen frame and emulsion 50 μm. The screen with the new design was fabricated in MCI Cambridge Ltd using the mesh count 200 per inch also with 45° filaments direction but emulsion 20 μm. The lower emulsion helps to print a line with better defined edges while the lower mesh count results in a slightly higher printed thickness.

At the start of the printing process, the screen is fitted into a semi-automatic screen printing machine AUREL C880, the thick film paste is spread on the screen and a few patterns are printed on testing substrates. Then the conductive pattern is printed on the 350 μm thick alumina tape, the printed pattern is left to create a smooth surface (levelling) and dries out at the room temperature. Usually the levelled printed patterns are placed into the belt driers where they are exposed to temperature above 100 °C for about 10 minutes. However this quick drying cannot be used for the alumina tape because the tape would loose some of its organic binders which would decrease its flexibility and ability to be well hot-pressed.

4.2.2. Hot Pressing

After the conductive pattern is created on the alumina tape, all electrically conductive parts of the THW sensor, which are to be immersed into the measured liquid, are sealed inside the alumina material. Prior to that, a 25 μm platinum wire (hot wire) is placed carefully on the printed conductive pattern a shown in Figure 4.2 or Figure 4.5.

The platinum wire is the core of the THW sensor and its geometry and material properties are the key parameters for accurate measurements of the temperature rise. The wire is supplied by Goodfellow, which provides material properties as stated in Table 4.II. Unfortunately the given properties are defined only over a narrow range of temperature or just at the room temperature. That is why it is essential to either individually measure hot wire properties at every temperature or use reliable and acknowledged standards for the platinum material. The wire geometry is also inspected under microscope for any mechanical cracks or deformed cross-sectional area which would result in non-uniformity of the generated heat flux.

Table 4.II Properties of the supplied platinum wire

Wire diameter	25 μm
Purity	99.99 %
Temper	annealed
Temperature coefficient of resistance at 0-100°C	0.00392 K^{-1}
Electrical resistivity at 20 °C	1.058E-09 Ω·m
Thermal conductivity at 0-100°C	71.6 $W \cdot m^{-1} \cdot K^{-1}$
Density at 20°C	21 450 $kg \cdot m^{-3}$
Specific heat at 25°C	133 $J \cdot kg^{-1} \cdot K^{-1}$
Coefficient of thermal expansion at 0-100°C	9 $ppm \cdot K^{-1}$
Melting point	2045 K (1772°C)

When the platinum wire is placed on the conductive pattern, the printed leads to the wire are extended to the outside of the alumina tape by platinum foils (thickness 0.2 mm, purity 99.98 %, supplied by Goodfellow). The platinum foils, which function as the contact terminals of the sensor, are positioned as illustrated in Figure 4.2 or Figure 4.5. Subsequently a blank sheet of the alumina tape is placed on the top and the whole 'sandwich' is hot-pressed under pressure of 35 MPa (cca 5000 psi) at a temperature of 180 °C for 20 minutes. The alumina tapes are separated from the pre-heated hot plates by two sheets of 275 μm thick Kapton® film 300HN otherwise the tapes would stick to them. At the end of the hot-pressing, the Kapton® films are carefully removed.

4.2.3. Sintering

When the hot wire is encapsulated between two flexible alumina tapes, the whole module is sintered (cured) at a high temperature in order to remove all organic binders and transform flexible alumina into a rigid substrate. In previous work at Imperial College, the alumina tape was sintered at 1873 K, i.e.1600 °C, and it was reported that the resulted thermal conductivity at the room temperature was about 25 $W \cdot m^{-1} \cdot K^{-1}$ [13]. Unfortunately, such laboratory equipment is not available at School of Engineering Sciences at University of Southampton satisfying the specific temperature and dimensional requirements. Thus a Lenton chamber furnace with maximum temperature 1723 K (1450 °C) is used instead. The substrate cured at this temperature is rigid but less transparent and its thermal conductivity is about 20 $W \cdot m^{-1} \cdot K^{-1}$ at room temperature. Although this is a major difference which results in a different thermal performance of the sensor, it has no influence on the measurements because the method is capable of

accommodating such differences as long as the heat wave produced by the encapsulated hot wire reaches the edge of the substrate within a suitable time.

The temperature profiles of the both current and original sintering processes are illustrated in Figure 4.9. Besides the maximum temperature, significant differences can be also observed at the cooling stage. A lower temperature slope 60 °C/h is applied because the furnace does not allow active cooling and is not capable of cooling down its chamber quickly with a good temperature distribution around the fired sample.

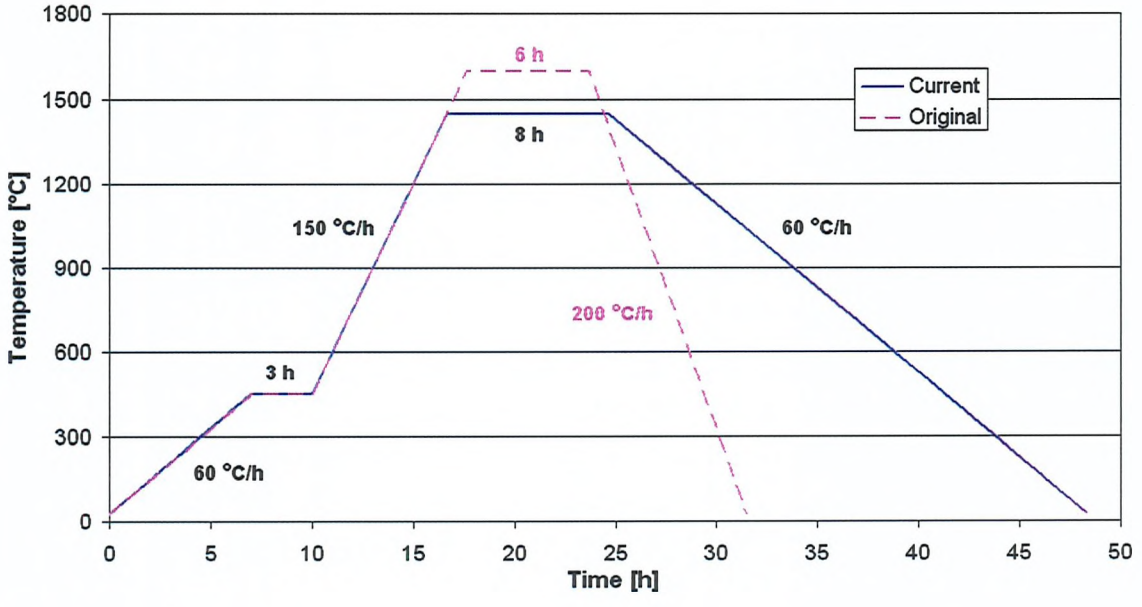

Figure 4.9 Temperature profiles of the sintering process

During the cooling stage, the alumina tape shrinks by about 6 % and such forces can result in bending or deformation of the thin substrate. Therefore it is necessary to place the HTCC tape in-between two similar solid alumina blocks with dimensions of 144 mm × 70 mm × 15 mm. In the same way as for the hot-pressing, the alumina tape is separated from the blocks by thin layers of zirconium powder in order to avoid adhesion.

After the cooling stage, the surface of the alumina sensor is cleaned of any remains of the zirconium powder. The sintered sensor is about 580 μm thick and the conductive pattern buried within the substrate together with platinum wire is visible because the fired sensor is semi-transparent as it can be seen in Figure 4.10. This feature allows measurements of the geometry of the encapsulated hot wire.

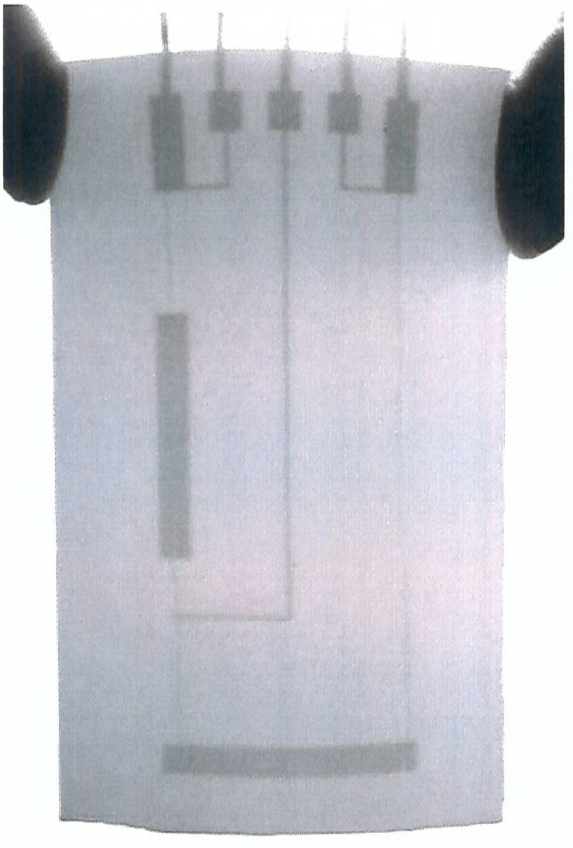

Figure 4.10 Sintered semi-transparent sensor (new design)

4.2.4. Post-Sintering Processes

The platinum foils that are protruding from the sintered sensor as shown in Figure 4.10 are spot-welded to a nickel wire (diameter 0.5 mm, 99.98 % pure, supplied by Goodfellow). Before the spot-welding, the wires ends are slightly hammered out and cleaned from oxide layers in order to create reliable mechanical and electrical contact. The nickel wires provide electrical connection between the hot zone of the high temperature furnace and the top cap of the furnace chamber where they are soldered to metal contacts. The rest of the connection outside the furnace is handled by copper wiring. The only requirements are that the wiring has to be able to accommodate electrical current of about 0.6 A without self-heating and must be suitable for carrying small voltage signals, i.e. a shielded cable is preferable.

The spot-welded Pt-Ni contacts are buried in the high temperature glue which fills a gap between two solid alumina blocks with dimensions 51 mm × 17 mm × 0.6 mm. This final step increases robustness of the final instrument and its contacts and the sensor is ready to be calibrated and mounted into the furnace chamber.

4.3. Sensor Calibration

Throughout the current research, five sensors with the original design and five sensors with the new design were fabricated and experimentally tested. It has been observed that every manufactured sensor is a unique unit with its own specific geometric and electric parameters. The differences between sensors are mainly caused by the technique of placement of the hot wire on the leads and also by the fact that the alumina tape shrinks during the sintering process. The shrinking process is governed by the temperature distribution on the tape during the cooling stage and amount of the zirconium powder used to avoid sticking to the alumina blocks. Both parameters cannot be precisely controlled and this results in slight variations among all fabricated sensors. Therefore it is necessary to calibrate every sensor in order to extract correct values of the thermal conductivity.

4.3.1. Sensor Dimensions

It has been mentioned in chapter *3.Transient Hot-Wire Technique*, that there are two main geometrical dimensions of the THW instrument which have to be known with adequate accuracy:

- the length of the finite part of an infinite hot wire, because the heat input to the hot wire is defined as a heat flux per unit length (see sections *3.1. Background Theory* and *3.4.Discussion*)
- the thickness of the substrate of the sensor (isolation of the hot wire), because it affects the temperature response of the sensor (see section *3.4.Discussion*).

The thickness of the substrate of the sensor is relatively easier to be identified. The thickness of the sintered alumina substrate can be measured directly by a micrometer with 1 μm resolution. It has been observed that the thickness is usually greater by up to 20 μm at places, where the wide thick film lines are buried. Therefore the thickness is evaluated at places where the heat transfer really occurs, i.e. along the hot wire. The measured thickness along the wire varies slightly within range of about ±8 μm. An average value of the thickness is calculated and used in subsequent calculations.

The length of the hot wire cannot be measured so precisely because the hot wire is already embedded inside the sintered alumina substrate and its ends cannot be clearly distinguished. In order to minimise errors, the semi-transparent sensor is placed on a glass holder with a light source beneath and a calliper with resolution 10 μm is used for repetitive measurements of the long part of the hot wire. The measurements are carried out from both sides of the substrate several times. Usually, the standard deviation for the length measurements is below 0.2 mm. However this deviation is relatively large especially in comparison with the length of the short wire.

It should be also noted, that due to a manual placement of the tiny platinum wire, it is rather difficult to produce an ideal straight line heat source. It is quite common that the bare wire is slightly off-position (see Figure 4.10) and its shape cannot be fully defined prior to hot-pressing and sintering. The length measurements assume that a straight wire is placed between the leads. Therefore the measurement of hot-wire length should be substituted by measurements of electrical properties wherever it is possible.

Table 4.III shows a comparison of the measured length of the long part of the hot wire, l_{long}, for all employed sensors. The derived electrical resistivity of the hot wires encapsulated in sensors is also listed and directly compared to the measured electrical resistivity of the 81.85 ±0.15 mm long, straight bare platinum wire diameter of 25 μm. In the table, the sensor numbers, which start with letter A, indicate the original design while the letter B means that the new design was used.

Table 4.III Electrical resistivity of the hot wire measured at 293 K (20 °C)

Sensor	*Measured l_{long} [mm]*	*El. resistivity [$\times 10^{-7}$ Ω·m]*	*Rel. difference from bare wire*	*Calculated l_{long} [mm]*
Bare wire	81.85	10.655	---	---
A1	56.75	10.799	1.35%	57.52
A2	57.74	10.783	1.20%	58.43
A3	59.87	10.927	2.56%	61.40
A4	56.73	10.528	-1.19%	56.06
A5	57.58	10.802	1.39%	58.38
B1	81.71	10.890	2.21%	83.52
B2	82.16	10.888	2.19%	83.96
B3	79.66	10.658	0.03%	79.68
B4	80.37	10.662	0.07%	80.43
B5	79.85	10.587	-0.64%	79.34

It can be seen in Table 4.III that the most sensors are within the range of ±1.5 % from the resistivity measured for the bare wire and can be used for the thermal conductivity measurement without any corrections. However three sensors show higher resistivity from +2 % to +3 % differences and the measurements of the straight length of the wire cannot be used for the heat flux calculations. The geometric shape of the hot wires has to be taken into account and the true length of the curved wire evaluated. The deviation of the electrical resistivity of ±1.5 % means that the heat flux value applied on the hot wire is also known with similar uncertainty. This uncertainty directly affects the accuracy of the whole method because the temperature rise of the wire linearly depends on the applied heat flux as shown in the equation (3-8). Therefore it can be concluded, that the inaccurate measurements of the length of the encapsulated hot wire introduce a major error into the measurements and for the above listed sensors, the derived thermal conductivity cannot be evaluated with accuracy better than ±1.5 %.

However the accurate length can be calculated assuming that the electrical resistivity and the cross-sectional area of the hot wire, i.e. wire diameter, do not change during the fabrication of the sensor. Hence knowing the resistance of the hot wire measured at given temperature and resistance of the bare platinum wire at the same temperature, the length of the finite part of an infinite hot wire can be calculated for both designs as

$$l_{\mathrm{w}} = \frac{R_{\mathrm{w}}}{R_{\mathrm{bare}}} \cdot l_{\mathrm{bare}} = \frac{R_{\mathrm{long}} - R_{\mathrm{short}}}{R_{\mathrm{bare}}} \cdot l_{\mathrm{bare}} \tag{4-3}$$

where R_{bare}, R_{long} and R_{short} are the resistances measured by 4-wire technique with a very high accuracy, l_{bare} is the length of the bare wire and measured with the accuracy of ±0.15 mm, i.e. less than ±0.2 %. The lengths calculated using equation (4-3) can be also seen in Table 4.III. They have been used for the evaluation of the heat flux, which is applied on the hot wire during the THW measurements, because this allows bypassing the inaccurate measurement of the length of the encapsulated hot wire.

This is a novel approach if compared to the calculation of the applied heat flux in previous work [13]. The new approach has been validated by the measurements of the thermal conductivity of the same sample with a number of sensors of both new and original design. However it should be emphasized that the measurements of the length of the hot wire are still essential. The comparison between measured and calculated length may help to reveal a faulty sensor if both values differ by more than 5 %.

4.3.2. Temperature Coefficient of Resistance

The temperature coefficients of resistance (TCR) of the hot-wire material are other important parameters for every transient hot-wire technique. They are used to calculate the temperature increase of the hot wire from the change of the wire resistance and that is why the use of proper TCRs is essential. The European Standard EN 60751:1995 [85] provides the recommended TCR values for platinum thermometers in the range from 0 °C to 850 °C as

$$R_1 = R_0 \cdot (1 + \alpha \cdot T_C + \beta \cdot T_C^{\,2}) \tag{4-4}$$

where R_0 is resistance at temperature 0 °C, R_1 is resistance at temperature T_C [°C] and the temperature coefficients are defined in the standard as

$$\alpha = 0.0039083\ ^\circ\mathrm{C}^{-1}$$

$$\beta = -5.775 \cdot 10^{-7}\ ^\circ\mathrm{C}^{-2}$$

The TCR of the hot wire have been also calculated from the resistance measurements of all sensors at temperatures from 17 °C (290 K) to about 450 °C (720 K). Although the accuracy of the resistance measurements was high, the calculated TCR coefficients could not be used for an accurate extraction of the hot-wire temperature rise because an accuracy of the measured absolute temperature is stated by the supplier of thermocouple as ±1.5 °C and it is also very likely that a different temperature gradient occurs along the hot wire at every measured temperature. Additionally, the studied range of temperatures is narrower than one presented in European Standard. This makes the extrapolation of the true quadratic curve difficult and results in large uncertainty of the derived TCR coefficients.

Therefore it has been decided to use standardised TCRs for the platinum material and not to introduce a likely source of error into the thermal conductivity measurement. The standard may be applied because our THW sensor meets the requirements that an annealed platinum wire is used as a heat source [3] and the thermal conductivity measurements are carried out below 1120 K (850 °C). Otherwise an accurate calibration in a chamber with well defined temperature distribution would be necessary and experimentally derived TCRs would have to be used.

4.4. Experimental Configuration and Equipment

The measuring system was originally built in Imperial College London and was moved to the University of Southampton at the end of 2002. The current configuration is a slightly upgraded version of the original system as some of the measuring devices were replaced or brought to their cutting edge. The system, which is illustrated in Figure 4.11, is capable of highly accurate transient measurements of voltage and can store up to two thousand acquired samples with a minimum sampling rate of 20 μs. If a higher number of samples or a better sampling rate would be required, the system would have to be significantly upgraded which would result in major changes virtually in all parts of the system. The following sections provide closer look at the most important parts of the experimental configuration.

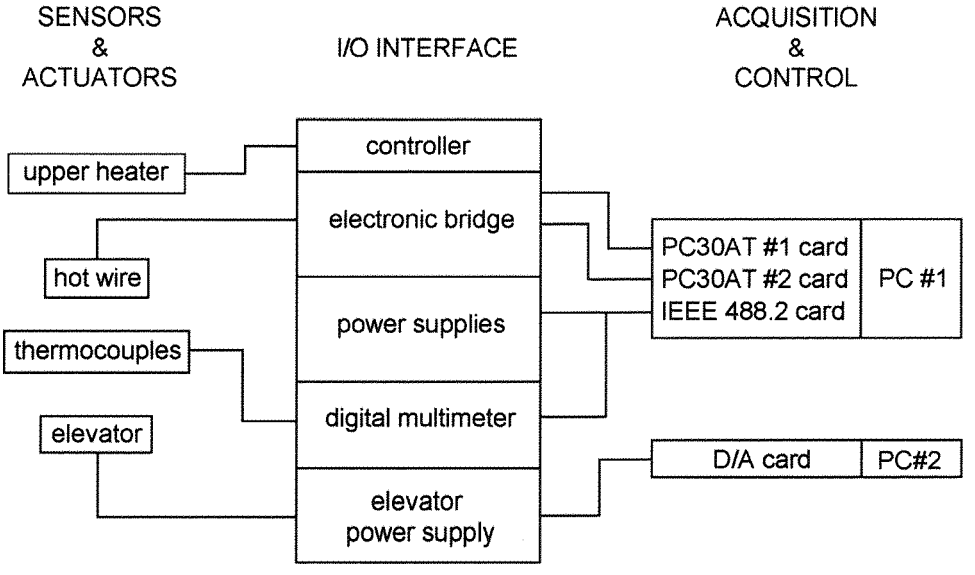

Figure 4.11 Schematic drawing of the experiment configuration

4.4.1. High Temperature Furnace

The high temperature furnace from Thermal Technology Inc is the core of the whole measuring system. The sensors (the hot-wire sensor and thermocouples) and actuators (the upper heater and elevator) are mounted in a tubular, water cooled furnace chamber with a 70 mm inner diameter and a 300 mm long cylindrical carbon heating element. According to the manufacturer, the temperature in the chamber can reach up to 2500 °C

(about 2800 K) if an inert gas is surrounding the carbon heating element. The chamber configuration also allows the usage of a different inert atmosphere around the sample because the cylindrical heating element is separated from its inner space by a sealed alumina tube. The furnace and the configuration inside its chamber are illustrated in Figure 4.12.

The gas management system of the furnace allows regulation of the pressure of the nitrogen gas (purity 99.998 %) around the heating element. The flow of the argon gas (purity 99.998 %) is also controlled separately and it has been found that the direction of its mild flow does not significantly contribute to the thermal distribution within the chamber. That is why the top-to-bottom argon flow is applied, which helps to avoid any condensation on the sensor support and leaves the vapours of molten materials to be condensed in the colder bottom part of the furnace chamber. The furnace chamber is also equipped with an exhaust line with a cold trap which filters any remaining metal vapour residues.

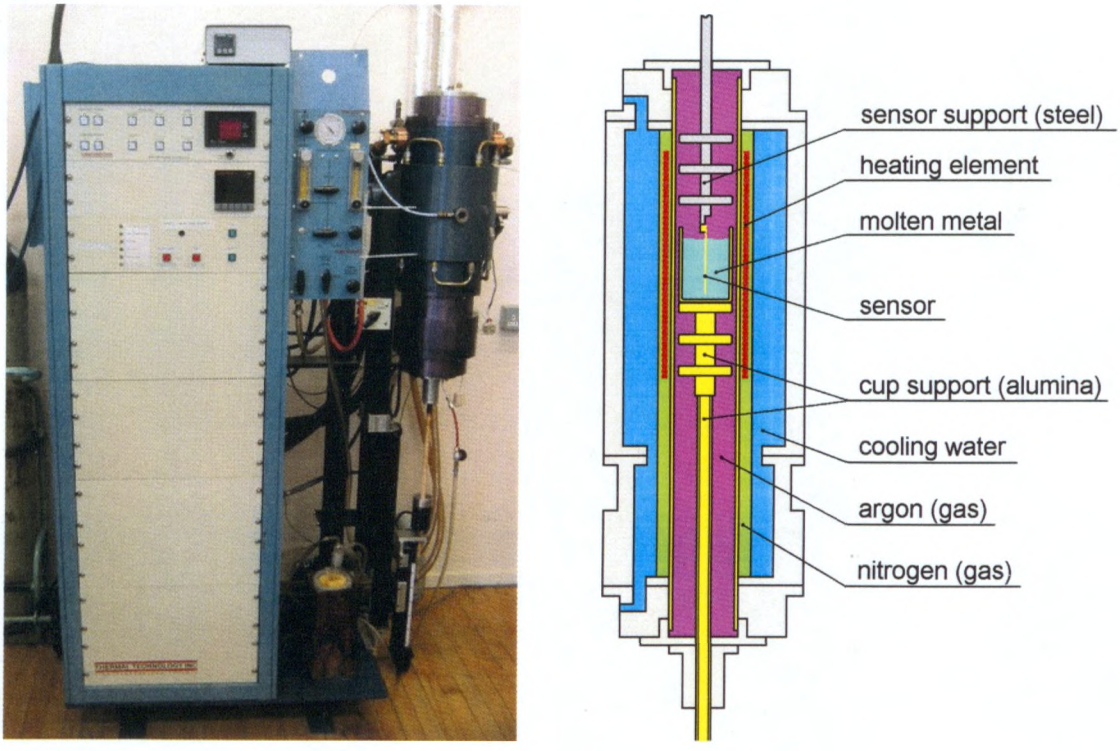

a) b)

Figure 4.12 The high temperature furnace (a) and schematics of its chamber (b)

4.4.2. Sensor Support

The hot-wire sensor is mounted on the stainless steel support, which was manufactured in Imperial College mechanical workshop, and it is illustrated and described in Figure 4.13. Thin alumina tubes and Kaowool plates are used for electrical insulation of the nickel leads from the electrically conductive support. The Kaowool plates also provide thermal insulation from the top and help to create more uniform thermal distribution within the measured sample. The space between the Kaowool plates is filled with glass wool in order to further enhance the thermal insulation effect.

The hot-wire sensor has to be connected to the measurement system with wiring made of electrically conductive materials which can withstand high temperatures in the chamber. The leads to the sensor are made of 0.5 mm nickel wire and the wiring changes to classic copper wires at the exit from the furnace chamber.

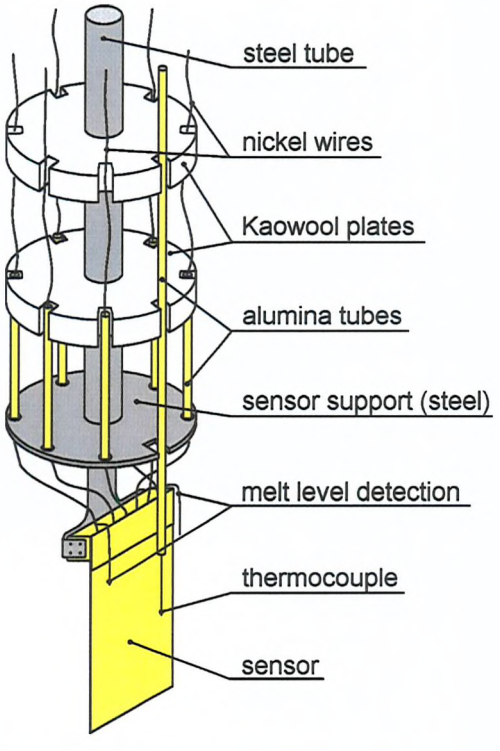

Figure 4.13 Schematic of the sensor support

Figure 4.13 also shows wires that are used to detect the level of the measured liquid around the sensor. These wires are used as resistance measurement terminals when the sensor is being immersed into the melt and again they are formed from the 0.5 mm

nickel wires. Supposing that the molten material is more conductive than air (which almost always happens), a quick drop of the resistance between these terminals indicates that the level of the melt has reached the desired position. For molten metals, the resistance drops from several MΩ in air to a few Ω when the wires are in contact with the melt.

Alternatively, the melt level can be also detected during the immersion process by the thermocouple shown also in Figure 4.13, because the level of the molten material causes a steep temperature change in the thermocouple readings during the immersion. If the position of the thermocouple junction is measured relatively to the top of the sensor prior to experiment, the desired position of the level of the molten material can be set.

The stainless steel sensor support has one additional important feature. It allows placement of a 9.52 mm diameter heater inside the carrier tube. The heater and another thermocouple are fitted into a stainless steel jacket which is used as a taper plug of the tube. The heater is employed to cancel the heat conduction from the sensor to the support and also to maintain the temperature of the upper part of the sample to overcome problems of convection owing to inappropriate temperature gradient along the molten sample.

In previous works, the additional 70 W low-watt-density heater (supplied by RS Components, Ltd) was reported to be insufficient at temperatures above 723 K (450 °C) and moreover further experiments showed that electrical insulation of this heater quickly degraded at such temperatures. Therefore a new heater is employed in this work (manufactured by Dalton Electric Heating Co., Inc and supplied by Engelmann & Buckham Ltd), which provides a heating power of 300 W and withstands temperatures up to 1273 K (1000 °C).

It should be emphasized that the upper heater does not guarantee that the convection inside the crucible is fully cancelled. It has been observed during a number of experiments that convection may occur even if the upper heater temperature is set well above the furnace temperature and it has been found that the vertical position of the crucible is the most important parameter for the control of the temperature gradient in the melt. The chamber has a certain temperature distribution along its cylinder axis and the crucible should be placed in a region where a temperature gradient in the chamber helps to avoid convection within the melt. In other words, the top edge of the crucible

should be placed in the hottest zone in the chamber. This suggests that, ideally, the whole crucible should be positioned below the geometric centre of the heating element. At the same time, the cylinder axis of the crucible should be identical with the cylinder axis of the chamber, otherwise horizontal misplacement occurs and this may also introduce unfavourable temperature gradients.

4.4.3. Electronic Bridge and Acquisition System

The electronic bridge and the acquisition system were also designed and manufactured in Imperial College London during previous work [8] and it is shown together with its simplified schematics in Figure 4.14. The main function of the electronic bridge is monitoring and amplification of the voltage difference during the transient run. The transient measurement starts at the moment when the DC voltage is applied to the whole circuit and heat starts to be generated within the hot wire. It results in a change of hot-wire resistance which causes a change of the voltages in the bridge arm. The output of the unbalanced Wheatstone bridge is amplified by a factor of one hundred, read by acquisition cards and transferred into a PC where the data are collected and subsequently processed.

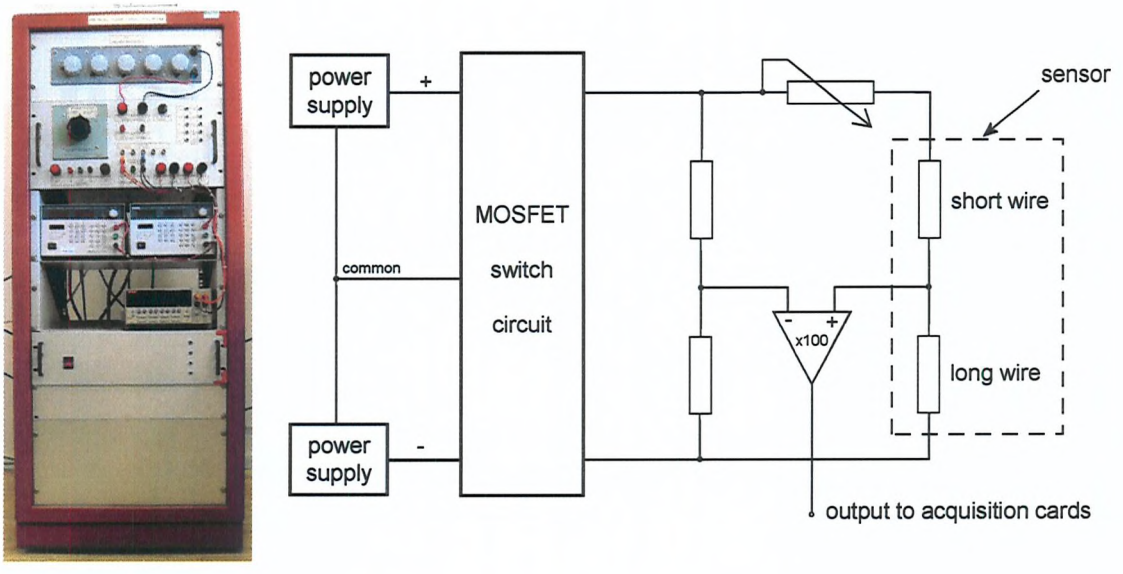

Figure 4.14 Electronic bridge and its schematic diagram

The experimental configuration of the acquisition devices requires several important parameters to be met. One of the key features is a precise time alignment of the power source and acquisition devices. The current measuring system is capable of switching the devices with a delay of less than a few microseconds from each other and such a difference between the starting points has a very minor effect on the thermal conductivity measurements.

In order to closely investigate the time response within the first second of the transient run, an adequate sampling rate of the acquisition system is set. The time interval that should be analysed is approximately from 100 μs to 1 s from the start. Due to the specific characteristic of the response, it is necessary to apply higher sampling rates at shorter times but such rates are not essential for the times from 0.01 s to 1 s. Therefore the acquisition system consists of two PC30AT acquisition cards from Amplicon Liveline Ltd. One card is set to a sampling rate of 20 μs and the sampling rate of the second card is 1 ms.

The PC30AT cards are equipped with 12-bit A/D converters with a stated accuracy of ±4 LSB (Least Significant Bits), which for the range ±10 V gives an absolute uncertainty of approximately ±20 mV with a minimum measurable voltage increment of 5 mV. The whole system is regularly calibrated by measurements of test voltages (from 0 V to 0.09 V) in order to minimize linearity and offset errors of the voltage amplifier and A/D converters. Each acquisition card is capable of acquiring and storing one thousand samples and both cards are controlled simultaneously during measurements via a computer with on-site written software. The program is written in QuickBasic® and besides the acquisition cards, it controls the electronic bridge, digital multimeter and power supplies via an IEEE 488.2 interface (GPIB).

The unique configuration of the electronic bridge also significantly eases measurements of the steady-state resistances. The bridge electronically switches a measuring arm between the sensor terminals as described in the section *4.5.2. Steady-State Resistance Measurements* and connects them to the Keithley 2000 digital multimeter with built in 28-bit A/D converter which is used for precise steady-state voltage and resistances measurements with an uncertainty of ±0.005 % for voltage and ±0.015 % for resistance measurements.

The source of the electric current, which generates heat within the hot wire, consists of a circuit with MOSFET switches and two DC voltage supply units. The switching circuit allows quick and precise switching of the heat flux applied on the hot wire and works in parallel with the acquisition cards. The two power supplies TSX3510P units are products of Thurlby Thandar Instruments Ltd.

4.5. Measurements

The fabricated THW sensor is firstly placed on the sensor support as shown above and the support is mounted inside the furnace chamber by fixing its stainless steel tube to the top cap of the chamber. The crucible with a sample is placed on an alumina support which is a part of an elevating mechanism. The alumina support, illustrated in Figure 4.12b, consists of the base made of machinable 960 alumina (supplied by Cotronics Corp.) and an alumina tube of 730 mm length and 15 mm diameter with 3 mm wall thickness. The alumina tube is connected to a stepper motor which is controlled electronically from a PC and allows usage of various lifting speeds. The mechanism also allows accurate vertical placement of the crucible.

Prior to melting, the crucible is placed immediately below the bottom edge of the sensor. The furnace chamber is then evacuated, filled with argon gas and the furnace is turned on. The furnace temperature is usually set to be about 70 K above the melting point of the measured material and this ensures that the measured material is liquid throughout the whole of its volume. The controlled temperature rise is recommended to be about 3 K per minute. Once the chamber reaches the desired temperature, the furnace is left for another hour to allow proper melting of the material inside the crucible. The crucible is then lifted slowly, approximately 5 mm per minute, towards the sensor. When the resistance between the level detector terminals drops significantly, the hot wire inside the sensor is fully immersed in the molten material and the lift is stopped. The transient response measurements are taken once the temperature of both thermocouples inside the crucible stabilizes, which usually takes additional two hours.

4.5.1. Temperature Measurements

The temperature of the molten material is measured by a pair of thermocouples, type K, supplied by Labfacility Ltd, with maximum application temperature 1373 K (1100 °C). The thermocouples are encapsulated in a stainless steel coating with diameter 0.5 mm. The same type of thermocouple is also used for the temperature control of the furnace heating element as well as for the additional upper heater mounted inside the sensor support. The two thermocouples are connected to the digital multimeter which is also used for voltage measurements during the transient run. The accuracy of the

thermocouple is stated by the manufacturer as ±1.5 °C and the overall accuracy of absolute temperature measurements is estimated to ±2 °C after considering the calibration of the digital multimeter. The overall temperature of the melt is calculated as an average of both thermocouple readings.

The main purpose of placing two thermocouples in the crucible with the melt is for measuring the stability of the temperature within the melt and insuring that a convective flow within the melt does not exist. One thermocouple is placed close to the top of the platinum wire and the second thermocouple is fixed near the bottom of the crucible. When the temperature measured by the upper thermocouple is greater than for the lower thermocouple, the convective flow inside the crucible is suppressed.

4.5.2. Steady-State Resistance Measurements

The electronic bridge can operate in two different modes. The first, resistance (steady-state) mode, allows precise resistance measurements of the sensor and paths of electrical current. The second, transient mode is used to monitor the voltage response of the sensor during the transient run.

Before the steady-state resistances are measured, the electronic bridge is set to the transient mode, a small voltage is applied on the sensor and the bridge is balanced by adjustments of the resistances R_1 and R_2, i.e. the voltage output of the Wheatstone bridge is minimized. Subsequently the bridge is switched to the resistance mode and the 4-wire resistance measurements are carried out as it is illustrated in Figure 4.15. The description of the sensor terminals (A, B, C, D and E) can be found in section *4.1.Sensor Design.* A small measuring current I_m is applied through the arm containing the hot wire and several essential resistance values are measured:

- R_{total} – overall resistance of the path of electrical current, i.e. 2-wire measurements

$$R_{\text{total}} = R_1 + R_{\text{leadin}} + R_{\text{short}} + R_{\text{long}} + R_{\text{leadout}} + R_2 \tag{4-5}$$

- R_{sensor} – resistance of the sensor between terminal A and C, including lead resistances

$$R_{\text{sensor}} = R_{\text{leadin}} + R_{\text{short}} + R_{\text{long}} + R_{\text{leadout}} + R_2 \tag{4-6}$$

- R_{LL} – resistance of the long part of the hot wire, including one lead resistance, measured between terminals B and C

$$R_{LL} = R_{long} + R_{leadout} + R_2 \tag{4-7}$$

- R_{long} – resistance of the long part of the wire, excluding lead resistances, measured between terminals B and D

$$R_{long} = R_w + R_{short} \tag{4-8}$$

- R_{short} – resistance of the short part of the wire, excluding lead resistances, measured between terminals B and E

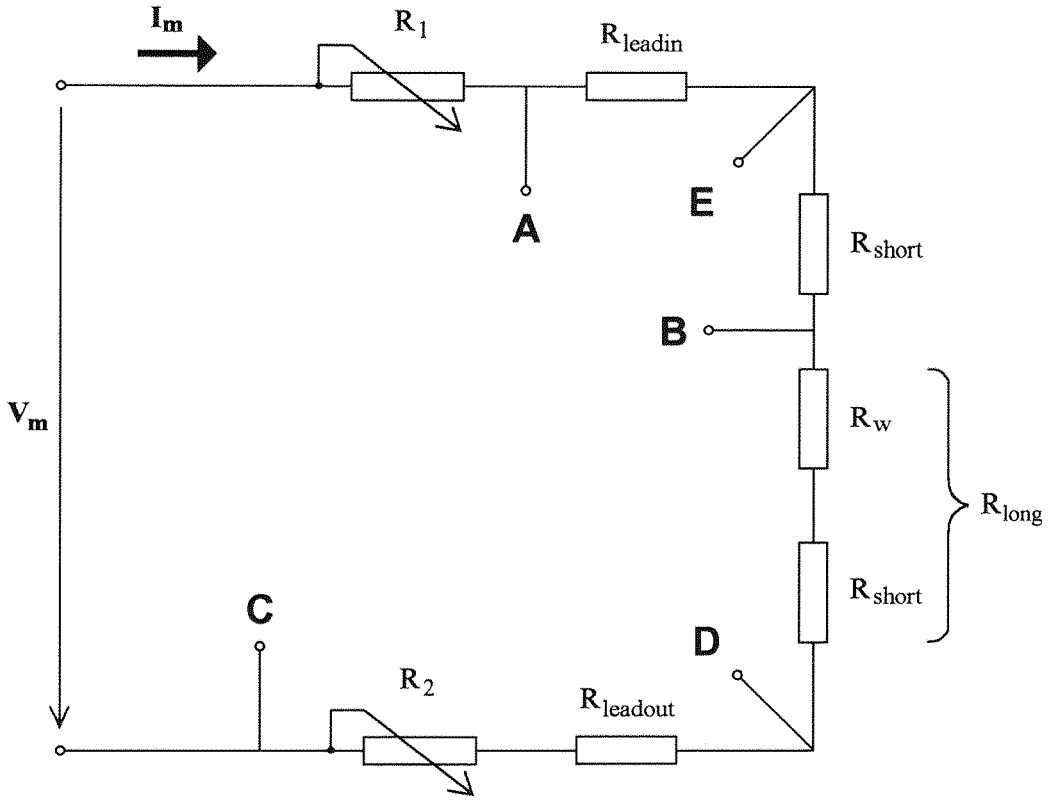

Figure 4.15 Schematic of steady-state resistance measurements

The steady-state measurements are always repeated several times because the high-power furnace influences small signals and introduces noise and inaccuracy into resistance and temperature readings. However, once repeatable values are obtained, the transient response can be acquired.

4.5.3. Transient Response Measurements

Prior to transient measurements, the balanced bridge is set back to the transient mode. In this mode, the bridge arm with the hot wire is connected to the voltage supply terminals and the terminal B output, which is the point where an unbalanced bridge voltage is measured, is switched to the inputs of both acquisition cards. The start of the transient run is controlled by a voltage pulse which turns the both acquisition cards and the MOSFET circuit on at the same time.

The transient response of the sensor is measured within one second from the moment after the voltage V_S is applied to the Wheatstone bridge. The voltage difference in the unbalanced bridge is amplified by factor of one hundred and read by the acquisition cards. During the time when very small voltage differences are being acquired, the high temperature furnace is turned off or the electrical current, which flows through the furnace heating element, needs to be diverted. It has been observed that otherwise the amplified signal contains noisy peaks with a frequency 50Hz induced by the heating element. At the end of the acquisition process, the furnace is turned on again and left for several minutes until a new steady state is reached.

Figure 4.16 shows the resistance changes in the bridge arm caused by the heating electric current $I(t)$. Compared to the steady state, new time-dependent resistances (red colour resistors) have to be introduced, $\Delta R_w(t)$ and $\Delta R_{short}(t)$, in order to describe appropriate resistance increases in the circuit. However the acquired bridge output voltage $\Delta V(t)$ depends only on $\Delta R_w(t)$ because the other two voltage increases across the short wires cancel each other out. After the transient response is acquired, the voltage values are saved into a file together with all steady-state parameters and experimental conditions.

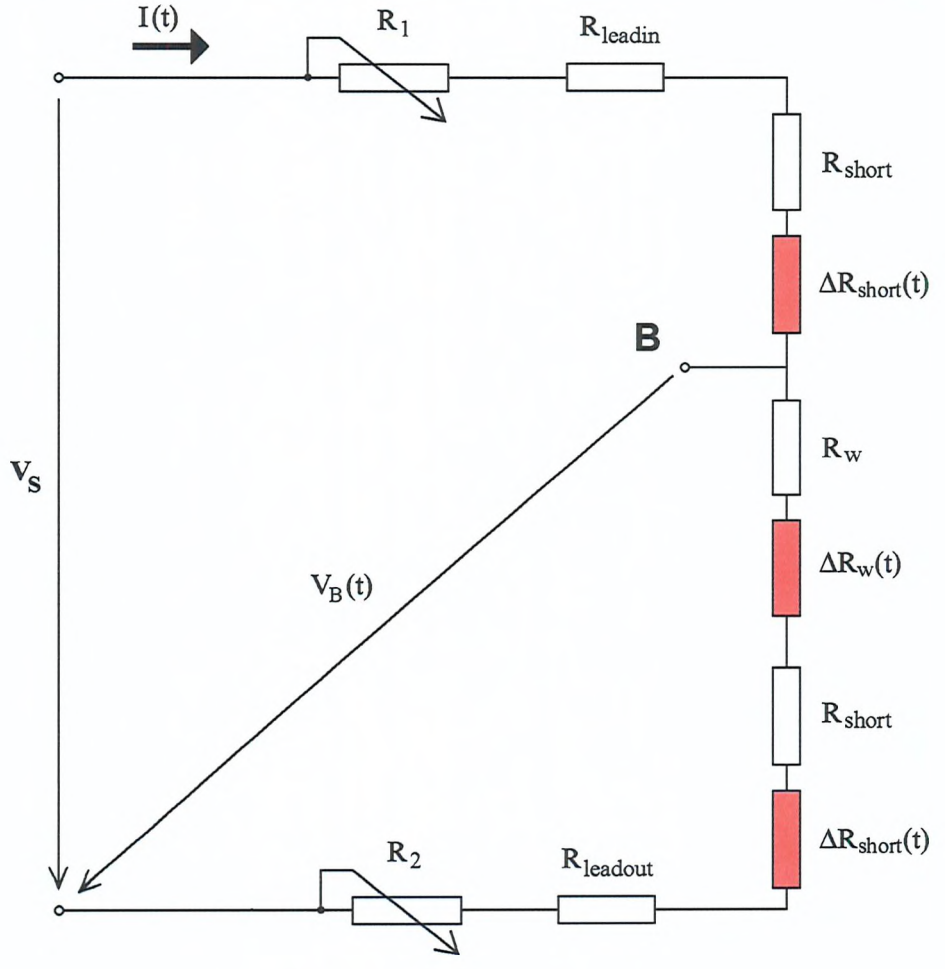

Figure 4.16 Schematics of the bridge arm with THW sensor during the transient measurements

4.6. Derivation of the Hot-Wire Temperature Rise

4.6.1. Voltage to Resistance Calculations

It can be seen from the schematic of the bridge arm in Figure 4.16 that the measured transient voltage can be defined as

$$\Delta V(t)=V_B(t)-V_B(0) \tag{4-9}$$

which can be re-written as

$$\Delta V(t)=\frac{V_S}{R_{total}+\Delta R_w(t)+2\cdot\Delta R_{short}(t)}\cdot\left(R_{LL}+\Delta R_w(t)+\Delta R_{short}(t)\right)-\frac{V_S}{R_{total}}\cdot R_{LL} \tag{4-10}$$

After extracting $\Delta R_w(t)$ we obtain

$$\Delta R_w(t)=\frac{\frac{\Delta V(t)}{V_S}\cdot\left(R_{total}^2+2\cdot\Delta R_{short}(t)\cdot R_{total}\right)+2\cdot\Delta R_{short}(t)\cdot R_{LL}-\Delta R_{short}(t)\cdot R_{total}}{R_{total}-R_{LL}-R_{total}\cdot\frac{\Delta V(t)}{V_S}} \tag{4-11}$$

It is clear from the above equations that the precise calculation of the resistance change of a part of the infinitely long hot wire requires that the resistance change of the short part of the wire needs to be known. However, this would involve additional precise and complex transient voltage measurements at the terminal E. Therefore it has been investigated how the resistance change of the short wire influences the calculations. The short wire resistance change was expressed as a proportional change of the hot-wire resistance

$$\Delta R_{short}(t)=n\cdot S_L\cdot\Delta R_w(t) \tag{4-12}$$

where n is a real constant from interval <0;1> and S_L is the ratio between the short and long wire resistances measured at steady state. If $n = 0$, it is assumed that there is no temperature increase of the short wire during the experiment and all heat generated within the wire is transferred to contacts. The opposite case, $n = 1$, assumes that the short wire temperature change follows the temperature increase of infinite wire, i.e. no heat is transferred to the contacts (ends of the wire). Common sense suggests that the true value of n can be found somewhere between those extremes. Also it is reasonable

to conclude that longer the short wire is, the value n is closer to 1. In order to evaluate the importance of a proper setting of n, the equation (4-12) is substituted into equation (4-10) and $\Delta R_w(t)$ is written as

$$\Delta R_w(t) = \frac{\frac{\Delta V(t)}{V_S} \cdot R_{total}^2}{R_{total} - R_{LL} - R_{total} \cdot \frac{\Delta V(t)}{V_S} + n \cdot S_L \cdot \left(R_{total} - 2 \cdot R_{LL} - 2 \cdot R_{total} \cdot \frac{\Delta V(t)}{V_S} \right)} \tag{4-13}$$

and calculated for different n. The $\Delta R_w(t)$ is then plotted as a function of $\Delta V(t)$ and different values of n for the original and new design sensors at temperature 570 K (297 °C) are plotted in Figure 4.17.

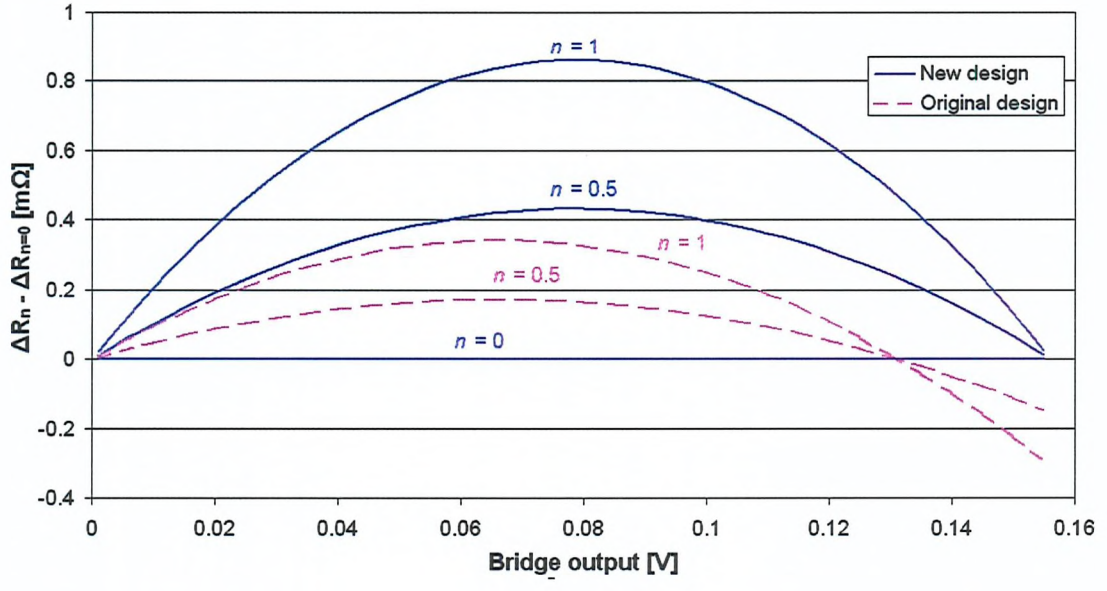

Figure 4.17 Absolute differences between several approaches for calculation of the hot-wire resistance at temperature 570 K (297 °C)

It can be seen that the differences between several approaches for the calculation of the resistance rise are less then 1 mΩ and it equates to a relative error of approximately 0.3 % of the total resistance. In previous works [13] the short wire resistance was experimentally evaluated by measurements of small voltage changes that the 'real' value of $\Delta R_w(t)$ was closer to the boundary for $n = 0$. However the accuracy of the small voltage measurements was not taken into account and the temperature, at which such tests were carried out, was not stated. The value of n greatly depends on the thermal

conductivity of the material around the hot wire and therefore it is expected to be greater at higher temperatures.

The analysis above, the experiments with infrared camera and the FE model of the hot-wire ends, which is illustrated in Figure 4.18, showed that n equals 1 just after the heat flux is applied on the hot wire and the value of n decreases with time. At the end of the first second of the transient run, n was found to be typically between 0.9 and 0.6 depending mainly on the thermal conductivity of the substrate material at given temperature.

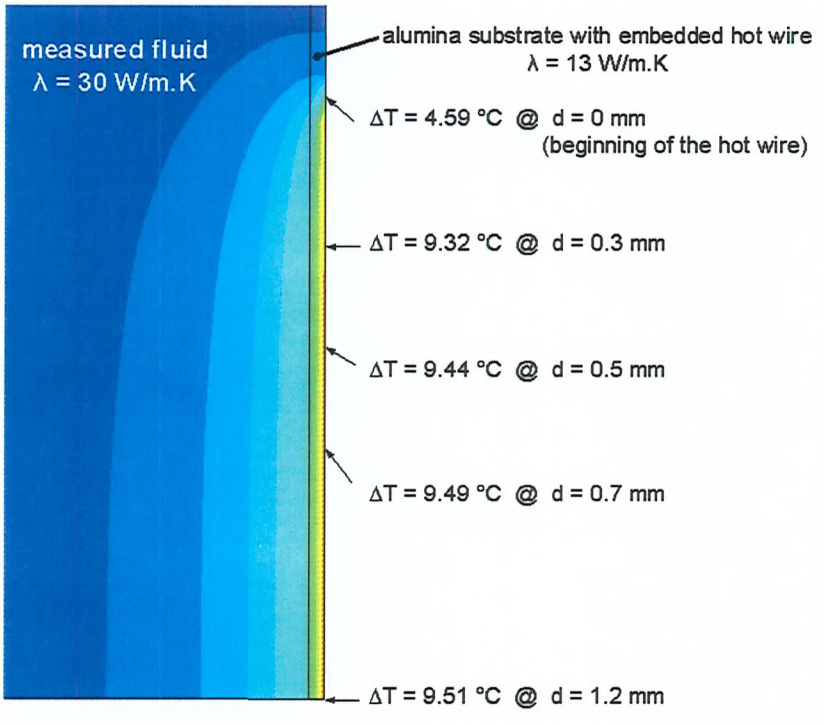

Figure 4.18 FE model of the thermal distribution at the end of the hot wire embedded in the substrate when the heat flux 100 $W \cdot m^{-1}$ applied for 1s

4.6.2. Extraction of Temperature Rise

The temperature rise of the hot wire is derived from several known or measured parameters. At the start of the temperature rise, $R_w(0)$ is known from steady-state measurements (equation (4-8)) as

$$R_w(0) = R_{long} - R_{short} = R_{long} \cdot (1 - S_L) \tag{4-14}$$

and it can be also evaluated using temperature coefficients of resistance as

$$R_w = R_w(0) = R_0 \cdot \left[1 + \alpha \cdot T_C(0) + \beta \cdot T_C(0)^2\right] \tag{4-15}$$

During the temperature rise, the hot-wire resistance is defined as

$$R_w(t) = R_0 \cdot \left[1 + \alpha \cdot T_C(t) + \beta \cdot T_C(t)^2\right] \tag{4-16}$$

The change of the hot-wire resistance is then given as

$$\begin{aligned} \Delta R_w(t) &= R_w(t) - R_w(0) = R_0 \cdot \left[\alpha \cdot (T_C(t) - T_C(0)) + \beta \cdot (T_C(t)^2 - T_C(0)^2)\right] = \\ &= R_0 \cdot \left[\alpha \cdot (T_C(t) - T_C(0)) + \beta \cdot (T_C(t) - T_C(0))^2 - 2 \cdot \beta \cdot T_C(t) \cdot T_C(0) - 2 \cdot T_C(0)^2\right] = \\ &= R_0 \cdot \left[(\alpha - 2 \cdot \beta \cdot T_C(0)) \cdot (T_C(t) - T_C(0)) + \beta \cdot (T_C(t) - T_C(0))^2\right] \end{aligned} \tag{4-17}$$

After substitution $\Delta T(t) = T_C(t) - T_C(0)$ and extraction of R_0 from the equation (4-15) the quadratic equation

$$\beta \cdot \Delta T(t)^2 + (\alpha - 2 \cdot \beta \cdot T_C(0)) \cdot \Delta T(t) - \frac{\Delta R_w(t)}{R_w(0)} \left(1 + \alpha \cdot T_C(0) + \beta \cdot T_C(0)^2\right) = 0 \tag{4-18}$$

can be solved and its sensible root is found as

$$\Delta T(t) = \frac{(2 \cdot \beta \cdot T_C(0) - \alpha) + \sqrt{(\alpha - 2 \cdot \beta \cdot T_C(0))^2 + 4 \cdot \beta \cdot \frac{\Delta R_w(t)}{R_w(0)} \left(1 + \alpha \cdot T_C(0) + \beta \cdot T_C(0)^2\right)}}{2 \cdot \beta} \tag{4-19}$$

This calculation is straightforward and that is why the accuracy of the temperature rise $\Delta T(t)$ fully depends on the correctness of the temperature coefficients of resistance, preciseness of the temperature and resistance measurements at steady state and accuracy of the resistance change calculations. All of them were described and discussed in the previous sections of this chapter. A typical example of a final transient temperature response acquired from the sensor is illustrated in Figure 3.6.

4.7. Heat Input Calculation

Two approaches may be used for the calculation of the heat flux which is applied on the hot wire during the experiment. The first approach works with an assumption that the change of the hot-wire resistance is negligibly small and does not significantly influence the overall value of the electrical current through the electronic bridge arm. The heat flux can be then written as

$$q = \frac{V_S^2 \cdot R_w}{R_{total}^2 \cdot l_w} \tag{4-20}$$

It has been proved [13] that if resistances R_1 and R_2 in the bridge arm are set appropriately, the value of the heat flux varies by about 0.04%, which is more than adequate for our purpose.

Alternatively the heat flux can be calculated even if the resistance boxes R_1 and R_2 cannot be set high enough to provide unchanging electrical current. In that case the value of heat flux can be evaluated as

$$q(t) = \frac{V_S^2 \cdot \left(R_{long} - S_L \cdot R_{long} + \Delta R_w(t)\right)}{\left(R_{total} + \Delta R_w(t) + n \cdot S_L \cdot \Delta R_w(t)\right)^2 \cdot l_w} \tag{4-21}$$

It should be also mentioned that especially at elevated temperatures the resistance R_2 can be totally removed from the circuit because the overall resistance of the balanced bridge is high enough to provide an almost constant electric current through the hot wire. A detail analysis and description of the heat flux calculation can be found in previously published works [13, 86].

4.8. Discussion and Error Analysis

All calculations in the previous chapters work with an assumption that the both short and long parts of the hot wire have identical cross-sectional area and therefore the same electric resistivity, i.e. electric resistance per unit length. The influence of the geometry differences between short and long hot wire were investigated by Kestin and Wakeham [86] and the temperature correction was introduced as

$$\Delta T_{\mathrm{corr}}(t)=\frac{\Delta T(t)}{1+\varepsilon} \tag{4-22}$$

where

$$\varepsilon=\frac{R_{\mathrm{short}}}{R_{\mathrm{long}}-R_{\mathrm{short}}}\cdot\frac{1+\ln\left(\frac{4\cdot a\cdot t}{r^2e^{\gamma}}\right)}{\ln\left(\frac{4\cdot a\cdot t}{r^2e^{\gamma}}\right)}\cdot\left(1-\frac{R_{\mathrm{short}}\cdot l_{\mathrm{long}}}{R_{\mathrm{long}}\cdot l_{\mathrm{short}}}\right) \tag{4-23}$$

Kestin and Wakeham [86] investigated a set of 150 mm long wires with diameter from 5 μm to 10 μm and found that their resistance might have differed by as much as 4 % although the wires were taken from the same roll. They also stated typical values of ε for the hot wires to be at most 0.02, which resulted in the deviation of the temperature rise to be less than 2 %. It should be noted that a is an approximated value of the thermal diffusivity of the material surrounding the hot wire.

For our purposes the conclusions stated by Kestin and Wakeham and the temperature correction cannot be fully applied because the hot wire is buried in a sintered alumina substrate, which disallows accurate length measurements and subsequently introduces error into the calculation of the temperature correction. However it is likely that the hot wire used in our experiment do not exhibit as large deviations as observed by Kestin and Wakeham because the overall hot-wire length is about 70 mm to 80 mm for the original sensor design and 100 mm to 110 mm for the new design, which decreases the possibility of greater change of the wire diameter. Furthermore the platinum wire is 25 μm in diameter, which is easier to manufacture with a more uniform diameter over the length. Therefore it has been decided not to use such a correction and all transient

voltage responses are transformed into temperature rises with an assumption that the diameter of the hot wire is the same over the whole length.

It has been shown above that the temperature rise of the hot wire is calculated from the following measured variables:

- temperature at steady state (averaged value of two thermocouples with accuracy ±2 °C)
- resistances at steady state (Keithley 2000 digital multimeter 4-wire resistance, uncertainty approximately ±0.015 %)
- ratio between short and long wire resistances (approximately ±0.03 %)
- length of the encapsulated hot wire (less than ±0.2 %)
- temperature coefficients of resistance (taken from European standard EN 60751:1995 [85], error estimated to ±0.5 %)
- transient voltage acquired from the electronic bridge (exact accuracy unknown, background noise of amplified voltage ±5 mV, error estimated to less than ±0.1 %)
- supply voltage (Keithley 2000 digital multimeter with 28-bit A/D converter, uncertainty ±0.005 %)

The overall error of the measurement of the temperature rise can only be estimated because there are many input variables which may not be accurately evaluated. However an approximate magnitude of the overall experimental error can be evaluated from the data presented above using basic rules of propagation of errors. It can be concluded that the overall uncertainty of the measured temperature rise is less than ±1 % and it mainly originates from inability to accurately measure the absolute temperature and geometric and material properties of the hot wire (the cross-sectional area, the length and the temperature coefficients of resistance).

5. Results

The chapter summarizes all measured data obtained during the course of the project. Various metals or alloys have been studied at temperatures from their melting points up to 750 K which is the maximum temperature possible for the application of the current sensor fabrication technology. The thermal conductivity of the alumina substrate, in which the hot wire is embedded, is firstly discussed and then the thermal conductivity data for pure tin, indium and lead are presented. Additionally four metallic alloys were also investigated and in a later section the results are discussed.

5.1. Alumina Substrate

The thermal properties of the alumina substrate are unknown prior to any of the measurements conducted here because the properties of the material are determined in a significant way by its heat treatment and purity so that they cannot be taken from a handbook. On the other hand these properties are essential for accurate extraction of the thermal conductivity of the measured fluid. Our THW technique and the experimental set-up allow accurate measurements of the thermal parameters of the substrate as has been presented in section *3.3.6.Material Properties Measurements*. The thermal conductivity of the sintered alumina material has been measured individually for every sensor and Figure 5.1 illustrates the data obtained from the measurements with sensors of both the original and new design. The red trend line in the figure represents a typical temperature dependence of the thermal conductivity of the sintered alumina tape in the temperature range studied. The thermal conductivity of alumina decreases with the temperature rather significantly from 20 $W \cdot m^{-1} \cdot K^{-1}$ at room temperature to about 12 $W \cdot m^{-1} \cdot K^{-1}$ at 475 K (200 °C). It can be seen in Figure 5.1 that further temperature increase imposes a smaller decrease of the thermal conductivity to about 8 $W \cdot m^{-1} \cdot K^{-1}$ at 725 K (450 °C).

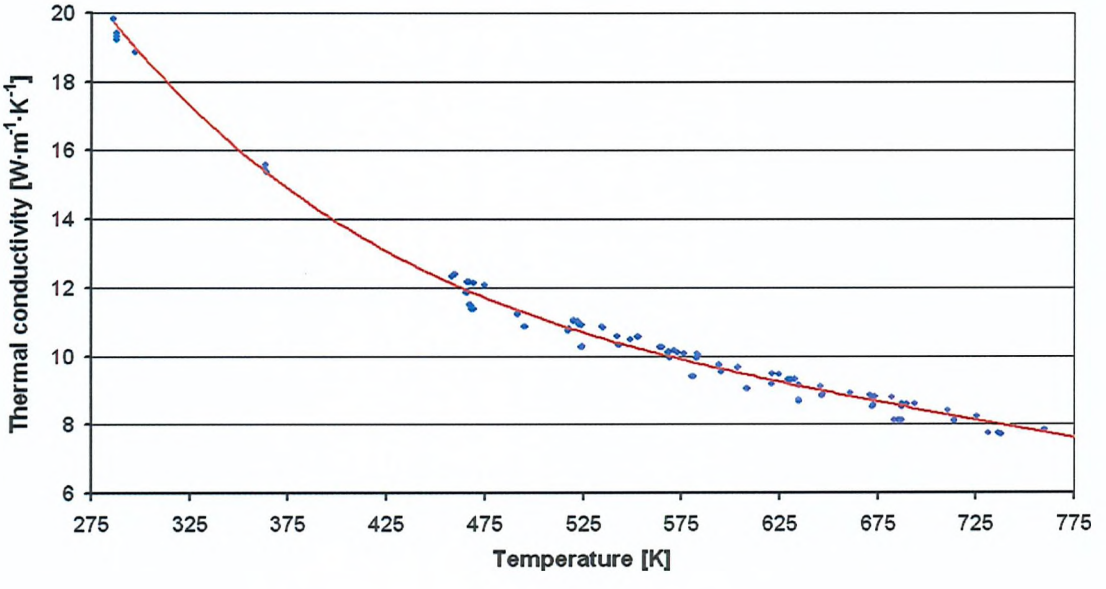

Figure 5.1 Thermal conductivity of the sintered alumina substrate

The temperature dependence of the thermal conductivity can be generally used to represent that of any substrate, which is manufactured using the same alumina tape. However, it has been found during the measurements that the absolute value of thermal conductivity of individual substrates can differ by up to about ±6 % from the trend line. Such a relatively large variation can be explained by small differences in applied curing profiles and the usage of different amounts of zirconium powder during each sintering process.

The knowledge of the thermal conductivity of the alumina substrate as a function of the temperature is also used to improve the accuracy of the FE model. The temperature increase of the hot wire imposes a temperature increase on the alumina substrate and it results in slightly lower thermal conductivity of the substrate. The FE model is able to accommodate the temperature dependence of the thermal conductivity hence the FE model is even more realistic. The effect of the temperature increase on the thermal conductivity of the substrate is not very big at small temperature gradients but once a wide range of heat fluxes is applied and the temperature rise of the wire is more than 5 K, this feature of the FE model is necessary especially at temperatures below 575 K (approx 300 °C).

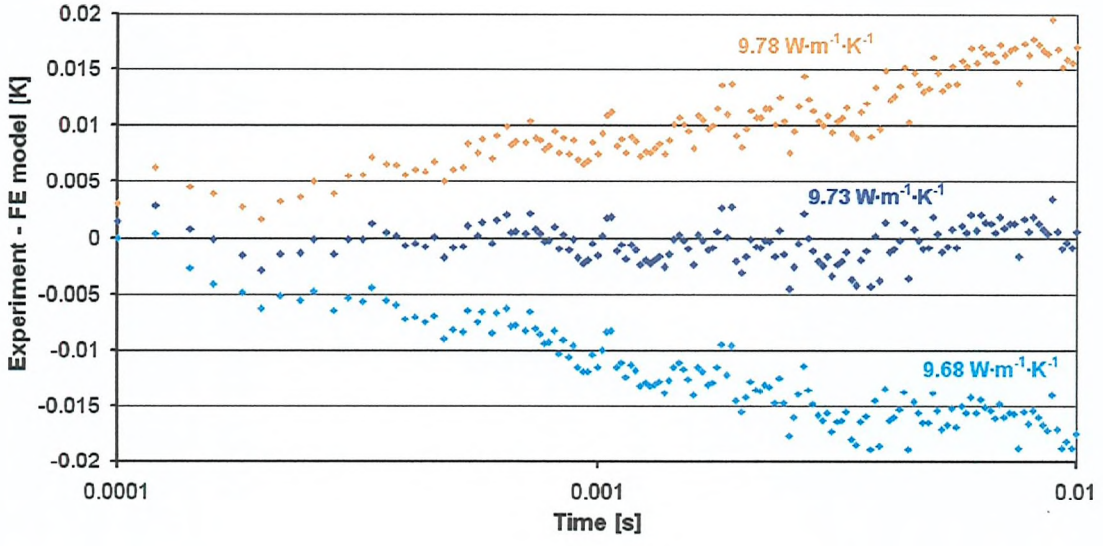

Figure 5.2 Sensitivity of the measurements of the thermal conductivity of the alumina substrate (sensor B5 at temperature 654 K, applied heat flux 80 $W \cdot m^{-1}$)

The ability of the method to derive a highly accurate value of the thermal conductivity of the substrate is demonstrated in Figure 5.2. It can be observed that the change of the substrate thermal conductivity by only 0.5 % results in clearly distinguishable differences in the discrepancy between the experimental temperature and that observed experimentally in the time region from 0.1 ms to 10 ms.

The other two thermal parameters of the sintered alumina, density and specific heat capacity, cannot be extracted from the temperature rise with such high accuracy and only their product, $\rho \cdot C_P$, can be identified with a certain degree of confidence. In our analysis, the derived value of $\rho \cdot C_P$ is typically between 3.4 $MJ \cdot m^{-3} \cdot K^{-1}$ and 3.6 $MJ \cdot m^{-3} \cdot K^{-1}$ at 475 K (200 °C) and rises slightly with temperature to about 3.8 $MJ \cdot m^{-3} \cdot K^{-1}$ at 750 K (450 °C). These values are quite typical of the values obtained from several suppliers of solid alumina substrates as is shown in Table 5.I. The table also shows that less dense and less pure alumina substrate provides lower thermal conductivity. In our case the inferior purity is caused by lower sintering temperature.

Table 5.I Thermal properties of alumina at room temperature (about 295 K)

Supplier	*Material*	λ $[W \cdot m^{-1} \cdot K^{-1}]$	ρ $[kg \cdot m^{-3}]$	C_P $[J \cdot kg^{-1} \cdot K^{-1}]$	$\rho \cdot C_P$ $[MJ \cdot m^{-3} \cdot K^{-1}]$
Goodfellow	Alumina - Al_2O_3	26 - 35	3900	850 - 900	3.32 - 3.51
Coorstek	96% Alumina	24.7	3720	880	3.27
Coorstek	94% Alumina	22.4	3700	880	3.26
Coorstek	90% Alumina	16.7	3600	920	3.31

5.2. Pure Materials

Almost all materials, which are investigated in this section, were inherited from previous research at Imperial College London. At the beginning of the current work, it was decided not to use any potential hazardous materials, such as mercury or gallium, in order to ease health and safety requirements on the measuring equipment and procedures. This decision narrowed the choice of materials to tin, indium and lead. Although lead was also investigated during the research at Imperial College London, its thermal conductivity has not been published and the data are not available. Therefore only the thermal conductivity of pure tin and indium can be compared to the values previously measured with a similar, but not identical experimental configuration. The material purities have not been measured and data from original suppliers are used instead.

The measurements of the thermal conductivity of each metal requires about five days. During the first day the sensor is placed in the furnace, the metal is brought into the liquid phase and the sensor is immersed within it. At the end of the first day, the first temperature point can be measured. The sensor is left in contact with the molten metal overnight and from three to five temperature points are measured the following day. This process is repeated on successive days until the desired temperature range is investigated and the last day is reserved for cooling the furnace chamber back to room temperature. Such a measurement protocol puts high requirements on the sensor and its contacts and that is why the mechanical and electrical performance of the sensor must be checked after every experiment.

It has been found that it is not desirable to replace the sensor on the support rod unless it is damaged because the nickel wiring looses its mechanical strength when exposed to high temperatures and becomes extremely difficult to manipulate. Furthermore one sensor can usually only be used to measure two or three molten metals before it is damaged. After every cycle of measurements, the residues of the metal or a thin oxide layer occur on the surface of the sensor and they have to be cleaned before any following measurements. The cleaning process necessarily imposes mechanical stress on the sensor and its contacts and this may result in damaging the sensor or its wiring.

The procedure for the extraction of the thermal conductivity from the measured responses of the sensor has been presented in section *3.3.6.Material Properties Measurements*. The ability of the method to derive highly accurate values of the thermal conductivity is demonstrated in Figure 5.3. In this figure, taken from measurements on molten lead at 682 K, it can be seen that changes in the thermal conductivity of molten lead of 1% can easily be discerned in the deviation plot between simulation and experimental temperature rises at long times. This is indicative both of the sensitivity of the measurements and the precision with which it can be determined from the measurements.

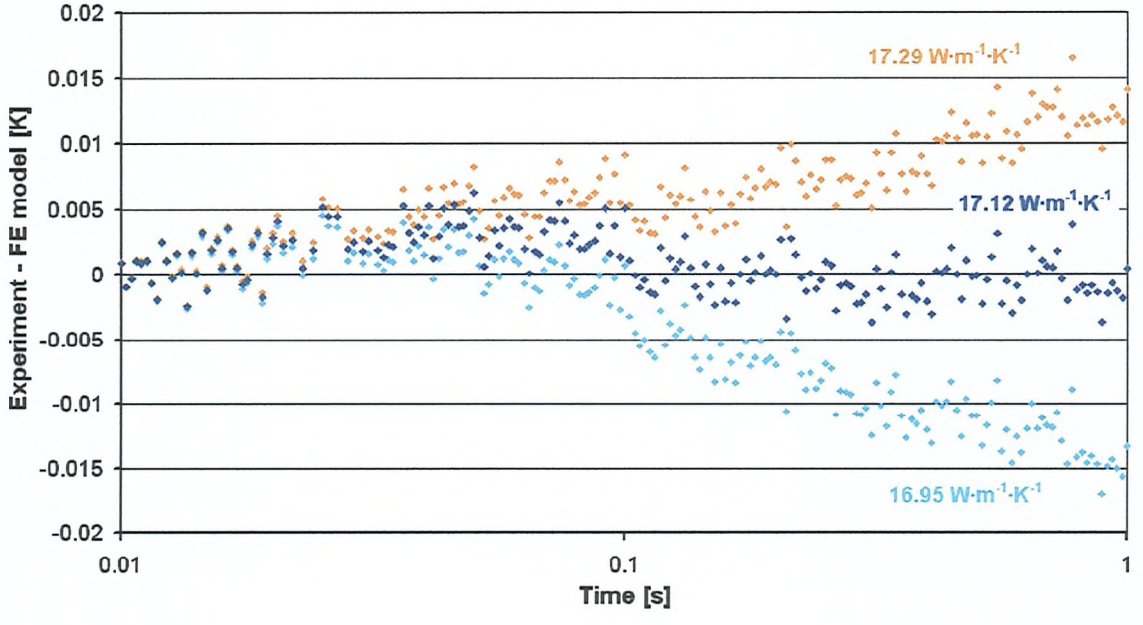

Figure 5.3 Sensitivity of the measurements of the thermal conductivity of the molten lead (sensor B5 at temperature 682 K, applied heat flux 79 W·m^{-1})

This relative sensitivity can be achieved by our technique for any measured molten material if the newly designed sensor is used. However, it should be noted, that the sensitivity is also linearly dependent on the heat flux that is applied on the hot wire and the length of the hot wire, i.e. the differences shown in Figure 5.3 will not be so clear if a lower heat flux is applied to the hot wire. Measurements such as those contained in Figure 5.3 were repeated for each fluid in order to estimate the precision of the measurements.

The following sections present the results from the measurements of the thermal conductivity of three pure molten metals and four metallic alloys. In most experiments, about six temperature responses of the hot wire are acquired from one sensor at one temperature with a variation of heat fluxes from 45 $W \cdot m^{-1}$ to 85 $W \cdot m^{-1}$ across the sequence of runs. The different applied heat fluxes result in different temperature rises of the hot wire and are typically from about 3 K to approximately 7 K depending on the temperature and the thermal conductivity of the measured metal.

It has been observed that the thermal conductivity derived from such different responses varies typically by no more than ±1 %. If more sensors, with both new and original design, are used to measure the same metal, the values of the thermal conductivity obtained from all sensors are typically within ±2 %. The influence of the temperature gradient within the measured sample, which is employed in order to suppress the convectional flow, has been calculated as $d\lambda/dT$. The applied gradient along the hot wire is always below 5 K and the imposed relative error has been evaluated to less than 0.5 % for all metals at all temperatures.

After evaluation of other possible deviations, which originate from the FE model (section *3.4.Discussion*) and the experimental configuration (section *4.8.Discussion and Error Analysis*), it has been estimated that the total uncertainty of our technique is one of approximately ±3 %. This uncertainty region encompasses all currently known deviations and errors, both systematic and random, which may occur during the measurements of the thermal conductivity of molten materials using the described THW technique, and is supported by a large number of experiments, which were carried out throughout the period of the postgraduate research. All the measured values of the thermal conductivity presented in the sections below are accompanied with error bars, which illustrate the ±3 % accuracy band.

The results are also accompanied with the data of the thermal conductivity experimentally measured by other researchers. All the methods for the measurements of the thermal conductivity used by other researchers have been introduced and discussed in chapter *2.Methods for the Measurements of the Thermal Conductivity*. A separate comparison is also made with so-called 'recommended values', i.e. the data which have been based on a critical review and evaluation of all the thermal conductivity values reported at a particular time. These data are usually defined with a rather large uncertainty and their accuracy cannot be assessed because the methodology behind this estimate is usually

unknown. When the recommended values are used in the figures below, they are distinguished by an asterisk.

The recommended values of the thermal conductivity published by Mills [72], Ho [71] and Touloukian [70] are illustrated in figures together with the thermal conductivity calculated using Wiedemann-Franz (W-F) law. This law was first originated in the second half of the 19th century and is still used for the estimation of the thermal conductivity of metals owing to the difficulty of measurement. The W-F law is based upon a simple approximate theory for perfect crystals of solid metals but also represents the only available theoretical approach to the molten state metals. In the theory of metals, in the solid state, the thermal conductivity is assumed to have two distinct contributions, the electronic and phonon contribution. The electronic contribution arises from heat transport by electrons, the phonon contribution from heat transfer by the ions in a lattice. For the case of pure metals it is considered that the thermal conductivity is mainly attributed to the free motion of electrons so that the thermal conductivity is related to the electrical conductivity. The W-F law then states that

$$L_0 = \frac{\lambda}{\sigma \cdot T} = 2.445 \cdot 10^{-8} \quad V^{-2} \cdot K^{-2} \tag{5-1}$$

where L_0 is the Lorentz number and σ is electrical conductivity of the molten metal at temperature T. The more comprehensive theory, which leads to equation (5-1), can be found in a good overview of the W-F law given by Peralta [13]. However it should be emphasized that the W-F law has never been fully validated for liquids and in particular molten metals at high temperatures owing to difficulties of the evaluation of the thermal conductivity by other means.

5.2.1. Indium

The indium used for the measurements was supplied by Lowden Metals Ltd with a stated purity of 99.99 %. Indium has the lowest melting point of all the metals that have been investigated, i.e. 156.6 °C ($T_{m,\,In}$ = 429.8 K). The thermal conductivity of indium has been extracted from the transient responses of the sensor measured at temperatures from 450 K to 750 K. The density and specific heat capacity data for molten indium has been obtained from several sources [70, 87-89] and they are illustrated in Figure 5.4 and Figure 5.5.

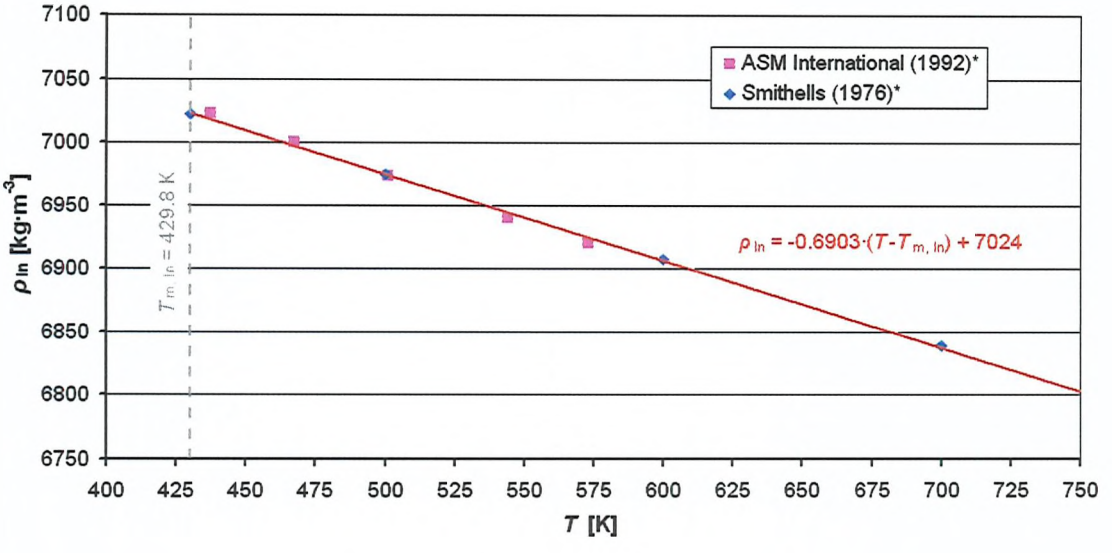

Figure 5.4 Density of molten indium

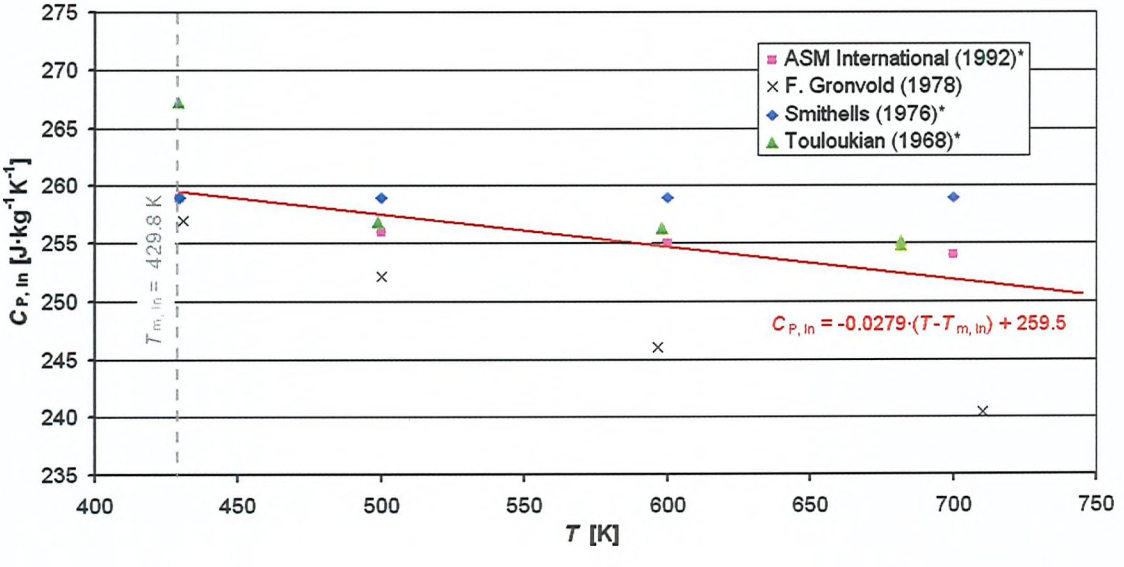

Figure 5.5 Specific heat capacity of molten indium

It can be seen that the data for pure molten indium show relatively large deviations, in particular specific heat capacity values vary up to ±4 % from an average value. That is why the trend lines are added into the figures and the equations of the trend lines are used to describe material properties of the molten indium in the FE model. These approximations allow evaluation of the product $\rho \cdot C_P$ at any temperature within the studied range. The uncertainty of the product $\rho \cdot C_P$ for molten indium is estimated as ±5 % and it may introduce an uncertainty of about 0.8 % into the measurements of the thermal conductivity of the molten indium (refer to section *3.4.Discussion* for explanation). However this uncertainty has been incorporated within the overall ±3 % accuracy region which was discussed above.

Table 5.II Thermal conductivity of molten indium as a function of temperature

T [K]	T [°C]	λ_{In} [W·m^{-1}·K^{-1}]
467.0	193.8	**36.3**
495.4	222.2	**37.0**
522.2	249.0	**38.2**
575.9	302.8	**40.0**
608.8	335.7	**41.4**
630.2	357.1	**42.2**
684.5	411.3	**44.0**
711.0	437.8	**44.4**
734.1	461.0	**45.3**

The measured values of the thermal conductivity of the molten indium are listed in Table 5.II. The table contains the average values of the thermal conductivity as a function of temperature obtained from experiments with four sensors (three sensors with original design and one newly-designed sensor). The average thermal conductivity values are used to define a linear trend line, which represents the rise of the thermal conductivity of molten indium within the studied temperature range. The equation of the linear trend line, which is valid for temperature T from 430 K to 750 K, is written as

$$\lambda_{In} = 0.0345 \cdot (T - T_{m,In}) + 35.0 \quad \text{W·m}^{-1}\text{·K}^{-1} \tag{5-2}$$

The trend line and the values from Table 5.II are illustrated in Figure 5.6 together with previously measured values published by Peralta [11], Goldratt [22], Duggin [20] and Yurchak [45]. The measured thermal conductivity reported here is generally up to 5 %

lower than the values by Peralta [11], who used the same THW sensor with the original design of the sensor but different configuration of the FE model. The differences in the measured thermal conductivity from this work are also found for the results obtained for pure tin and they will be discussed in detail later in section *5.4.Discussion*.

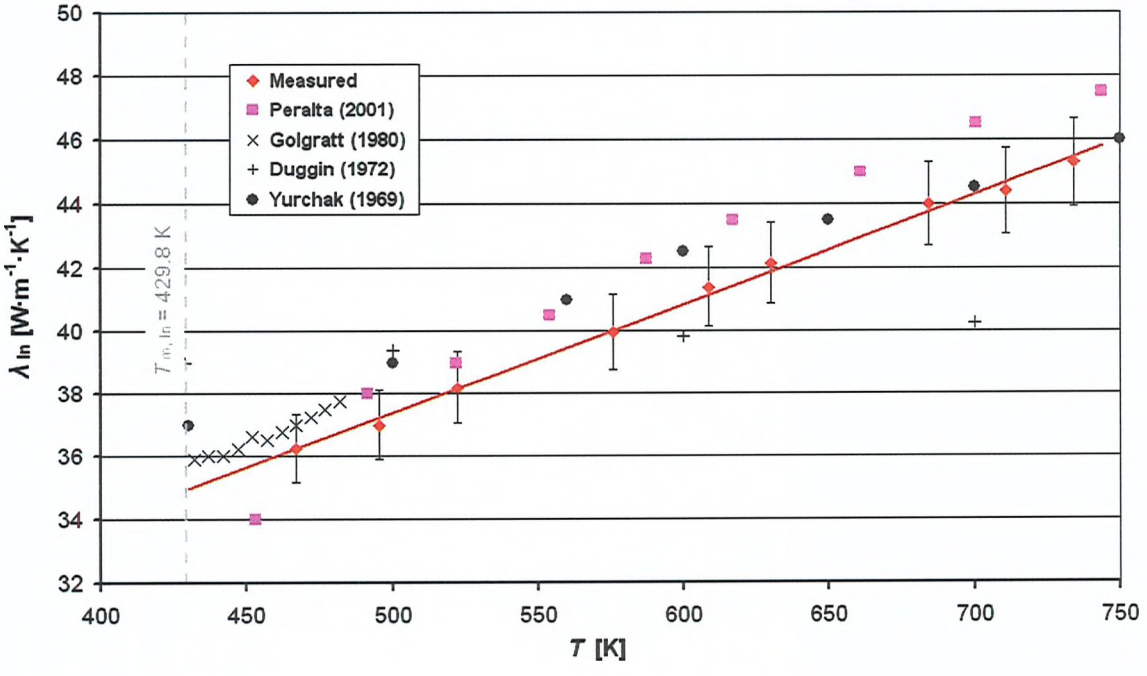

Figure 5.6 Thermal conductivity of molten indium as a function of temperature

If the measured values are compared to other available data for molten indium, good agreement with Goldratt [22], who claimed accuracy of ±1%, can be observed. Data published by Yurchak [45], who estimated the experimental error to approximately 4 %, can be found within the 5 % region. The thermal conductivity of molten indium presented by Duggin [20], who used an axial flow method, is an approximation of the data of very large scatter of up to ±4 W·m^{-1}·K^{-1} (10 %). It can be concluded that the measured values in this work do not disprove the data from previous works and at the same time offer a higher accuracy of ±3 % over a wide range of temperatures.

Figure 5.7 then presents a comparison with recommended values of the thermal conductivity. Touloukian [70] estimated uncertainty of the thermal conductivity of molten indium to 10 %, Ho [71] suggested even higher uncertainty of 15 % and data recommended by Mills [72] were given without specific uncertainty. The W-F law for molten indium has been calculated using average values of electrical resistivity

published by Dyos [90] for pure molten indium and their uncertainty is estimated to less than 5 %. It can be seen in Figure 5.7 that all the recommended values are within ±8 % of the measured thermal conductivity and the values calculated using W-F law can be found within the 3 % region of the measured results at temperatures above 500 K.

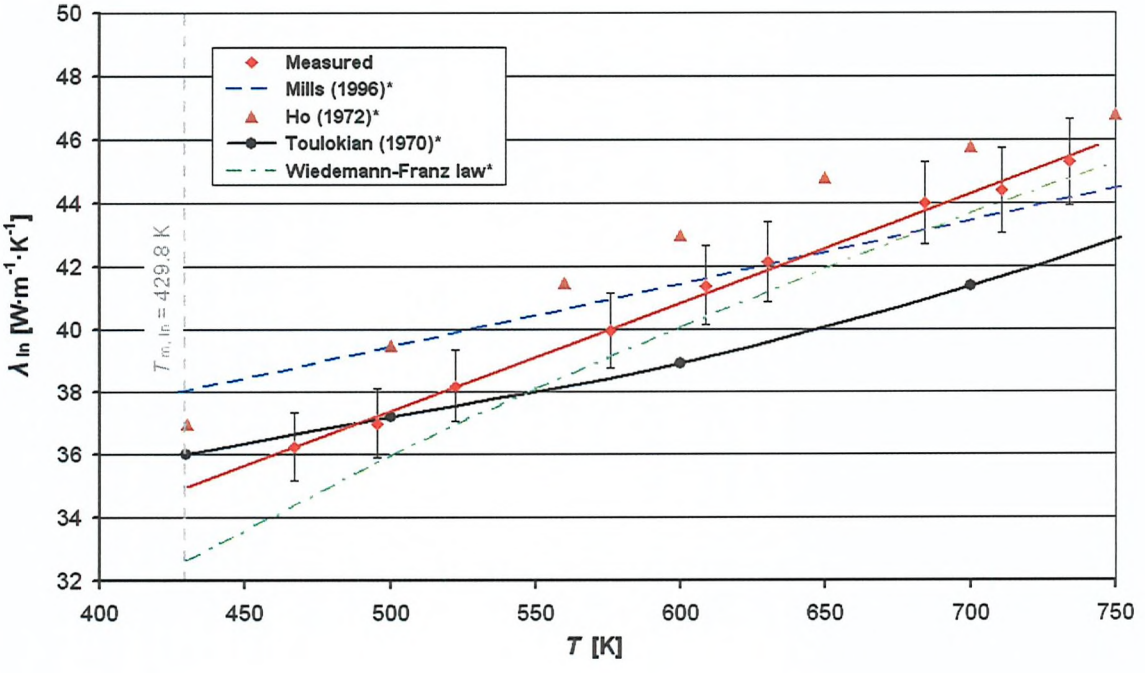

Figure 5.7 Thermal conductivity of molten indium (comparison with recommended values)

5.2.2. Tin

Two different samples of pure tin were used for measurements of its thermal conductivity in the liquid phase. The first sample was tin inherited from the previous research in Imperial College London and was supplied by MCP with a stated purity of 99.99 %. The second sample was supplied by The Solder Connection Ltd and again the purity stated by the supplier was 99.99%. Pure tin has a melting point at 232 °C ($T_{m,\,Sn}$ = 505.1 K) and the transient responses of the sensor have been measured from about 520 K to 750 K.

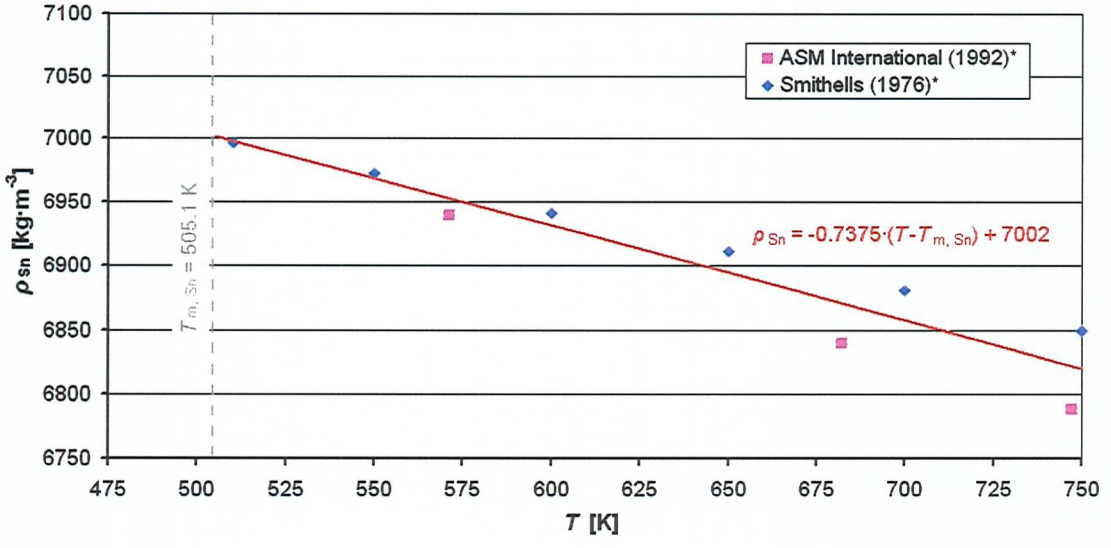

Figure 5.8 Density of molten tin

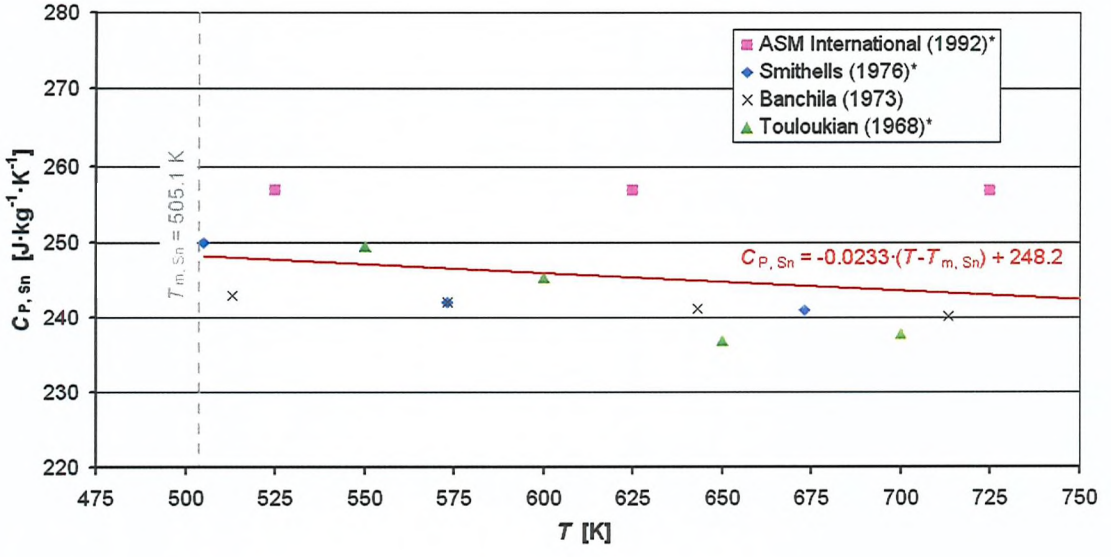

Figure 5.9 Specific heat capacity of molten tin

The data available for the calculation of the product $\rho \cdot C_P$ for pure tin [26, 70, 87, 88] are illustrated in Figure 5.8 and Figure 5.9. In a similar manner to that observed for molten indium, the calculated product $\rho \cdot C_P$ for the molten tin shows deviation within the range of ±6 %, which may result in an uncertainty of the measured thermal conductivity by about ±1 %. Again this value is well within the overall accuracy region of ±3 %.

Two sensors with the original design and one newly designed sensor were used to analyse the thermal conductivity of liquid tin. Table 5.III lists average values of the measured thermal conductivity of molten tin as a function of temperature.

Table 5.III Thermal conductivity of molten tin as a function of temperature

T [K]	T [°C]	λ_{Sn} [$W \cdot m^{-1} \cdot K^{-1}$]
523.1	249.9	**27.3**
549.2	276.0	**28.0**
580.0	306.8	**28.6**
603.7	330.6	**29.1**
634.9	361.8	**30.0**
657.0	383.8	**30.6**
683.8	410.7	**31.4**
707.6	434.4	**31.9**
733.2	460.1	**32.5**

The measured values of the thermal conductivity are also shown in Figure 5.10 and a linear trend line was found adequate to characterise the rise of the thermal conductivity of molten tin with temperature. The equation of the trend line can be written for temperatures T from $T_{m,Sn}$ to 750 K as

$$\lambda_{Sn} = 0.025 \cdot (T - T_{m,Sn}) + 26.8 \quad W \cdot m^{-1} \cdot K^{-1} \tag{5-3}$$

The values of the thermal conductivity for molten tin show large deviations from the values published by Sklyarchuk [14] and Osipenko [16]. They both used steady-state techniques and estimated the uncertainty to 7 % and 5 % respectively. The scale of deviations suggests that they both were probably not able to control the convective flow within the molten tin. On the contrary, values published by Hemminger [17], who also used steady-state technique, are found within the ±3 % accuracy region presented here and this leads to the assumption that Hemminger was able to suppress the convectional

flow experimentally and evaluate suitable correction for the radiative heat transfer. Yamasue et al [69] used a modified transient hot-wire technique and reported even lower values of the thermal conductivity of molten tin but they stated the standard deviation of their experiment up to 2.5 $W \cdot m^{-1} \cdot K^{-1}$, i.e. almost 10 %. However the deviations of the measured thermal conductivity from the values obtained by Peralta [11], of about 3 $W \cdot m^{-1} \cdot K^{-1}$, are found to be the most alarming because she used the same instrument and similar technique to the one presented in this work. A detail analysis of such departures will be carried out later in section *5.4.Discussion*.

It can be concluded that the measured thermal conductivity of molten tin does not show as good agreement with other researchers as presented for molten indium. However, the measured data are supported by measurements of two independent samples and usage of three different transient hot-wire sensors. Despite such variations in the set-up, the measurements have still resulted in the same overall uncertainty of ±3 %.

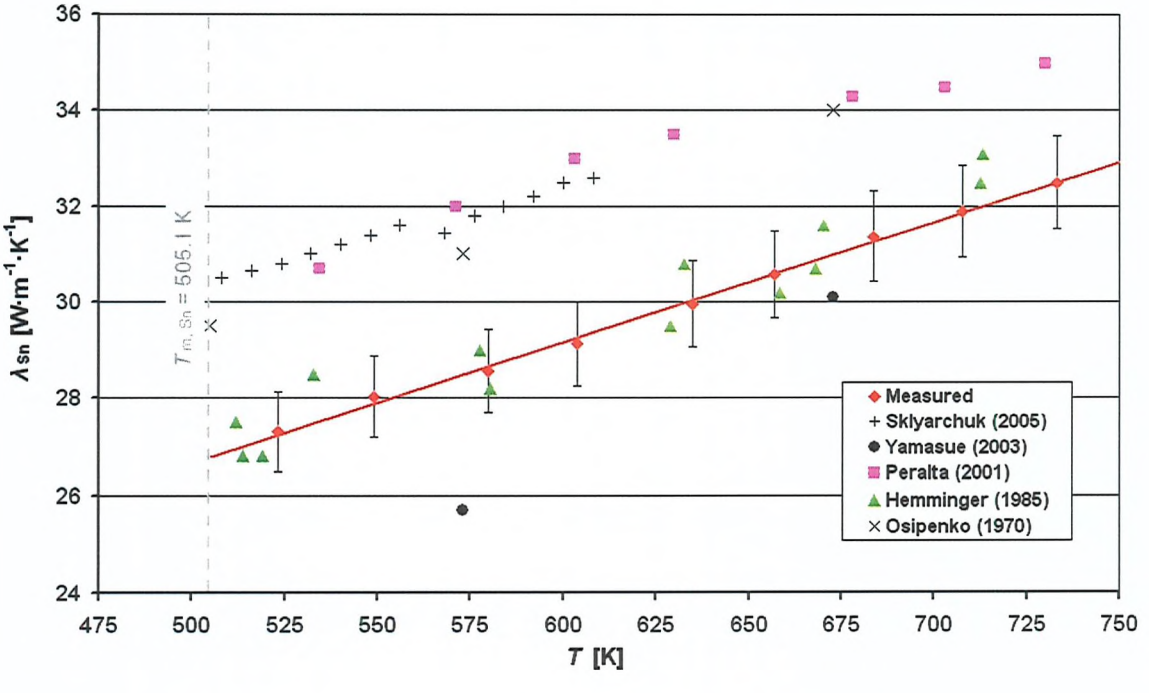

Figure 5.10 Thermal conductivity of molten tin

Figure 5.11 illustrates a comparison of the measured thermal conductivity with recommended values. Touloukian [70] estimated uncertainty of the thermal conductivity of molten tin to 15 %, Ho [71] stated that the accuracy is 'probably good to ±5 % near the melting point, but an increasing uncertainty to be resolved at higher temperatures'

and data recommended by Mills [72] were given without specific uncertainty. The W-F law has been calculated using the electrical resitivity as a function of temperature published by Monaghan [91] who estimated an uncertainty of his method to approx. ±3 %.

It can be seen in Figure 5.11 that data recommended by Touloukian [70] and Ho [71] are identical and differ significantly from the other two recommended functions. Both the W-F law and Mills [72] then show very good agreement with the measured values of the thermal conductivity of molten tin and the differences are at most ±3 %.

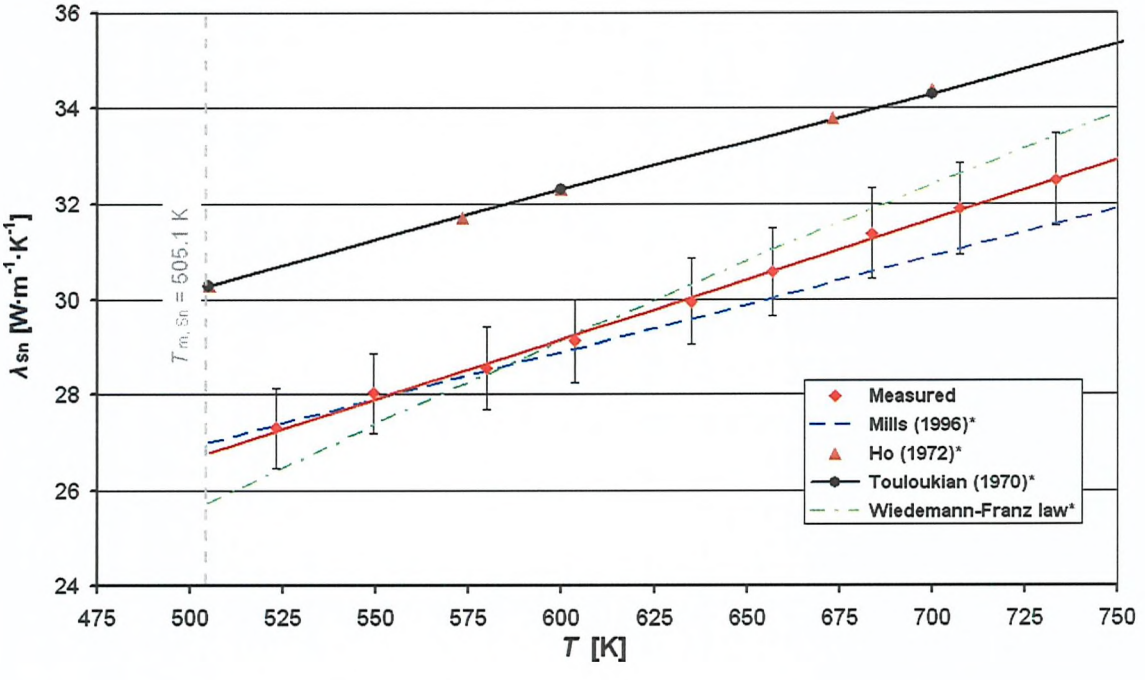

Figure 5.11 Thermal conductivity of molten tin (comparison with recommended values)

5.2.3. Lead

The lead used for the measurements was supplied by MCP with a purity of 99.99 %. The temperature of the melting point of the pure lead is 327.6 °C ($T_{m,\,Pb}$ = 600.7 K) and the transient responses of the sensor have been measured from about 615 K to approx. 750 K. Figure 5.12 and Figure 5.13 illustrate the data, which are used for calculation of $\rho \cdot C_P$ for molten lead at studied temperatures [87, 88, 92]. The uncertainty of $\rho \cdot C_P$ is at most ±5 %, which may result in a contribution of about ±0.8 % to the uncertainty in the measured thermal conductivity.

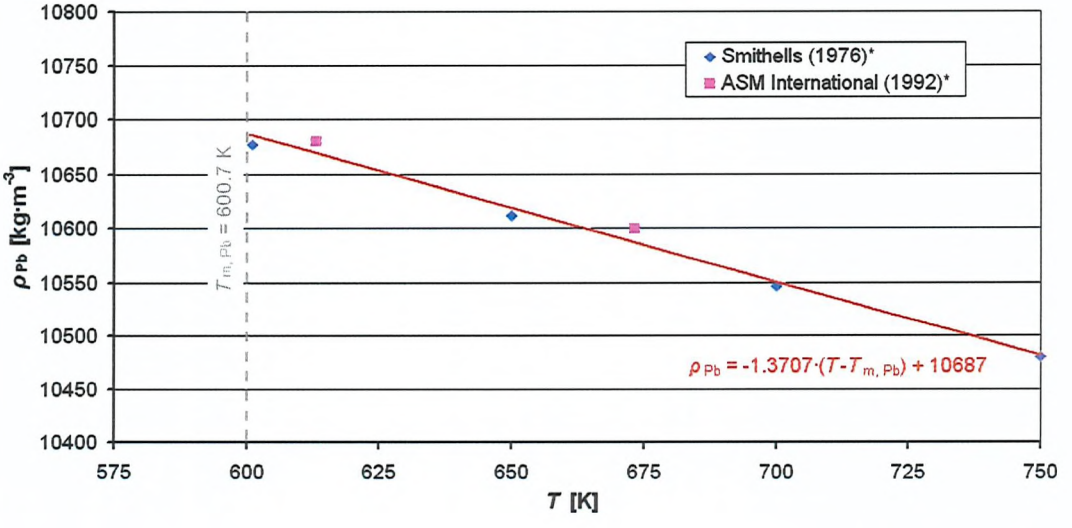

Figure 5.12 Density of molten lead

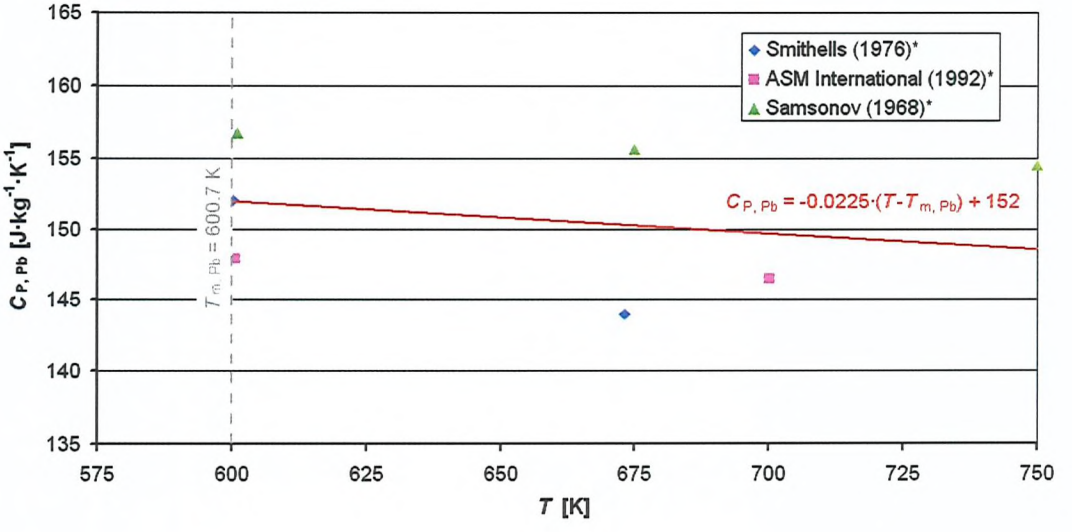

Figure 5.13 Specific heat capacity of molten lead

Two newly designed sensors were used to determine the thermal conductivity of liquid lead. Table 5.IV lists average values of the measured thermal conductivity of molten lead at specific temperatures and Figure 5.14 graphically represents the data from the table.

Table 5.IV Thermal conductivity of molten lead as a function of temperature

T [K]	T [°C]	λ_{Pb} [W·m^{-1}·K^{-1}]
620.3	347.1	**16.2**
678.1	404.9	**17.0**
729.5	456.3	**17.6**

In a similar way to that observed for the molten indium and molten tin, a linear trend line was found to be adequate to characterise the rise of the thermal conductivity of molten lead with temperature and its equation valid for T from 600 K to 750 K can be written as

$$\lambda_{Pb} = 0.0128 \cdot (T - T_{m,Pb}) + 15.95 \quad \text{W·m}^{-1}\text{·K}^{-1} \tag{5-4}$$

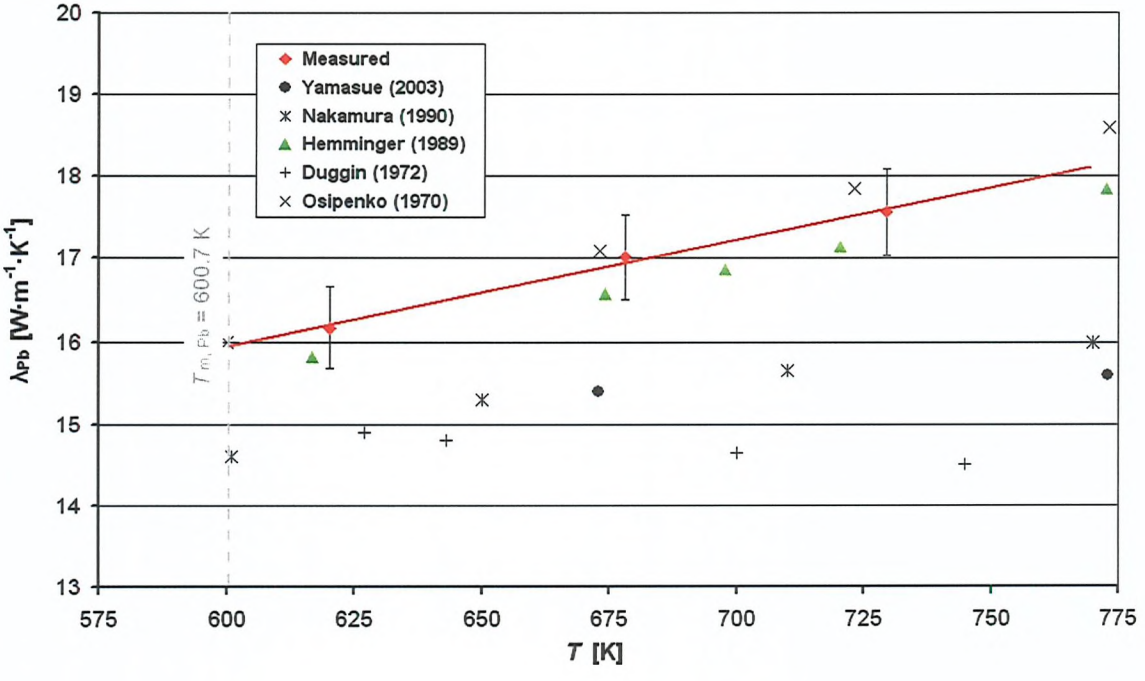

Figure 5.14 Thermal conductivity of molten lead

The measured values are in a very good agreement with the thermal conductivity data published by Hemminger [19] and Osipenko [16] who both used steady-state methods and stated uncertainty of ±3 % and ±5 % respectively. Values published by Yamasue et al [69], who employed a transient hot-wire instrument, are much lower but the standard deviation of their experimental values was 1.2 $W \cdot m^{-1} \cdot K^{-1}$. Moreover their method suffers many potential uncertainties as discussed in section *3.2.Modified Techniques*. Nakamura et al [66] also used an instrument based on the transient hot-wire method but they employed simplified analytical equations and did not evaluate the accuracy of the technique. And finally the data published by Duggin [20] differ significantly from all other sources, because his results suggest that the thermal conductivity of molten lead should be decreasing with the increasing temperature rather than increasing. The values cannot be accepted with confidence also because of their very large scatter of almost ±8 % of the measured thermal conductivity.

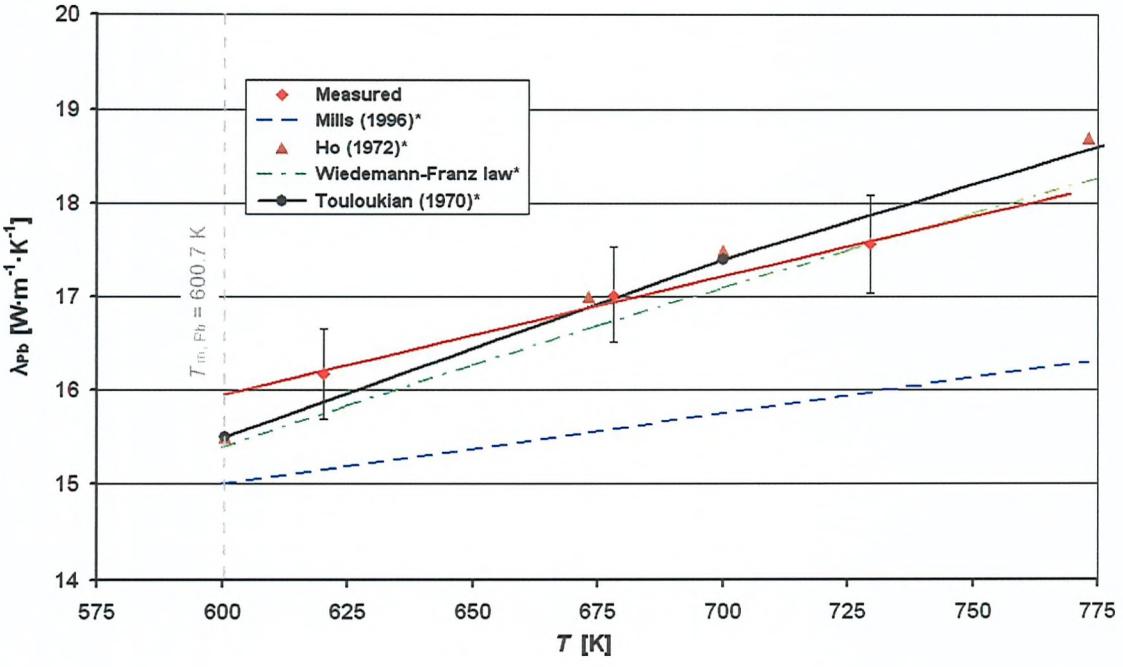

Figure 5.15 Thermal conductivity of molten lead (comparison with recommended values)

If a comparison is made with recommended values, as shown in Figure 5.15, the very good agreement of ±3 % is found with Touloukian [70] and Ho [71] although they both stated an uncertainty of 10 %. The W-F law was again calculated using electrical resitivity published by Monaghan [91] with uncertainty of about ±3 % and the

calculated thermal conductivity is also found within ±3 % of the measured data. The values recommended by Mills [72] more or less follow the values measured by Nakamura [66] because Mills believed that the measurements by Hemminger and Osipenko (steady-state techniques) were more affected by convection within the measured sample.

5.3. Solders

Besides the pure molten metals, which were presented above, several alloys have been investigated. The accessibility, common usage in industry and suitable temperature of the melting point were the most significant parameters, which influenced the choice of the materials. Solders comfortably met all of these criteria, because they are widely used in the electronics industry and their melting point is usually within the temperature range from 180 °C (approx. 450 K) to 250 °C (approx. 520 K). The research was also driven by the fact that a comprehensive study of the thermal conductivity of the molten solders has not been yet carried out and such data may become very important once the manufacturers of the electronics are forced to adjust their technological processes to different soldering materials that are free of lead.

For example, from July 1, 2006 onward, any electrical or electronic goods (subject to some limited exceptions) placed on the market in the EU cannot contain materials mentioned in WEEE (Waste Electrical and Electronic Equipment) and RoHS (Restriction of Hazardous Substances) directives [93]. Lead is also listed as a hazardous substance and therefore must be excluded from the manufacturing processes if the products are designed for the European market. That is why the electronics industry has had to change their soldering material from the commonly used leaded solders to lead-free alternatives.

A comparison between leaded and lead-free solders is one of the main goals of the analysis of the thermal conductivity of the soldering alloys. The alloys for soldering are usually defined as a sequence of symbols of the elements from the periodic table and numbers, which represents the percentage of the element in the solder by mass. For example, 1 kg of Sn60Pb40 solder (sometimes also defined as 60Sn40Pb) contains 600 g of pure tin and 400 g of pure lead. The following sections present the data of the thermal conductivity of molten Sn60Pb40, Sn62Pb36Ag2, Sn99.3Cu0.7 and Sn95.5Ag3.8Cu0.7.

The experiments with the solders were carried out in two stages. The first stage started in January 2004 and was one of the first measurements of the thermal conductivity of molten materials at University of Southampton. The thermal conductivity of the molten solders was measured with a sensor, which was fabricated in Imperial College London

in 2000, and the equipment, measuring devices and procedures were the same as in previous work carried out by Peralta [13]. The FE analysis employed was also very similar to a previously used technique and the only differences were that the rectangular cross-section of the hot wire in the FE analysis was replaced by a circular cross-section and ANSYS software was used to carry out the FE analysis. The first stage was concluded in May 2004 with the publication of the data of the thermal conductivity of molten leaded and lead-free solders up to 625 K (approx. 350 °C) [94, 95].

At the end of 2005, the experiments with the molten solders were repeated, because the technique of measurements of the thermal conductivity had been significantly upgraded. Besides other minor improvements, the newly designed sensors were used, the upper heater placed in the furnace was replaced by a more powerful and reliable heat source, the accuracy of the FE model was significantly improved by changes in time-stepping and the thermal conductivity was measured up to about 725 K (approx. 450 °C).

5.3.1. Leaded Solders

The Sn60Pb40 solder was supplied by MBO UK Ltd in the form of bars and the specified temperature from which the composition is in the liquid phase is 191 °C ($T_{m,\,Sn60Pb40}$ = 464 K) [96]. The Sn62Pb36Ag2 solder was supplied by ESL in the form of powder and the temperature of its melting point is 179 °C ($T_{m,\,Sn62Pb36Ag2}$ = 452 K) [96].

The density and specific heat capacity data, which are required for the thermal conductivity measurements, are not available and therefore must be calculated using the 'Rule of Mixtures' as suggested in [97]. However the usage of this rather simple rule may result in inaccurate values of the density and specific heat capacity of the measured solders. Therefore it should be noted that the uncertainty of the measurement of the thermal conductivity, when the presented technique is used, is stated as being ±3 % only if the product of density and specific heat capacity of the molten metal is know with an uncertainty of less than ±10 %. The uncertainty, which originates from the 'Rule of Mixtures' is unknown, and has not been investigated, hence the region of ±3 % presented in the figures below is only to be considered as an expected uncertainty.

For the Sn60Pb40 solder, the density and specific heat capacity is calculated at every temperature as

$$\frac{1}{\rho_{Sn60Pb40}} = \frac{0.60}{\rho_{Sn}} + \frac{0.40}{\rho_{Pb}} \tag{5-5}$$

$$C_{P,\,Sn60Pb40} = 0.60 \cdot C_{P,\,Sn} + 0.40 \cdot C_{P,\,Pb} \tag{5-6}$$

The temperature of the melting point of the Sn60Pb40 solder is approximately 40 K lower than for the melting point of the pure tin and about 140 K lower than for the melting point of the pure lead. It is assumed that the material properties of the solder at its melting point are calculated using material properties of composites at their melting points. For example, the density of the Sn60Pb40 solder at its melting point (464 K) is defined as

$$\frac{1}{\rho_{Sn60Pb40}(T_{m,\,Sn60Pb40})} = \frac{0.60}{\rho_{Sn}(T_{m,\,Sn})} + \frac{0.40}{\rho_{Pb}(T_{m,\,Pb})} \tag{5-7}$$

The similar assumption is also made for higher temperatures, e.g. the density of the solder at temperature 50 K above the melting point is derived from the density of its composites also at temperature 50 K above their melting points. Therefore the equation, which describes the change of the density of the Sn60Pb40 solder with the temperature, can be then written as

$$\rho_{\mathrm{Sn60Pb40}}(T) = -0.91 \cdot (T - T_{\mathrm{m,\,Sn60Pb40}}) + 8122 \quad \mathrm{kg \cdot m^{-3}} \tag{5-8}$$

and is valid at temperatures $T \geq T_{\mathrm{m,\,Sn60Pb40}}$, i.e. at temperatures above the melting point of the Sn60Pb40 solder. A similar technique is used for the calculation of the specific heat capacity of the molten Sn60Pb40 solder and the temperature dependence can be written for $T \geq T_{\mathrm{m,\,Sn60Pb40}}$ as

$$C_{\mathrm{P,\,Sn60Pb40}}(T) = -0.023 \cdot (T - T_{\mathrm{m,\,Sn60Pb40}}) + 209.7 \quad \mathrm{J \cdot kg^{-1} \cdot K^{-1}} \tag{5-9}$$

Similar rules have also been applied to the second leaded solder, Sn62Pb36Ag2, with the only difference that the solder consists of three pure metals, i.e. tin, lead and silver. The density and specific heat capacity of the molten silver was again obtained from the same reference sources as material properties of other pure metals [88]. The equations which describe the temperature dependence of the density and specific heat capacity of the molten Sn62Pb36Ag2 solder can be then written as

$$\rho_{\mathrm{Sn62Pb36Ag2}}(T) = -0.896 \cdot (T - T_{\mathrm{m,\,Sn62Pb36Ag2}}) + 8041 \quad \mathrm{kg \cdot m^{-3}} \tag{5-10}$$

$$C_{\mathrm{P,\,Sn62Pb36Ag2}}(T) = -0.023 \cdot (T - T_{\mathrm{m,\,Sn62Pb36Ag2}}) + 214.3 \quad \mathrm{J \cdot kg^{-1} \cdot K^{-1}} \tag{5-11}$$

Both equations are valid for $T \geq T_{\mathrm{m,\,Sn62Pb36Ag2}}$. Similar to the measurements of the thermal conductivity of pure metals, it is estimated that the uncertainty of the density and specific heat capacity results in an additional uncertainty of approximately ±1 % in the measured thermal conductivity, which is again included within the overall ±3 % accuracy region.

Table 5.V and Table 5.VI present the measured thermal conductivity of the molten leaded solders as a function of temperature and Figure 5.16 then graphically presents the data from the tables.

Table 5.V Thermal conductivity of the molten Sn60Pb40 solder

2005

T [K]	T [°C]	$\lambda_{Sn60Pb40}$ [W·m^{-1}·K^{-1}]
466.2	193.1	20.1
491.9	218.7	21.0
517.8	244.6	21.7
543.4	270.2	22.1
569.5	296.3	22.6
595.4	322.2	23.5
621.3	348.2	23.8
647.2	374.0	24.5
673.1	399.9	25.0
714.2	441.0	25.7

2004

T [K]	T [°C]	$\lambda_{Sn60Pb40}$ [W·m^{-1}·K^{-1}]
471.3	198.2	23.3
518.2	245.1	25.2
571.5	298.4	25.9
621.8	348.7	26.2

Table 5.VI Thermal conductivity of the molten Sn62Pb36Ag2 solder

2005

T [K]	T [°C]	$\lambda_{Sn62Pb36Ag2}$ [W·m^{-1}·K^{-1}]
466.9	193.7	20.9
492.9	219.7	21.6
518.9	245.8	22.2
545.5	272.3	23.0
570.5	297.4	23.9
596.9	323.7	24.4
623.0	349.9	25.1
648.7	375.6	25.6
675.0	401.8	26.3
716.0	442.8	27.0

2004

T [K]	T [°C]	$\lambda_{Sn62Pb36Ag2}$ [W·m^{-1}·K^{-1}]
466.8	193.7	22.8
485.3	212.2	23.7
518.5	245.4	24.9
560.1	287.0	26.0
618.7	345.6	26.3

It can be seen that the results measured in 2004 are about 2 W·m^{-1}·K^{-1} above the values measured in 2005. The adoption of the newer measured data is strongly recommended, because they offer much higher degree of accuracy. The explanation of the higher accuracy of the latest data will be presented in section *5.4.Discussion.*

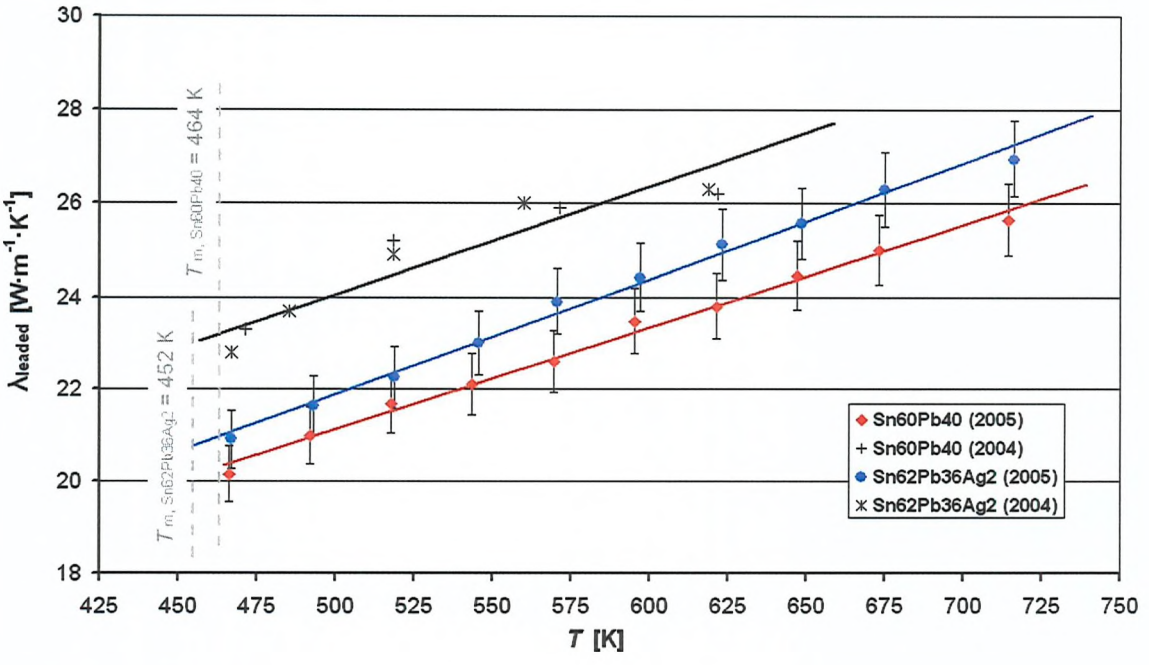

Figure 5.16 Thermal conductivity of molten leaded solders

The trend lines of the measured thermal conductivity of molten leaded solders are also shown in Figure 5.16. The thermal conductivity of the molten Sn60Pb40 solder can be written for T from $T_{m,\,Sn60Pb40}$ to750 K as

$$\lambda_{Sn60Pb40} = 0.0221 \cdot (T - T_{m,\,Sn60Pb40}) + 20.35 \quad W \cdot m^{-1} \cdot K^{-1} \tag{5-12}$$

and the thermal conductivity for the molten Sn62Ag36Ag2 solder is defined for T from $T_{m,\,Sn62Pb36Ag2}$ to750 K as

$$\lambda_{Sn62Pb36Ag2} = 0.0249 \cdot (T - T_{m,\,Sn62Pb36Ag2}) + 20.66 \quad W \cdot m^{-1} \cdot K^{-1} \tag{5-13}$$

5.3.2. Lead-free solders

The two most common lead-free solders have been investigated. The Sn99.3Cu0.7 solder was supplied by MBO UK Ltd. It is an eutectic solder and the temperature of its melting point is 227 °C ($T_{m,\,Sn99.3Cu0.7}$ = 500 K) [96]. The Sn95.5Ag3.8Cu0.7 solder was supplied by ESL and the tabulated temperature, from which the solder is in the liquid phase, is 220 °C ($T_{m,\,Sn95.5Ag3.8Cu0.7}$ = 493 K) [96]. The density and specific heat capacity are again calculated using the rules of mixtures and data from other sources [88] as was described above for leaded solders. The material properties of the lead-free solders are then defined as

$$\rho_{Sn99.3Cu0.7}(T) = -0.738 \cdot (T - T_{m,\,Sn99.3Cu0.7}) + 7008 \quad \text{kg·m}^{-3} \tag{5-14}$$

$$C_{P,\,Sn99.3Cu0.7}(T) = -0.023 \cdot (T - T_{m,\,Sn99.3Cu0.7}) + 250 \quad \text{J·kg}^{-1}\text{·K}^{-1} \tag{5-15}$$

for $T \geq T_{m,\,Sn99.3Cu0.7}$ and

$$\rho_{Sn95.5Ag3.8Cu0.7}(T) = -0.744 \cdot (T - T_{m,\,Sn95.5Ag3.8Cu0.7}) + 7076 \quad \text{kg·m}^{-3} \tag{5-16}$$

$$C_{P,\,Sn95.5Ag3.8Cu0.7}(T) = -0.023 \cdot (T - T_{m,\,Sn95.5Ag3.8Cu0.7}) + 251.3 \quad \text{J·kg}^{-1}\text{·K}^{-1} \tag{5-17}$$

for $T \geq T_{m,\,Sn95.53Cu0.7}$. The uncertainties of the density and specific heat capacity are again expected to impose less than ±1 % uncertainty into the thermal conductivity measurements.

Table 5.VII Thermal conductivity of the molten Sn99.3Cu0.7 solder

2005

T [K]	T [°C]	$\lambda_{Sn99.3Cu0.7}$ [W·m^{-1}·K^{-1}]
623.2	350.1	**30.1**
518.4	245.2	**26.8**
570.5	297.4	**28.5**
726.9	453.7	**32.9**
675.2	402.0	**31.4**
704.0	430.9	**32.1**
548.0	274.9	**27.6**

2004

T [K]	T [°C]	$\lambda_{Sn99.3Cu0.7}$ [W·m^{-1}·K^{-1}]
507.3	234.2	**27.4**
541.6	268.5	**29.3**
577.1	304.0	**31.3**
619.4	346.3	**32.1**

Table 5.VIII Thermal conductivity of the molten Sn95.5Ag3.8Cu0.7 solder

2005

T [K]	T [°C]	$\lambda_{Sn95.5Ag3.8Cu0.7}$ [W·m^{-1}·K^{-1}]
515.5	242.3	26.7
548.0	274.9	27.9
579.4	306.3	28.7
605.4	332.3	29.8
632.6	359.4	30.5
658.5	385.3	31.0
685.2	412.1	31.9
712.1	439.0	32.4
737.4	464.3	33.3

2004

T [K]	T [°C]	$\lambda_{Sn95.5Ag3.8Cu0.7}$ [W·m^{-1}·K^{-1}]
501.4	228.3	27.4
533.3	260.2	29.3
564.0	290.9	30.4
608.6	335.5	31.6

The measured thermal conductivity of molten lead-free solders are presented in Table 5.VII and Table 5.VIII and illustrated in Figure 5.17 as a function of temperature. The thermal conductivity of pure tin is also shown in the figure because the measured lead free solders contain more than 95% of pure tin.

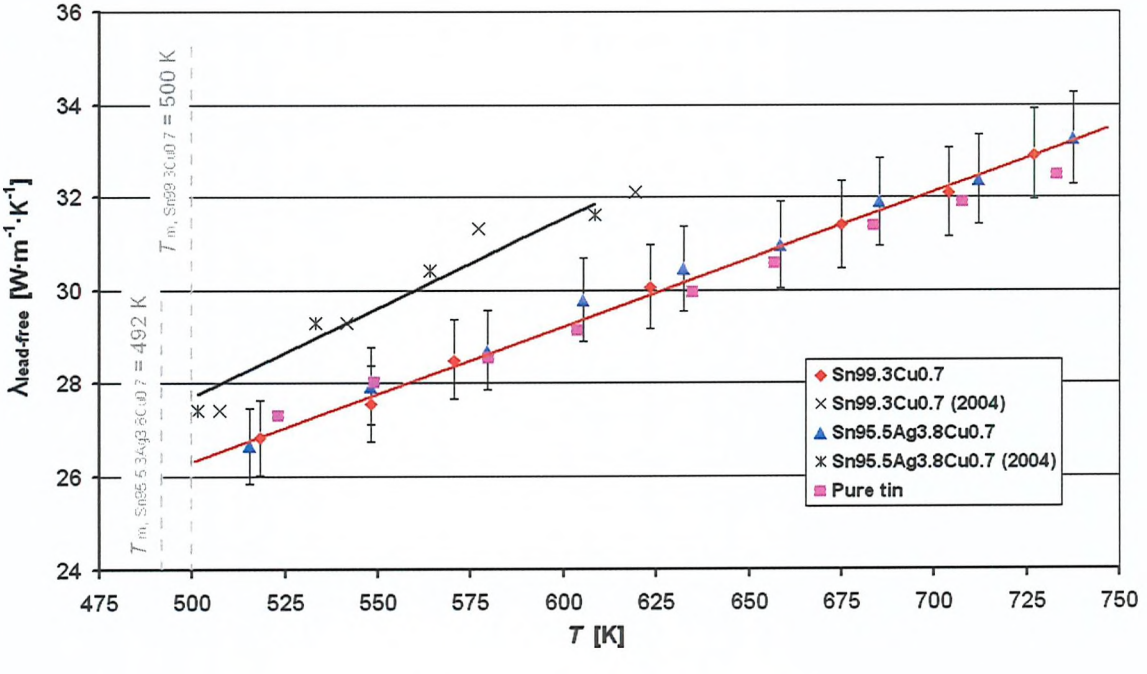

Figure 5.17 Thermal conductivity of molten lead-free solders

It can be seen in Figure 5.17 that the thermal conductivity of both lead-free solders is almost identical although the molten Sn95.5Ag3.8Cu0.7 solder contains more silver which is a better thermal conductor. However no significant differences were observed during the measurements and one linear relationship can be used to evaluate the measured thermal conductivity as a function of temperature

$$\lambda_{Sn99.3Cu0.7} = \lambda_{Sn95.5Ag3.8Cu0.7} = 0.0294 \cdot (T - T_{m,Sn99.3Cu0.7}) + 26.3 \quad W \cdot m^{-1} \cdot K^{-1} \qquad (5\text{-}18)$$

The thermal conductivity of pure tin can be found within the 2 % uncertainty region, therefore it can be concluded that the thermal conductivity of the molten lead-free solders, which contain at least 95 % pure tin can be characterised by the thermal conductivity of pure tin unless an accuracy of better than 2 % is required.

Figure 5.17 also illustrates the thermal conductivity which was measured and published in 2004 and it can be seen that those values are again about 2 $W \cdot m^{-1} \cdot K^{-1}$ higher than the newly measured data. Similar to the case of leaded solders, it is recommended to use the newly measured thermal conductivity because it offers higher accuracy. A further explanation is presented in the following section.

5.4. Discussion

The thermal conductivity data, which have been presented for molten indium, tin, lead and four alloys, have been measured using an upgraded transient hot-wire technique. Each molten material was measured with at least two different sensors. Additionally, both the original and new design of the sensor has been employed and it has been observed that the new design improves the electrical performance of the sensor and it allows the measurement of the thermal conductivity with higher sensitivity. The responses of the original and newly designed sensor are shown in Figure 5.18 and Figure 5.19.

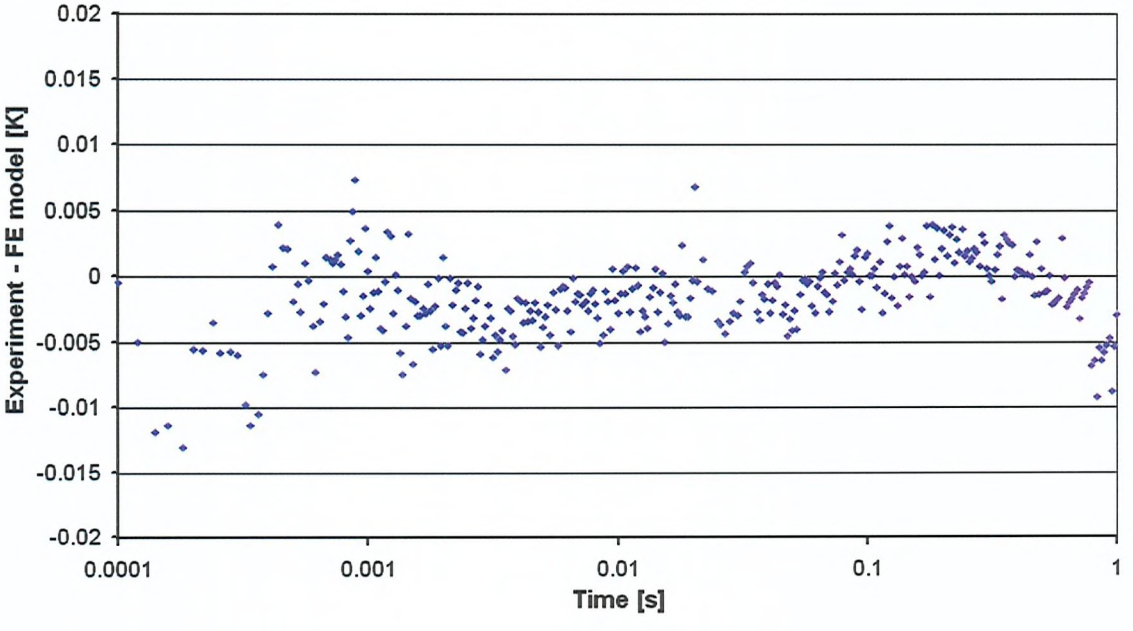

Figure 5.18 Comparison between FE model and temperature rise of the hot wire measured with sensor A5 (measured in molten Sn60Pb40 solder at 543 K, applied heat flux 64 $W \cdot m^{-1}$)

Figure 5.18 shows the differences between the FE model and a response measured by an original sensor when a heat flux of 64 $W \cdot m^{-1}$ is applied. The response is noisy especially at short times and the level of noise is up to ±5 mK on the temperature scale. Figure 5.19 then illustrates the noise when a new design of the sensor is used. The noise level is similar to that for the original design, about ±3 mK, but this level is reached with a

heat flux of only 53 $W \cdot m^{-1}$. Therefore it can be concluded that the new design offers better signal-to-noise ratio by approximately 18 %. It confirms the theoretical assumption that if the length of the hot wire is extended by 18 %, the signal-to-noise ratio should also improve by about 18 %.

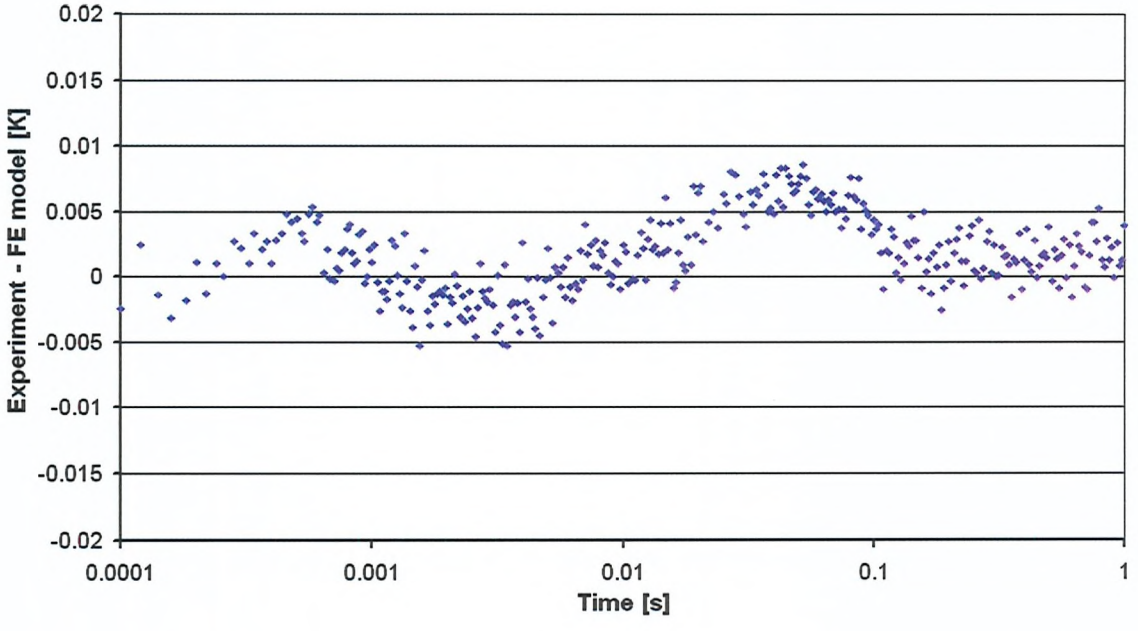

Figure 5.19 Comparison between FE model and temperature rise of the hot wire measured with sensor B1 (measured in molten Sn62Ag3.8Cu0.7 solder at 548 K, heat flux 53 $W \cdot m^{-1}$)

The repeated experiments also helped to analyse the influence of convection within the molten metals. Different positions of the crucible in the high temperature furnace have been tested, together with various temperatures of the upper heaters, in order to comprehensively evaluate the convectional heat transfer in the crucible containing the molten sample. That is, convection in the fluid within the crucible caused by a steady-state temperature distribution. It has been found that such convection may significantly affect the measurements of the thermal conductivity if it is not totally suppressed with a suitable temperature gradient.

The influence of the convection within the measured sample can be revealed only by repetitive measurements at the same steady temperature. During the measurements, different heat fluxes have to be applied and ideally the differences between applied heat fluxes should be large, even up to 100 %. If the measured thermal conductivity is the

same for all the applied heat fluxes or at least within a reasonably small range, the phenomenon of convection is suppressed and the values of the thermal conductivity are trustworthy.

It has been found during the measurements that the upper heater, which is placed inside the sensor support, needs to be set to more than 60 K above the temperature of the melt otherwise convection is very likely to occur. Figure 5.20 shows a comparison between the model and experimental results when the upper heater is set to only 20 K above the temperature of the measured sample. The first three time decades of the temperature can be matched to the FE model but significant differences are observed from time 0.1 s. In this time decade the steady-state convection heavily influences the temperature increase of the wire, i.e. the heat generated from the hot wire is absorbed in the measured liquid much quicker and an exact match between the FE model and the experiment is impossible. Therefore the temperature difference between the upper heater and the measured sample has to be more than 60 K in order to suppress the steady-state convection.

The low-wattage heater, which was used in previous work by Peralta [13] and for the measurements carried out before 2005, was not able to accommodate such temperature difference and that is why it had to be replaced by a more powerful heating element in this work.

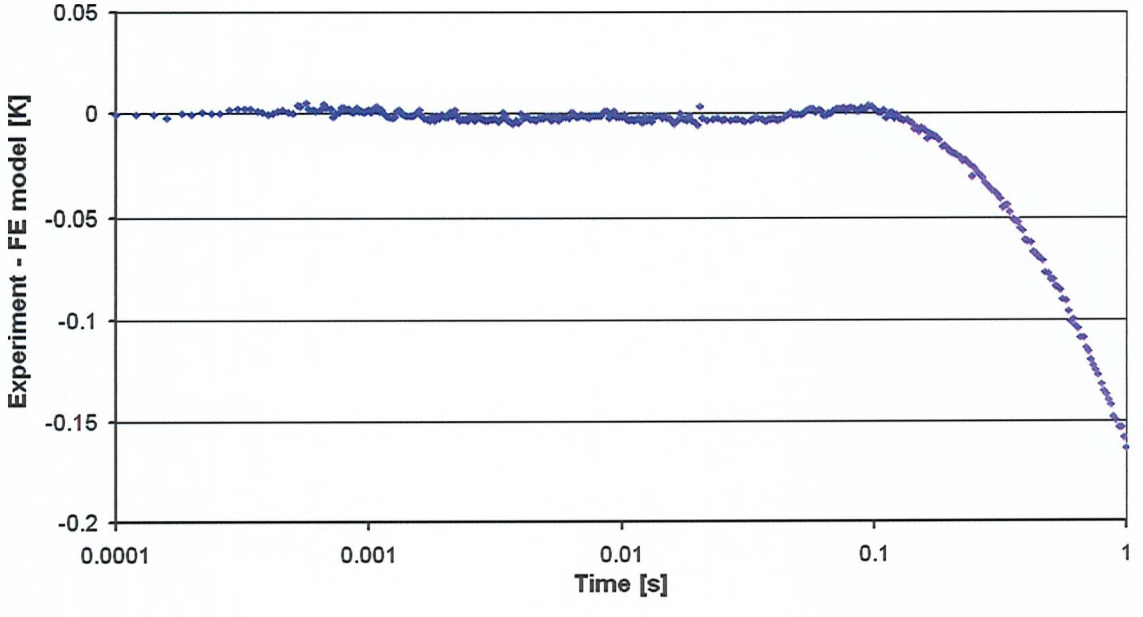

Figure 5.20 Influence of the convection within the molten indium (sensor A3 at temperature 521 K, heat flux 95 W·m^{-1}, upper heater set to 541 K)

The importance of such an upgrade can be observed by comparing the values of the thermal conductivity of molten solders in Figure 5.16 and Figure 5.17. The values measured in 2004 were obtained with low-wattage upper heater, which could not create a suitable temperature gradient along the molten material hence cancel the natural convection. Additionally the applied heat fluxes did not vary greatly and the FE model, which was used to extract the thermal conductivity from the measured temperature rises, used less accurate linear time stepping.

In September 2004, a newly designed sensor was introduced [98] and at the beginning of 2005, the first new sensors were manufactured. The new design of sensor led to different thermal conductivity values for a series of metals than those observed before. This led to further experimental work and improvements in the FE model and details of the experimental set-up. Among the latter was the inclusion of a more powerful upper heater, which could be set to higher temperature than the earlier one. It was at this stage that the earlier and the newer sensor designs provided similar thermal conductivity data and that tests using a wide variation of the applied heat fluxes on the hot wire were also successful.

The thermal conductivity data, which have been presented in this work, for some metals differ significantly from the values measured by Peralta [13] in her pioneering study, although she used the same THW sensor. The differences exceed the mutual estimated uncertainty of the two sets of work. It was assumed that such differences were caused mainly by the phenomenon of the steady, natural convection within the investigated molten metal. Peralta was able to cancel a part of the convectional flow, however the convection was probably not fully suppressed and it resulted in up to 10 % differences from the values of the thermal conductivity measured in this work. This assertion is also supported by the fact that Peralta used only one sensor for the measurements of each metal and therefore her values might have contained a systematic error which was extremely difficult to identify.

Wiedemann-Franz law can be also used for the analysis of the experimentally acquired values of the thermal conductivity. The measured thermal conductivity can be used to calculate constant L_T from the Wiedemann-Franz law defined in the equation (5-1) as

$$L_{\mathrm{T}} = \frac{\lambda}{\sigma \cdot T} \tag{5-19}$$

Then the constant L_T can be relatively compared to the theoretical Lorentz number L_0 and the comparison between the measured thermal conductivity and values published by Peralta can be presented in one graph as a relative deviation of the data from the Wiedemann-Franz law for all investigated molten metals. Such a comparison is illustrated in Figure 5.21.

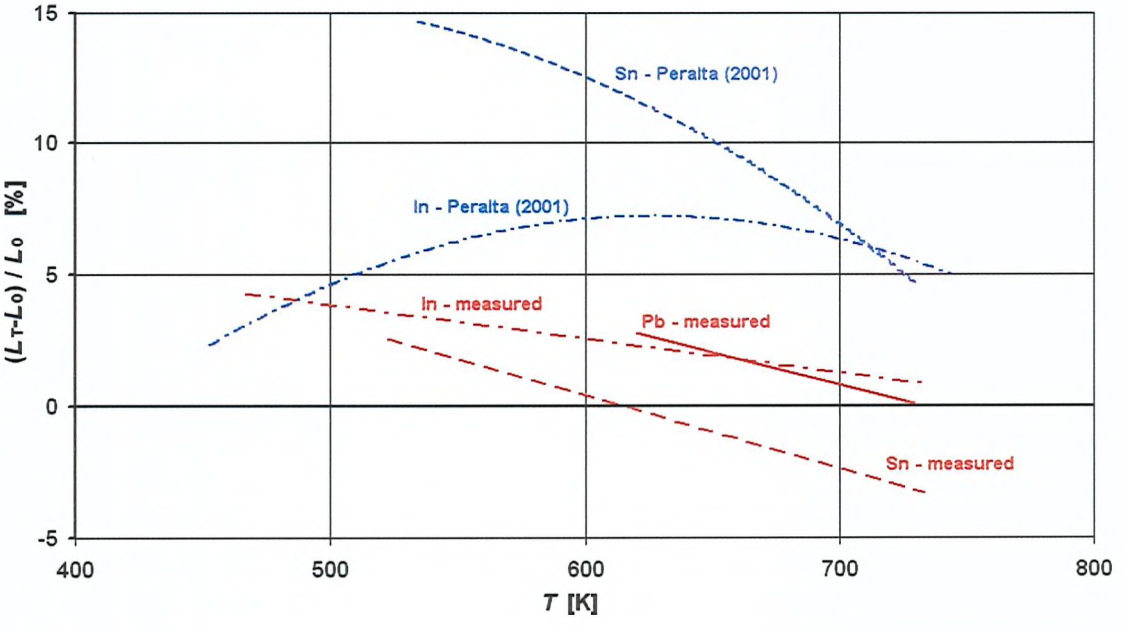

Figure 5.21 Comparison between the measured values and data published by Peralta [11] using W-F law

It can be seen that the measured thermal conductivities differ by less than 5 % from the theoretical W-F law and L_T decreases slightly with increasing temperature for all pure molten metals although it should be emphasized that the accuracy of the measured thermal conductivity is stated as ±3 % and the uncertainty of the data for electrical conductivity is from 3% to 5 %. However, L_T calculated from the thermal conductivity measured by Peralta show differences of up to 15% and its temperature dependence is not that consistent and therefore the comparison presented in Figure 5.21 can also be used as validation of the thermal conductivity data measured in this work.

Based on all the data presented in this chapter, it can be concluded that this work has contributed to a modified transient hot-wire technique for the measurements of the thermal conductivity of molten metals in a number of ways:

- The experimental set-up has been upgraded in order to improve the control of the temperature distribution within the measured material
- The FE model used for the extraction of the thermal conductivity from the measured temperature rise of the hot wire has been transferred into the commercially available software, significantly improved and validated.
- The new design of the transient hot-wire instrument have been introduced, manufactured and tested. The new design provides better electrical performance hence improving the measurements of the thermal conductivity.
- For the first time the instrument has been used to measure the thermal conductivity of molten pure lead and four metallic alloys which are used in the electronics industry.

6. Future Work

This chapter has been added to this work with the aim of describing tasks, which could not be completed within the time available for the current postgraduate research. The sections list challenges in several areas of the above presented transient hot-wire technique and sketch out possible directions for subsequent research.

6.1. Further Improvements of the Design

The design of the sensors of the THW instrument is one of the main improvements which have been introduced in this work. Experiments with a number of newly designed sensors have proved that the new design is capable of more sensitive and accurate measurements of the thermal conductivity of the molten materials than earlier examples. However, the design is not optimal and can be still further improved. The experiments with the infrared camera, described in chapter *4.Experimental Arrangements*, proved that the design could be more condensed, i.e. the three thermally independent parts of the hot wire may be placed closer to each other. Figure 6.1 suggest patterns of sensors which are expected to further improve the sensitivity of the measurements because the length of the hot wire increases so that the change of the hot wire resistance can be measured more precisely. The numbers in the figure illustrate lengths of the components of the new sensor in millimetres.

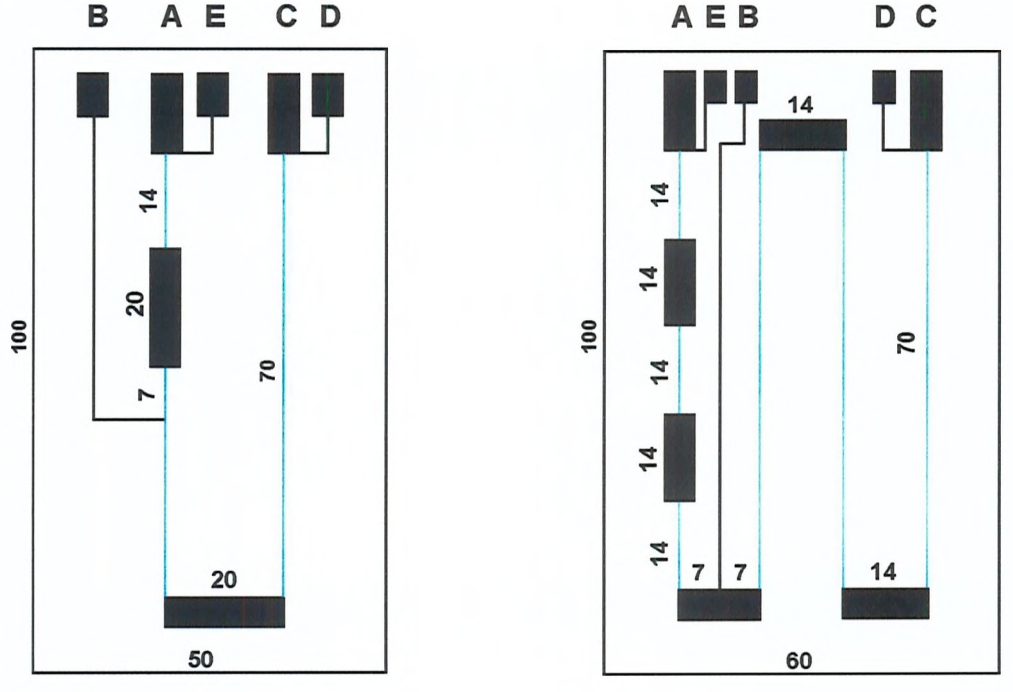

a) b)

Figure 6.1 Suggested future designs of the THW instrument (the blue lines show the position of the platinum wires)

Figure 6.1a shows an outline of the sensor, which is very similar to the new design presented in section *4.1.2.New Sensor Design*, with the length of the finite part of an infinitely long hot wire of 78 mm (i.e. an increase of 39 % compared to the original design). The design in Figure 6.1b then suggests a revolutionary configuration of six thermally independent parts of the hot wire. In this case, the finite part of the hot wire would be three times longer (168 mm) than in the original design.

The main advantage of such improvements is that the voltage acquired from the sensor will have better signal-to-noise ratio, which will allow better comparison between the measured and the modelled temperature rise of the hot wire. On the other hand, the new designs also provide a disadvantage, because the higher integration of the wires will result in even higher demands for proper placement and straightness of the thin platinum wires. At the same time the uncertainty of measurements of the length of the encapsulated hot wire will inevitably increase. Problems with the placement of the hot wire could be overcome by printing the hot wire using the same technology as for the printed conductive pattern. However, this will definitely mean that every sensor will have to be calibrated at all temperatures because the standards for pure and annealed platinum cannot be used for the platinum thick film paste used in printing. Also the cross-sectional area of the printed wire will differ along its length and for each sensor will have to be studied in detail in order to construct a reliable and trustworthy FE model of the resulting THW instrument.

6.2. Measurements at Higher Temperatures

Chapter *5.Results* contained the results from the measurements of the thermal conductivity of molten metals up to 750 K (470 °C). Beyond this temperature, the sensors started to produce occasionally faulty responses and the resistance of the hot wire apparently became very variable. This phenomenon was observed for all sensors, which were exposed to temperatures higher than 750 K (470 °C), and this suggests an inappropriate choice of materials during the fabrication process. Therefore some changes in the fabrication are necessary, if the present technique is required to be employed to measure the thermal conductivity of liquid materials at higher temperatures.

The response from the sensor can become noisy only if some of the contacts with the hot wire are faulty because the temperature 750 K (470 °C) cannot impose any changes upon the platinum wire itself. Between the platinum hot wire and measurement devices, there are several material junctions but only three of them are exposed to the high temperatures in the furnace chamber. One junction is the contact between the bare platinum wire and the printed platinum pattern, the second junction is a contact between the printed pattern and the platinum foil and the third junction is the spot-welded Pt-Ni joint between the foil and the nickel wire (refer to section *4.2.Fabrication Process*).

The first two junctions are mainly Pt-Pt contacts; however the thick film platinum paste which creates the conductive pattern of the sensor may also contain residues of other material such as glass and certain types of binders. Typically the platinum thick film pastes contain about 65 % of Pt particles (by weight) and the overall solid content is from 72 % to 78 % by weight. As the whole sensor is sintered at 1720 K (approx 1450 °C) it is assumed that the liquid content of the paste plus most of the non-metallic solids evaporate.

This suggests that the main cause of the inappropriate behaviour of the sensor above 450 °C is the junction created by the spot-welding of two different metals: platinum and nickel. These two metals have very different melting points (for Pt it is 2041.4 K or 1768.3 °C, for Ni it is 1728 K or 1455 °C) and this may result in a spot-welded junction of a poor quality. Although every effort had been made to clean the Pt foil and Ni wires from any oxide layer, the spot-welding process could not be carried out in a non-oxidising atmosphere and therefore it was very likely that a thin oxide layer between the

two bulk materials had been created and as a consequence the joint lost a certain amount of its robustness. Additionally, platinum has a much lower thermal coefficient of expansion ($8.8 \cdot 10^{-6}$ K^{-1}) than nickel ($13.4 \cdot 10^{-6}$ K^{-1}) and this imposes mechanical stress on the spot-welded joints. In the end, the combination of the mechanical stress and spot-welded joints that are not ideal may result in a small layer between the two metallic materials and so that there is a further resistance in the circuit which is very variable and militates against trustworthy measurement of the resistance and voltage.

In order to eliminate this effect and enable operation at higher temperatures than those employed here, the nickel wire should be substituted with platinum wires. The spot-welding of platinum foil to platinum wires should provide a more reliable contact and mechanical stress should not occur at any temperature. However, the main disadvantage of such a solution is the cost of platinum material because it is necessary to use a wire about 20 mm long for each terminal of which there are five. Thus whereas platinum has higher electrical conductivity ($10.6 \cdot 10^{-8}$ $\Omega \cdot m$) than nickel ($7 \cdot 10^{-8}$ $\Omega \cdot m$) and therefore the diameter of the wires can be reduced slightly, the cost of of the five connections is quite substantial.

Although the performance of the sensor became very poor at temperatures above 750 K, a couple of high temperature tests were carried out in order to investigate whether the sensor itself could withstand very high temperatures. During the first test, the sensor was exposed to a temperature of approximately 1270 K (1000 °C) for about two hours. After the test, the mechanical strength of the sensor was unaffected and neither the printed pattern nor the encapsulated hot wire showed any changes. The second test was carried out above 1470 K (1200 °C) and this time there were visible changes in the printed platinum pattern. The printed paste filled the gap between the hot wire and the alumina substrate (caused by the difference in coefficients of thermal expansion) so that the sensor was destroyed. That is why it has been estimated that the maximum application temperature of the current technique is about 1370 K (1100 °C) supposing that the material junctions in the sensor can provide reliable electric contact throughout the whole range of temperatures.

6.3. Experimental Configuration

The devices used for the measurements of the temperature rise of the hot wire were described in section *4.4.Experimental Configuration and Equipment* and they have remained almost the same for last ten years. The current configuration of the whole experiment consists of three main processing units. The first processing unit is a 286 computer (running on MS DOS) with built-in 8-bit D/A ISA card, which controls the lifting mechanism of the high temperature furnace. The card cannot be placed in a computer with a newer operating system because it requires a specific driver (Dynamic Link Library), which is not available.

The second processing unit is the computer that controls the THW measurements. This computer had been upgraded and two different systems (Windows NT and MS DOS) are available. The computer must be switched to the MS DOS system for the THW measurements because the program, which controls the experiment, uses a DMA channel and this causes great difficulties in multitasking systems. Once the data are measured the computer is switched back to the Windows NT system and acts as a file server. The last processing unit is a modern computer outside the lab, which processes the measured data, solves FE models and is used as an archive of all analysed responses.

It can be seen that the configuration is rather complicated and not efficient. Ideally only one computer should be used to provide control of the lifting mechanism, carry out all measurements and analyse the measured results. However it would mean major upgrade of most of the components. The two acquisition cards would have to be replaced by one modern card, which allows application of different time steps during the run and is able to run on machines with a modern operating system. Ideally this new acquisition card would also provide a D/A converter, which would be used to control the lifting mechanism of the crucible. And finally, the computer would be also equipped with ANSYS software and allow instant analysis of the measured results. Alternatively, the computer would use the computational grid of University of Southampton, which serves for highly demanding analyses of FE models. The connection to the internet would also allow distant monitoring of the temperature of the melt measured by the thermocouples.

Such a major upgrade of the equipment would result in much more efficient use of time and resources. On the other hand, I estimate the overall cost of such improvements to be

about £2000-£4000 and also the time, which would be necessary to re-write the computer programs for the transient measurement and operation of the lifting mechanism, would not be negligible. At present the upgrade of the devices is not the priority, because the current equipment can still provide highly precise measurements of temperature and time. However, once one of the main components in the measurement system is damaged or stops working properly, the upgrade of the whole system and the integration of the three independent computing units should be considered.

6.4. Improvements in Post-Processing of FE Analysis

It was described in section *3.3.6.Material Properties Measurements* how the material properties are iteratively derived from the measured temperature rise of the hot wire. Currently the iterative analysis requires manual adjustments of the material properties before/after every analysis in ANSYS. The ANSYS software includes advanced analysis techniques such as Design Optimisation and Probabilistic Design, which may be used to automate the iterative analysis. However, the transient analysis of our FE model consists of altogether about 600 time points and the optimisation process can result in a much slower overall analysis if compared to the analysis completed within few runs if an experienced user is involved.

Therefore I recommend that the first few runs of the FE analysis should be completed with a very rough time stepping (about 60 time points, i.e. each time decade divided into just ten steps) and once a reasonably accurate match between the measured and modelled temperature rise is obtained, the time stepping can be refined and a more accurate model optimised again. Therefore the automated FE analysis has to be capable of recognition of the moment when the refinement of the time steps should be applied. At the same time it would be convenient if the transient FE analysis may be stopped during its run once a significant departure between the modelled and measured temperature rise is observed. Also, the model should prevent changes in the material properties if another temperature rise measured at the same temperature with different applied heat flux is entered.

Such requirements mean that the automation of the analysis will result in significant changes in the code of the ANSYS model that is currently used. The changes have to be carried out cautiously and must be verified by comparison with either analytical solutions or previous models. Again this will be a very time demanding procedure, but once the reliable and trustworthy automation of the analysis is completed, it will significantly speed up the measurements of the thermal conductivity.

References

1. Kuang-O, Y., *Modelling for Casting and Solidification Processing*, 2002, New York, Marcel Dekker Inc.

2. Wunderlich, R.K., *High-Precision Thermophysical Property Data of Liquid Metals for Modelling of Industrial Solidification Processes* in *ESA Final Report Part A*, 2003 University of Ulm

3. Wakeham, W.A., Nagashima, A., Sengers, J.V., *Measurement of the Transport Properties of Fluids*, Experimental Thermodynamics, Vol. III, 1991, Blackwell Scientific Publications

4. Tye, R.P., *Thermal Conductivity*, Vol. 2, 1969, London, Academic Press

5. Jamieson, D.T., Irving, J.B., Tudhope, J.S., *Liquid Thermal Conductivity: A Data Survey to 1973*, 1975, Edinburgh, H.M.S.O.

6. Nieto de Castro, C.A., Wakeham, W.A., *Experimental Aspects of the Transient Hot-Wire Technique for Thermal Conductivity Measurements*, Proceedings of 15th International Conference on Thermal Conductivity, Thermal Conductivity 15, 1977, Ottawa, Ontario

7. Sakonidou, E.P., Assael, M.J., Nieto de Castro, C., Van den Berg, H.R., Wakeham, W.A., *A Review of the Experimental Data for the Thermal Properties of Liquid Mercury, Gallium and Indium*, Thermal Conductivity 24, Proceedings of 24th Internattional Thermal Conductivity Conference, 1999, Technomic Publishing Company, Inc.

8. Assael, M.J., Nieto de Castro, C.A., van den Berg, H.R., Wakeham, W.A., *An Instrument for the Measurement of the Thermal Conductivity of High-Temperature Melts*, in *Research report for European Project FP4 Commission*, 1997

9. Peralta-Martinez, V., Dix, M., Wakeham, W.A., *The Thermal Conductivity of Liquid Gallium*, Proceedings of 25th International Thermal Conductivity Conference, 1999, Ann Arbor, Michigan, USA

10. Peralta-Martinez, M.V., Dix, M., Lesemann, M., Wakeham, W.A., *Thermal Conductivity of Liquid Mercury*, High Temperatures – High Pressures, 2002, **34**(Proceedings of 15th ECTP): p. 35-39

11. Peralta-Martinez, M.V., Wakeham, W.A., *Thermal Conductivity of Liquid Tin and Indium*, International Journal of Thermophysics, 2001, **22**(2): p. 395-403

12. Peralta-Martinez, V., Dix, M., Wakeham, W.A., *The Thermal Conductivity of Several Molten Metals*, Proceedings of The 1st International Conference on Thermophysical Properties of Materials, 1999, Singapore

13. Peralta-Martinez, V.M., *Thermal Conductivity of Molten Metals*, Thesis, Imperial College, 2000

14. Sklyarchuk, V., Plevachuk, Yu. , *A Modified Steady State Apparatus for Thermal Conductivity Measurements of Liquid Metals and Semiconductors*, Meas. Sci. Technol., 2005, **16**: p. 467

15. Abdulagatov, I.M., Azizov, N.D., *Thermal Conductivity and Viscosity of Aqueous K2SO4 Solutions at Temperatures from 298 to 575K and at Pressures up to 30 MPa*, International Journal of Thermophysics, 2005, **26**(3): p. 593-635

16. Osipenko, V.P., *Thermal Conductivity of Alloys of the Systems Sn-Pb and Sn-In in the Solid and Liquid States*, Russian Physics Journal, 1970, **13**(12): p. 1570-1573

17. Hemminger, W., Jugel, R., *A Guarded Hot-Plate Apparatus for Thermal Conductivity Measurements over the Temperature Range -75 to 200°C*, International Journal of Thermophysics, 1985, **6**(5): p. 483-497

18. Hemminger, W., *Thermal Conductivity of Tin between 15 and 500 °C*, High Temperature-High Pressures, 1985, **17**: p. 465

19. Hemminger, W., *Thermal Conductivity of Lead in the Range -180 to 500 °C*, International Journal of Thermophysics, 1989, **10**(4): p. 765-777

20. Duggin, M.J., *The Thermal Conductivities of Liquid Lead and Indium*, J. Phys. F: Metal Phys., 1972, **2**: p. 433-440

21. Goldratt, E., Greenfield, A.J., *New Method for Measuring Thermal-Conductivity*, Review of Scientific Instruments, 1978, **49**(11): p. 1531-1536

22. Goldratt, E., Greenfield, A.J., *Experimental Test of the Wiedemann-Franz Law for Indium*, J. Phys. F: Metal Phys., 1980, **10**: p. L95-L99

23. Kubicar, L., Bohac, V., *Review of Several Dynamic Methods of Measuring Thermophysical Parameters*, Thermal Conductivity 24, Proceedings of 24th International Thermal Conductivity Conference, 1999, Technomic Publishing Company

24. Filippow, L.P., *Research of Thermophysical Properties at Moscow State University*, International Journal of Heat and Mass Transfer, 1973, **16**(5): p. 865-885

25. Yurchak, R.P., Filippov, L.P., *Measuring the Thermal Diffusivity of Molten Metals*, High Temperature, 1964, **2**: p. 628-635

26. Banchila, S.N., Filippov, L.P., *New Measurements of Complex of Thermal Properties of Liquid-Tin and Lead*, High Temperature, 1973, **11**(3): p. 602-605

27. Zinovyev, V.Y., Polev, V.F., Taluts, S.G., Zinovyeva, G.P., Ilinykh, S.A., *Temperature and Heat Conductivities of 3D-Transition Metals in Solid and Liquid States*, Fizika Metallov I Metallovedenie, 1986, **61**(6): p. 1128-1135

28. Parker, W.J., Jenkins, R.J., Butler, C.P., Abbott, G.L., *Flash Method of Determining Thermal Diffusivity, Heat Capacity, and Thermal Conductivity*, J. Appl. Phys., 1961 **32**(9): p. 1679-1684

29. Mathis, N., *Transient Thermal Conductivity Measurements: Comparison of Destructive and Nondestructive Techniques*, Proceedings of 15th European Conference on Thermal Properties, 1999, Wurzburg, Germany, Pion, Ltd., 2001

30. Baba, T., Ono, A., *Improvement of the Laser Flash Method to Reduce Uncertainty in Thermal Diffusivity Measurements*, Measurement Science & Technology, 2001, **12**(12): p. 2046-2057

31. Vozar, L., Hohenauer, W., *Flash Method of Measuring the Thermal Diffusivity. A Review*, High Temperature-High Pressures, 2003, **35/36**(3): p. 253-264

32. Vozar, L., Hohenauer, W., *Uncertainty of Thermal Diffusivity Measurements Using the Laser Flash Method*, International Journal of Thermophysics, 2005, **26**(6)

33. Ohta, H., Ogura, G., Waseda, Y., Suzuki, M., *Thermal-Diffusivity Measurements of Molten-Salts Using a 3-Layered Cell by the Laser Flash Method*, Review of Scientific Instruments, 1990, **61**(10): p. 2645-2649

34. Taylor, R.E., Groot, H., Goerz, T., Ferrier, J., Taylor, D.L., *Thermophysical Properties of Molten Aluminium Alloys*, High Temperatures-High Pressures, 1998, **30**(3): p. 269-275

35. Monaghan, B.J., Quested, P.N., *Thermal Diffusivity of Iron at High Temperature in Both the Liquid and Solid States*, ISIJ International, 2001, **41**(12): p. 1524-1528

36. Maeda, Y., Sagara, H., Tye, R.P., Masuda, M., Ohta, H., Waseda, Y., *A High-Temperature System Based on the Laser Flash Method to Measure the Thermal Diffusivity of Melts*, International Journal of Thermophysics, 1996, **17**(1): p. 253-261

37. Becker, H., Grigull, U., *Measurement of Thermal-Diffusivity and Conductivity of Carbon-Dioxide in Critical Region by Means of Holographic-Interferometry*, Warme Und Stoffubertragung-Thermo and Fluid Dynamics, 1978, **11**(1): p. 9-28

38. Nagashima, A., *Recent Development and Applications of an Optical Method for Measurements of Thermophysical Properties*, International Journal of Thermophysics, 1995, **16**(5): p. 1069-1086

39. Nagasaka, Y., Hatakeyama, T., Okuda, M., Nagashima, A., *Measurement of the Thermal-Diffusivity of Liquids by the Forced Rayleigh-Scattering Method - Theory and Experiment*, Review of Scientific Instruments, 1988, **59**(7): p. 1156-1168

40. Nagasaka, Y., Nagashima, A., *Measurement of the Thermal-Diffusivity of Molten KCl up to 1000-Degrees-C by the Forced Rayleigh-Scattering Method*, International Journal of Thermophysics, 1988, **9**(6): p. 923-931

41. Motosuke, M., Nagasaka, Y., Nagashima, A., *Measurement of Dynamically Changing Thermal Diffusivity by the Forced Rayleigh Scattering Method (Measurement of Gelation Process)*, International Journal of Thermophysics, 2004, **25**(2): p. 519-531

42. Borelius, G., *A Method for the Combined Measurements of Peltier Heat and Thermal Conductivity*, Ann. Physik, 1917, **52**(4): p. 398-414

43. Cutler, M., *Thermoelectric Measurements at Small-Area Contacts*, Journal of Applied Physics, 1961, **32**(6): p. 1075-1082

44. Yurchak, R.P., Smirnov, B.P., *Thermal Conductivity and Lorentz Number of Solid and Liquid Gallium*, Soviet Phys.-Solid State, 1968, **10**: p. 1065

45. Yurchak, R.P., Smirnov, B.P., *Thermal Conductivity and Lorentz Number of Indium in the Solid and Liquid States*, High Temperature, 1969, **7**: p. 163-164

46. Stalhane, B., Pyk, S., *New Method for Determining the Coefficient of Thermal Conductivity*, Teknisk Tidskrift, 1931 **61** p. 389-393

47. van der Held, E.F.M., van Drunen, F.G., *A Method of Measuring the Thermal Conductivity of Liquids*, Physica 1949 **15** (10): p. 865-881

48. Haran, E.N., Wakeham, W.A., *A Transient Hot-Wire Cell for Thermal Conductivity Measurements over a Wide Range of Temperature Range*, J.Phys. E: Sci.Instrum, 1982, **15**: p. 839

49. Assael, M.J., Charitidou, E., Wakeham W.A., *The Thermal Conductivity of Mixtures of Alcohols and Water*, International Journal of Thermophysics, 1989, **10**: p. 793-803

50. Assael, M.J., Gialou, K., *A Transient Hot-Wire Instrument for the Measurement of the Thermal Conductivity of Solids up to 590 K*, International Journal of Thermophysics, 2003, **24**(3): p. 667-674

51. Gustafsson, S.E., Karawacki, E., Khan, M.N., *Transient Hot-Strip Method for Simultaneously Measuring Thermal-Conductivity and Thermal-Diffusivity of Solids and Fluids*, Journal of Physics D-Applied Physics, 1979, **12**(9): p. 1411-1421

52. Hammerschmidt, U., *A Linear Procedure for Analyzing Transient Hot Strip Signals*, Thermal Conductivity 24, Proceedings of 24th International Thermal Conductivity Conference, 1999, Technomic Publishing Company, Inc.

53. Gustaffson, S.E., *Transient Hot Strip Technique for Measuring Thermal Conductivity and Thermal Diffusivity*, The Rigaku Journal, 1987, **4** (1/ 2): p. 16-28

54. Gustafsson, S.E., *Transient Plane Source Techniques for Thermal-Conductivity and Thermal-Diffusivity Measurements of Solid Materials*, Review of Scientific Instruments, 1991, **62**(3): p. 797-804

55. Gustavsson, M., Nagai, H., Okutani, T., *Measurements of the Thermal Effusivity of a Drop-Size Liquid Using the Pulse Transient Hot-Strip Technique*, International Journal of Thermophysics, 2005, **26**(6): p. 1803-1813

56. Xie, H., Gu, H., Fujii, M., Zhang, X., *Short Hot Wire Technique for Measuring Thermal Conductivity and Thermal Diffusivity of Various Materials*, Measurements science and technology, 2005, **17**: p. 208–214

57. Weisstein, E.W., *Convective Derivative*, MathWorld - A Wolfram Web Resource, 1999 [cited 2006]; Available from: http://mathworld.wolfram.com/ConvectiveDerivative.html

58. De Groot, J.J., Kestin, J., Sookiazian, H., *Instrument to Measure the Thermal Conductivity of Gases*, Physica, 1974, **75**(3): p. 454-482

59. Carslaw, H.S., *Conduction of Heat in Solids*, 1947

60. Abramowitz, M., *Handbook of Mathematical Functions*, 1964

61. Healy, J.J., de Groot, J.J., Kestin, J., *The Theory of the Transient Hot-Wire Method for Measuring Thermal Conductivity*, Physica, 1976, **92C**: p. 392-408

62. Nagasaka, Y., Nagashima, A., *Absolute Measurement of the Thermal Conductivity of Electrically Conducting Liquids by the Transient Hot-Wire Method*, J.Phys. E:Sci.Instrum., 1981, **14**: p. 1435

63. Nakamura, S., Hibiya, T., Yamamoto, F., *New Sensor for Measuring Thermal-Conductivity in Liquid-Metal by Transient Hot-Wire Method*, Review of Scientific Instruments, 1988, **59**(6): p. 997-998

64. Nakamura, S., Hibiya, T., Yamamoto, F., *Ceramic Probe for Measuring the Thermal-Conductivity of an Electrically Conductive Liquid by the Transient Hot-Wire Method*, Review of Scientific Instruments, 1988, **59**(12): p. 2600-2603

65. Takegoshi, E., Imura, S., Hirasawa, Y., Takenaka, T., *A Method of Measuring the Thermal-Conductivity of Solid Materials by Transient Hot-Wire Method of Comparison*, Bulletin of the Jsme-Japan Society of Mechanical Engineers, 1982, **25**(201): p. 395-402

66. Nakamura, S., Hibiya, T., Yamamoto, F., *Thermal-Conductivity of Gasb and Insb in Solid and Liquid States*, Journal of Applied Physics, 1990, **68**(10): p. 5125-5127

67. Nakamura, S., Hibiya, T., *Thermophysical Properties Data on Molten Semiconductors*, International Journal of Thermophysics, 1992, **13**(6)

68. Nakamura, S., Hibiya, T., Yamamoto, F., Yokota, T., *Measurement of the Thermal-Conductivity of Molten InSb under Microgravity*, International Journal of Thermophysics, 1991, **12**(5): p. 783-790

69. Yamasue, E., Susa, M., Fukuyama, H., Nagata, K., *Deviation from Wiedemann–Franz Law for the Thermal Conductivity of Liquid Tin and Lead at Elevated Temperature*, International Journal of Thermophysics, 2003, **24**(3): p. 713-730

70. Toulokian, Y.S., Powell,R.W., Ho, C.Y., Klemens, P.G., *Thermal Conductivity of Metallic Elements and Alloys*, Thermophysical Properties of Matter, 1970, New York,, IFI/Plenum

71. Ho, C.Y., Powell, R.W., Liley, P.E., *Thermal Conductivity of Elements*, J. Phys. Chem. Ref. Data, 1972, **1**: p. 279-421

72. Mills, K.C., Monaghan, B.J., Keene, B.J., *Thermal Conductivity of Liquid Metals*, Proceedings of 23rd International Thermal Conductivity Conference, 1996, Thermal Conductivity 23, Technomic

73. Zhang, X., Hendro, W., Fujii, M., Tomimura, T., Imaishi, N., *Measurements of the Thermal Conductivity and Thermal Diffusivity of Polymer Melts with the Short-Hot-Wire Method*, International Journal of Thermophysics, 2002, **23**(4): p. 1077-1090

74. Felippa, C.A., *A Historical Outline of Matrix Structure Analysis: A Play in Three Acts*, Computers and Structures, 2001, **79**: p. 1313-1324

75. Zienkiewicz, O.C., *The Birth of the Finite Element Method and of Computational Mechanics*, International Journal for Numerical Methods in Engineering, 2004, **60**: p. 3–10

76. Zienkiewicz, O.C., Cheung, Y.K., *The Finite Element Method in Structural Mechanics*, 1967, New York, McGraw-Hill

77. Mackerl, J., *Finite Element Books*, Dept. of Mechanical Engineering Div. of Solid Mechanics, Linköping Institute of Technology, 2005 [cited 2005]; Available from: http://www.solid.ikp.liu.se/fe/

78. Kohnke, P., *Ansys, Inc. Theory Reference*, in *ANSYS Release 8.0*, 2003, SIS IP, Inc

79. Dix, M., Drummond, I.W., Lesemann, M, Peralta-Martinez, V.M., Wakeham, W.A., Assael, M.J., Karagiannidis, L., van den Berg, H.R., *The Thermal Conductivity of Liquid Metals near Ambient Conditions*, Proceedings of 21st International Thermal Conductivity Conference, 2000, Cambridge, MA, USA, Plenum

80. Bilek, J., Atkinson, J.K., Wakeham, W.A., *Validation of FE Model for Transient Hot Wire Thermal Conductivity Measurements*, Proceedings of EuroSimE, 2005, Berlin

81. Palacín, J., Marco, S., Samitier, J., *Suboptimal Filtering and Nonlinear Time Scale Transformation for the Analysis of Multiexponential Decays*, IEEE Transactions on instrumentation and measurement, 2001, **50**(1): p. 135-140

82. Holmes, P.J., Loasby, R.G., *Handbook of Thick Film Technology*, 1976, Glasgow, Electrochemical Publications Ltd

83. Barnwell, P., Reynolds, Q., *A New, Very Low Loss LTCC Technology, Combined with Photo–Patterned Thick Film for Microwave Applications*, Proceedings of 36th IMAPS Nordic Conference, 1999, Helsinki

84. Mohammed, A.A., *LTCC for High–Power RF Applications*, in *Advanced Packaging*, 1999, p. 46

85. *Industrial Platinum Resistance Thermometer Sensors*, The European Standard EN 60751:1995, Editor. 1995.

86. Kestin, J., Wakeham, W.A., *A Contribution to the Theory of the Transient Hot-Wire Technique for Thermal Conductivity Measurements*, Physica A: Statistical and Theoretical Physics, 1978, **92**(1-2): p. 102-116

87. *ASM Handbook*, ed. ASM International Handbook Committee, 1992

88. Smithells, C.J., *Metals Reference Book*, 1976

89. Gronvold, F., *Heat Capacity of Indium from 300 to 1000 K*, Journal of Thermal Analysis and Calorimetry, 1978, **13**(3): p. 419-428

90. Dyos, G.T., Farrell, T., *Electrical Resistivity Handbook*, 1992, IEE

91. Monaghan, B.J., *A Four-Probe Dc Method for Measuring the Electrical Resistivities of Molten Metals*, International Journal of Thermophysics, 1999, **20**(2): p. 677-690

92. Samsonov, G.V., *Handbook of the Physicochemical Properties of the Elements*, 1968, New York, Plenum Press

93. *European Parliament Directive 2002/95/EC*, European Commission Official Journal, 2003, **L37**: p. 19-23

94. Bilek, J., Atkinson , J., Wakeham, W., *Thermal Conductivity of Molten Lead Free Solders*, Proceedings of European Microelectronics and Packaging Symposium, 2004, Prague

95. Bilek, J., Atkinson, J.K., Wakeham, W.A., *Thermal Conductivity of Molten Lead-Free Solders*, International Journal of Thermophysics, details to be specified, 2006

96. *Table of Specialty Alloys and Solders*, Indium Corporation of America, 2006 [cited 2006]; Available from: http://www.indium.com/products/sorted_by_temp.pdf

97. SOLDERTEC, *Thermal and Electrical Conductivity of Lead Free Solders*, 1996 [cited 2005]; Available from: http://www.tintechnology.biz/soldertec/

98. Bilek, J., Atkinson, J., Wakeham, W., *Design Issues of an Instrument for Measuring Thermal Conductivity of High Temperature Fluids*, Proceedings of Electronic Devices and Systems Conference, 2004, Brno

Appendix A
Summary of Material Properties

Thermal material properties of molten metals, which have been acquired from other sources and used to evaluate the thermal conductivity of the molten metals investigated in this work. The measured thermal conductivity is also listed. All equations are valid for temperatures T from the melting point of the material, T_m, to 750 K.

Indium

Melting point:	$T_m = 429.8$ K
Density (liquidus):	$\rho = -0.6903 \cdot (T - T_m) + 7024$ kg·m^{-3}
Specific heat capacity (liquidus):	$C_P = -0.0279 \cdot (T - T_m) + 259.5$ J·kg^{-1}·K^{-1}
Thermal conductivity (liquidus):	$\lambda = 0.0345 \cdot (T - T_m) + 35.0$ W·m^{-1}·K^{-1}

Tin

Melting point:	$T_m = 505.1$ K
Density (liquidus):	$\rho = -0.7375 \cdot (T - T_m) + 7002$ kg·m^{-3}
Specific heat capacity (liquidus):	$C_P = -0.0233 \cdot (T - T_m) + 248.2$ J·kg^{-1}·K^{-1}
Thermal conductivity (liquidus):	$\lambda = 0.025 \cdot (T - T_m) + 26.8$ W·m^{-1}·K^{-1}

Lead

Melting point:	$T_m = 600.7$ K
Density (liquidus):	$\rho = -1.3707 \cdot (T - T_m) + 10687$ kg·m^{-3}
Specific heat capacity (liquidus):	$C_P = -0.0225 \cdot (T - T_m) + 152$ J·kg^{-1}·K^{-1}
Thermal conductivity (liquidus):	$\lambda = 0.0128 \cdot (T - T_m) + 15.92$ W·m^{-1}·K^{-1}

Sn60Pb40 Solder

Melting point: $T_m = 464$ K

Density (liquidus): $\rho = -0.91 \cdot (T - T_m) + 8122$ kg·m^{-3}

Specific heat capacity (liquidus): $C_P = -0.023 \cdot (T - T_m) + 209.7$ J·kg^{-1}·K^{-1}

Thermal conductivity (liquidus): $\lambda = 0.0221 \cdot (T - T_m) + 20.35$ W·m^{-1}·K^{-1}

Sn62Pb32Ag2 Solder

Melting point: $T_m = 452$ K

Density (liquidus): $\rho = -0.896 \cdot (T - T_m) + 8041$ kg·m^{-3}

Specific heat capacity (liquidus): $C_P = -0.023 \cdot (T - T_m) + 214.3$ J·kg^{-1}·K^{-1}

Thermal conductivity (liquidus): $\lambda = 0.0249 \cdot (T - T_m) + 20.66$ W·m^{-1}·K^{-1}

Sn99.3Cu0.7 Solder

Melting point: $T_m = 500$ K

Density (liquidus): $\rho = -0.738 \cdot (T - T_m) + 7008$ kg·m^{-3}

Specific heat capacity (liquidus): $C_P = -0.023 \cdot (T - T_m) + 250$ J·kg^{-1}·K^{-1}

Thermal conductivity (liquidus): $\lambda = 0.0294 \cdot (T - T_m) + 26.3$ W·m^{-1}·K^{-1}

Sn95.5Ag3.8Cu0.7

Melting point: $T_m = 493$ K

Density (liquidus): $\rho = -0.744 \cdot (T - T_m) + 7076$ kg·m^{-3}

Specific heat capacity (liquidus): $C_P = -0.023 \cdot (T - T_m) + 251.3$ J·kg^{-1}·K^{-1}

Thermal conductivity (liquidus): $\lambda = 0.0294 \cdot (T - 500) + 26.3$ W·m^{-1}·K^{-1}

Appendix B
ANSYS Code of the FE model

ANSYS code, which is used to create the FE model. This code was developed throughout the course of the postgraduate project.

```
!------------------------- LOADING THE EXPERIMENTAL RESULTS FROM THE TEXT FILE ----------------
*DIM,Data,array,10,2,,,,
*VREAD,Data(1,1),trash,dat,d:\data\sensor,IJK,1,1,,1021
(f10.6)

*VREAD,Data(2,1),trash,dat,d:\data\sensor,IJK,2,1,,11
(f10.6)

*VREAD,Data(4,1),trash,dat,d:\data\sensor,IJK,1,1,,15
(f10.6)

*VREAD,Data(5,1),trash,dat,d:\data\sensor,IJK,1,1,,18
(f10.6)

*VREAD,Data(6,1),trash,dat,d:\data\sensor,IJK,1,1,,20
(f10.6)

*VREAD,Data(7,1),trash,dat,d:\data\sensor,IJK,1,1,,7
(f10.0)


*DIM,Voltage,array,1000,2,,,,
*VREAD,Voltage(1,1),trash,dat,d:\data\sensor,JIK,2,1000,,21
(2f10.6)

                        !LOADED EXPERIMENT CONSTANTS
Vss=Data(1,1)           !bridge voltage [V]
Lst=Data(2,1)           !long wire length [m]
StoL=Data(3,1)          !short/long wire ratio
Rtt=Data(4,1)           !bridge resitance [mOhm]
Rl=Data(5,1)            !long wire resistance [mOhm]
Rst=Data(6,1)           !long wire resistance 4-terminal measurements [mOhm]
T1=Data(7,1)            !Temperature measured displayed on the furnace
offset=1.5*(Voltage(2,2)-Voltage(1,2))          !Voltage offset

                        !TEMPERATURE RISE CALCULATION CONSTANTS
Alpha=3.9083e-3         !Thermal coeffiecient of resistance [1/K]
Beta=-5.775e-7          !Thermal coefficient of resistance [1/K^2]
PI=3.14159265358979323846264338327795           ! Ludolf's number

                        !CALCULATIONS
Rs=Rst*StoL             !Resistance of short wire
Rw=Rst-Rs               !Resistance of the wire without influence of the contacts

*DIM,V,array,1980,1,,,  !array of scaled measured voltage
*DIM,R,array,1980,1,,,  !array of calculated changes of resistance Rw
*DIM,Q,array,1980,1,,,  !array of applied heat input
*DIM,Qsub,array,7,1,,,  !array of applied heat input

!*DIM,dT,array,1980,1,,,  !array of calculated temperature rise
```

```
!SCALING THE VOLTAGE AND APPLYING OFFSET
*DO,I,1,1000
V(I)=(Voltage(I,2)/100)-((Voltage(1,2)-offset)/100)
*ENDDO
*DO,I,20,1000
V(I+980)=(Voltage(I,1)/100)-((Voltage(1,2)-offset)/100)
*ENDDO

!CALCULATING CHANGE OF RESISTANCE FROM CHANGE OF VOLTAGE
*DO,I,1,1980
R(i)=-(V(i)*Rtt*Rtt/Vss)/((Rtt*V(i)/Vss)-Rtt+RI) !Equation taken from QBasic, explanation in Vita's thesis


!CALCULATING HEAT FLUX
Corr=1 !1.04789  !1.01390

D=Vss*Vss*(Rw+R(i))
E=(Rtt+R(i))*(Rtt+R(i))*(Lst-Lst*StoL)
Q(i)=Corr*1000*D/E                    !Equation taken from QBasic, explanation in Vita's thesis
*ENDDO

Qsub(1)=Q(1)              !starting heat flux
Qsub(2)=Q(1)              !measured heat flux at t=0.00002s
Qsub(3)=Q(5)              !heat flux at t=0.0001s
Qsub(4)=Q(50)             !heat flux at t=0.001s
Qsub(5)=Q(500)            !heat flux at t=0.01s
Qsub(6)=Q(1080)           !heat flux at t=0.1s
Qsub(7)=Q(1980)           !heat flux at t=1s

!****** DIMENSIONS & MATERIAL PROPERTIES *****

!WIRE
Diameter=26e-6

!ALUMINA
Thickness=565e-6
Width=28e-3
roSub=3796                !Density
CPSub=880              !Heat capacity
TCSub=8.9                 !Thermal conductivity
TCcoef=-0.014             !Linear material property near measured temperature

!INTERFACE WIRE-SUBSTRATE
WiSub=1e-9                !interface thickness
roWiSub=roSub             !if values same as for substrate, there is no interface
CPWiSub=CPSub
TCWisub=0.02

!INTERFACE SUBSTRATE-MELT
SubMelt=0.42e-6           !interface thickness
roSubMelt=roSub           !if values same as for substrate, there is no interface
CPSubMelt=CPSub
TCSubMelt=0.08

!MELT
Melt=15e-3                                  !melt dimension (square)
roMelt=-0.744*(T1+273.15-493)+7076          !density of the melt [kg/m3]

!-0.7375*(T1+273.15)+7374.5                 !Tin
!-1.3707*(T1+273.15-600.7)+10687            !Lead

CPMelt=-0.023*(T1+273.15-493)+251.3         !specific heat capacity [J/Kg*K]
!-0.0233*(T1+273.15)+259.99                 !Tin
!-0.0225*(T1+273.15-600.7)+152              !Lead

TCMelt=32.3                         !thermal conductivity [W/m*K]
```

```
!****** TIMEPOINT OF THE TRANSIENT RUN ******
TimInit=1e-6
Substeps=10

!************* PREPROCESSOR **************
/PREP7

!******** Element type *******
ET,1,plane55
!ET,1,plane77

!******** Material properties ********
! 1-platinum, 2-interface wire-substrate, 3-alumina, 4-interface 5-melt

MP,dens,1,21472.19      !Platinum
MP,c,1,132.963
MP,kxx,1,70.35

MP,dens,2,roWiSub       !Interface wire-substrate
MP,c,2,CPWiSub
MP,kxx,2,TCWiSub

MP,dens,3,roSub         !Alumina
MP,c,3,CPSub
MP,kxx,3,TCSub,TCcoef

MP,dens,4,roSubMelt     !Interface substrate-melt
MP,c,4,CPSubMelt
MP,kxx,4,TCSubMelt

MP,dens,5,roMelt !Melt
MP,c,5,CPMelt
MP,kxx,5,TCMelt


!******** Geometry *******
!Wire
K,1,0,0
CIRCLE,1,diameter/2,,,90  !Line 1
L,1,2                     !Line 2
L,1,3                     !Line 3
AL,1,2,3                  !Area 1

!Interface
CIRCLE,1,diameter/2+WiSub,,,90  !Line 4
L,2,4                           !Line 5
L,3,5                           !Line 6
AL,4,5,1,6                      !Area 2

!Substrate -> areas 2,3,4
CIRCLE,1,thickness/4-diameter/2,,,90    !Line 7
L,5,7                                   !Line 8
L,4,6                                   !Line 9
AL,4,9,7,8                              !Area 3

K,8,thickness/2,0
K,9,0,thickness/2
K,10,thickness/2,thickness/2
K,11,width/2,0
K,12,width/2,thickness/2

L,7,9                   !Line 10
L,6,8                   !Line 11
L,8,10                  !Line 12
L,9,10                  !Line 13
AL,7,11,12,13,10        !Area 4
```

```
L,10,12                 !Line 14
L,8,11                  !Line 15
L,11,12                 !Line 16
AL,12,14,16,15          !Area 5
!Interface Substrate-Melt
K,13,0,SubMelt+thickness/2
K,14,thickness/2,SubMelt+thickness/2
K,15,width/2,SubMelt+thickness/2

L,9,13                  !Line 17
L,13,14                 !Line 18
L,10,14                 !Line 19
AL,13,17,18,19          !Area 6

L,14,15                 !Line 20
L,15,12                 !Line 21
AL,14,19,20,21          !Area 7

!Melt
K,16,0,SubMelt+thickness/2+Melt
K,17,4*thickness,SubMelt+thickness/2+Melt
K,18,width/2,SubMelt+thickness/2+Melt

L,13,16                 !21-left
L,16,17                 !23-top left
L,17,18                 !24-top right
L,15,18                 !25-right
L,14,17                 !26-midle

AL,18,26,23,22          !Area 8
AL,20,25,24,26          !Area 9


!******** MESHING *******
mshkey,2

MAT,1
lesize,1,,,14
lesize,2,,,14
lesize,3,,,14
amesh,1

mshkey,1
mshape,0,2D

MAT,2
lesize,4,,,14
lesize,5,,,2
lesize,6,,,2
amesh,2

MAT,3
lesize,7,,,14
lesize,8,,,20,5
lesize,9,,,20,5
amesh,3

Lesize,13,,,7,1.5
Lesize,12,,,7,1.5
lccat,13,12
lesize,10,,,15,1.5
lesize,11,,,15,1.5
amesh,4
```

```
lesize,14,,,40,60
lesize,15,,,40,60
amesh,5

MAT,4
lesize,17,,,3
lesize,19,,,3
lesize,18,,,7,1.5
amesh,6
lesize,20,,,40,60
lesize,21,,,3
amesh,7

MAT,5
lesize,22,,,40,150
lesize,26,,,40,150
lesize,25,,,40,150
lesize,23,,,7
lesize,24,,,40

amesh,8
amesh,9

/TRIAD,OFF
finish


!********* SOLUTION ***********
ASEL,s,,,1
NSLA,s,1
*GET,Nnode,NODE,,COUNT, , , ,          !number of nodes for the wire
ASEL,all
NSEL,all

/solu
ANTYPE,trans
outres,all,all
SOLCONTROL,on
AUTOTS,off

!tunif,T1
!tref,T1

!Applying loads

t=TimInit
Step=1-LOG10(TimInit)

*DO,J,1,Step

PowerIn=Qsub(J)/(Nnode*4)      !Heat generation in the wire [W/m], 4=one quater

*DO,I,1,Substeps
time,10**(I/SubSteps+Log10(t)-1)

NSEL,s,node,,1,Nnode,1
F,ALL,HEAT,PowerIn             !heat applied directly on nodes
NSEL,ALL

solve
*ENDDO

ti=t*10
t=ti
*ENDDO
```

```
!************************ POSTPROCESSOR *********************************
/post1

ASEL,s,,,1
NSLA,s,1
*GET,N,NODE,,COUNT, , , ,                    !number of nodes for the wire

Set,last
*GET,SetsNum,ACTIVE, ,SOLU,NCMLS      !NCMIT          !number of resultsets

*DIM,Twire,array,N,1,,,              !array of calculated temperature rise
*DIM,DeltaT,array,Setsnum,2,,,


*DO,I,1,Setsnum
SET,,,,,,,I
*VGET,Twire(1),NODE,1,TEMP
*VSCFUN,Taver,mean,Twire(1)      !average temperature of the wire

*GET,DeltaT(I),ACTIVE, ,SET,TIME
DeltaT(I,2)=Taver

*ENDDO

*CFOPEN,'deltaT','dat','D:\PhD\4_Measured'          !save the vector into file
*VWRITE,Diameter,Thickness,WiSub,TCcoef,RoSub,CPSub,TCSub,SubMelt,TCSubMelt,RoMelt,CPMelt,
TCMelt
(f18.10)
*VWRITE,deltaT(1),deltaT(1,2) , , , , , , , ,
(f12.10,'  ',f8.4)
*VWRITE,
(f18.10)
*VWRITE,Qsub(1),Qsub(2),Qsub(3),Qsub(4),Qsub(5),Qsub(6),Qsub(7)
(f18.10)
*CFCLOSE

finish
```

Appendix C
Publications

Papers, which contain results of the thermal conductivity of molten solders (values measured in 2004):

- Bilek, J., Atkinson , J., Wakeham, W., *Thermal Conductivity of Molten Lead Free Solders*, Proceedings of European Microelectronics and Packaging Symposium, 2004, Prague 150
- Bilek, J., Atkinson, J., Wakeham, W., *Thermal Conductivity of Molten Lead Free Solders*, International Journal of Thermophysics, 2006, paper presented at the Seventh Asian Thermophysical Properties Conference, August 23-28, 2004, Hefei and Huangshan, Anhui, P. R. China 156

Paper, which introduces the new design of the THW sensor:

- Bilek, J., Atkinson, J., Wakeham, W., *Design Issues of an Instrument for Measuring Thermal Conductivity of High Temperature Fluids*, Proceedings of Electronic Devices and Systems Conference, 2004, Brno 167

Paper, which analyses the solution of the FE model in the time domain:

- Bilek, J., Atkinson, J.K., Wakeham, W.A., *Validation of FE Model for Transient Hot Wire Thermal Conductivity Measurements*, Proceedings of EuroSimE, 2005, Berlin, p.134-138 173

Expected publications (not listed because the final versions are not completed):

- Bilek, J., Atkinson , J., Wakeham, W., *Repeatability and Refinement of a Transient Hot Wire Instrument for Measuring the Thermal Conductivity of High Temperature Melts*, to be published in International Journal of Thermophysics (the paper is now in the process of revision)
- Bilek, J., Atkinson , J., Wakeham, W., *Measurements of the Thermal Conductivity of Molten Lead Using a New Transient Hot Wire Sensor*, submitted to the Sixteenth Symposium on Thermophysical Properties and accepted for oral presentation

The following published papers were included in the bound thesis. These have not been digitised due to copyright restrictions, but the links are provided.

- Bilek, J., Atkinson, J. and Wakeham, W. (2004) Thermal conductivity of molten lead free solders. *European Microelectronics and Packaging Symposium, Prague, Czech Republic. 16 - 18 Jun 2004.* 6 pp. [Online]. Available at: http://eprints.soton.ac.uk/id/eprint/23346 [Accessed 16 December 2024].

- https://doi.org/10.1007/s10765-006-0035-4

- Bilek, J., Atkinson, J. and Wakeham, W. (2004) Design issues of an instrument for measuring thermal conductivity of high temperature fluids. *11th Electronic Devices and Systems Conference, Brno, Czech Republic. 08 - 09 Sep 2004.* 6 pp. [Online]. Available at: http://eprints.soton.ac.uk/id/eprint/23348 [Accessed 16 December 2024].

- Bilek, J., Atkinson, J.K. and Wakeham, W.A. (2005) Validation of FE model for transient hot wire thermal conductivity measurements. In *Proceedings of EuroSimE 2005.* IEEE. 720 pp. [Online]. Available at: http://eprints.soton.ac.uk/id/eprint/23348 [Accessed 16 December 2024].